Dynamical Mass Generation in Asymptotically Safe QED

Master's Thesis

seit 1558

A thesis in partial fulfillment
of the requirements for the degree of

Master of Science

submitted by

Ka Kit Kevin Tam

September 26, 2022

Primary examiner: Prof. Dr. Holger Gies
Secondary examiner: Dr. Georg Bergner

Abstract

While quantum electrodynamics (QED) is arguably the most attested theory in physics, perturbation theory suggests that the running gauge coupling diverges at a finite Landau pole, albeit at a regime $\sim 10^{286}$ eV far beyond the electroweak scale where the prediction is modified by a non-Abelian gauge symmetry. Nonetheless, the fundamental inconsistency of pure QED as an interacting theory is confirmed by lattice simulations and non-perturbative functional methods.

Recently, it has been shown that well-defined ultraviolet (UV) completions can be accommodated by including the next-to-leading-order Pauli operator of canonical dimension 5. This spin-field coupling term may be rendered relevant by quantum fluctuations, resulting in non-trivial fixed points of the non-perturbative functional renormalization group (FRG). One of these has been connected by a line of constant physics to phenomenological values of the gauge coupling and anomalous electron magnetic moment.

In this work, we apply FRG techniques to investigate whether such asymptotic safety scenarios are consistent with the small fermion masses of the Standard Model due to the Higgs mechanism. In particular, we consider the Nambu-Jonas-Lasinio (NJL) subspace of dimension-6 four-fermion operators, a simpler effective model for chiral symmetry breaking in quantum chromodynamics. While chiral symmetry is already explicitly broken by the Pauli term, divergences in the NJL couplings still herald dynamical generation of masses at a large UV scale.

Deriving the RG flow equations for the NJL couplings, we first consider a natural single-channel approximation in which all dependence on flavor number drop out incidentally. The observed fixed point collisions exclude the possibility of physically relevant asymptotic safety scenarios with light fermions. A more interesting case is given by a flavor-dependent two-channel model. For flavor number larger than one, we observe IR-stable fixed points, which safeguard against dynamical mass generation for UV values tuned in the appropriate phase, without introducing further physical parameter to the asymptotic safety scenarios in the gauge/Pauli sectors. Such fixed points persist despite the fermionic anomalous dimension rendering the NJL couplings perturbatively marginal.

The discovery of additional fixed points with relevant directions may extend asymptotic safety to the NJL sector, but the large deviations from canonical scaling necessitate further investigation by bosonization of the four-fermion interactions.

Acknowledgements

I would like to express my gratitude towards my supervisor Prof. Dr. Holger Gies, not only for the helpful feedback on the content of this thesis, but also for the reassuring support and empathy during difficult times. I am fortunate to have learnt as much as I did through your patient guidance in the many discussions which undoubtedly shaped the direction of this project. Thank you for your time and commitment.

I would also like to acknowledge the unconditional love and sacrifice of my parents Thomas and Angela, and sister Christy. Without your lifelong support, which transcends any geographical inconveniences, I would not be in this position to pursue my passions. I hope you can be proud of the work that I have managed and will continue to undertake. Matri meae recquiescas in pace et in paradiso tecum rursus erimus. Quos valde amas numquam vere moriuntur.

Finally, I would also like to thank my partner Michelle for the unwavering love and belief in my tenacity, especially in these final grueling weeks of trying to improve this thesis. We both know that your assistance with LaTeX has left very tangible contributions to the betterment of this document. I hope to be able to reciprocate the favour soon.

Declaration of Independent Work

I declare that I have independently written the work presented here, and I have not used any help other than from the stated sources and resources.

26.09.2022, Jena	
date, place of submission	signature

Contents

Chapter 1

Introduction

In quantum and statistical field theories, the renormalization group (RG) describes the running coupling upon coarse-graining of UV degrees of freedom. A well-known example is the gauge coupling e in quantum electrodynamics (QED), which is anticipated to increase with energy scale due to the screening nature of a vacuum populated by virtual fermion-antifermion pairs. Despite the remarkable agreement between theory and experiment [1, 2], such predictions are based solely on QED in the perturbative regime. In the ultraviolet (UV) limit, the gauge coupling e is expected to diverge at a finite scale. Phenomenologically, such a Landau pole occurs far above the electroweak scale where the physics of a non-Abelian gauge theory must be taken into account. Nonetheless, the Landau pole represents a fundamental inconsistency in pure QED as an interacting theory. Of course, this may simply signal the breakdown of perturbation theory for large coupling, but a similar conclusion is supported by lattice simulations and the non-perturbative functional renormalization group (FRG).

Without extending the particle spectrum beyond that of pure QED, a recently proposed resolution to the triviality of QED is to include the next-to-leading order Pauli term. As a dimension-5 operator in $d = 4$ spacetime dimensions, this spin-field coupling term is perturbatively non-renormalizable, but may become relevant at a non-Gaussian fixed point due to quantum fluctuations. This can provide a well-defined UV completion for QED. Such asymptotic safety scenarios were demonstrated by Gies and Ziebell and indeed, one such universality class is able to account for phenomeonological values of QED in the infrared [3].

A natural line of inquiry is to investigate the effects of including higher-dimensional operators. In this work, we focus on the dimension-6 four-fermion operators, particularly those channels belonging to the Nambu-Jonas-Lasinio (NJL) model. This provides an effective theory of spontaneous chiral symmetry breaking and the associated dynamical generation of mass, as observed in the constituent quarks of quantum chromodynamics (QCD). Similarly, we would like to investigate whether mass is generated at a UV scale in the strong coupling regimes of the aforementioned Pauli-induced asymptotic safety scenarios, which would contradict the light fermions of the Standard Model.

To establish the groundwork for our analysis, we revise in Chapter 2 the essential concepts behind the Wilsonian explanation for the universal scaling behavior among microscopically distinct systems. We then turn to the formulation of RG by Wetterich, with desirable properties for non-perturbative computations. We also develop intuition for dynamical mass generation by direct references to the low-energy phenomenology of QCD. In Chapter 3, we review in turn the application of FRG to the Pauli and NJL sectors which form the basis of our model in Chapter 4. There we derive the flow equations for the NJL couplings in the presence of a finite Pauli coupling, illustrating each term by its corresponding 1PI

Feynman diagram. Chapter 5 is then devoted to an analysis of the phase structure in the NJL sector, based on whether mass generation is triggered. For the sake of clarity, various simplifying approximations are employed before we examine the full model. As an epilogue, we summarize our findings and remark upon some interesting directions for further research in Chapter 6.

Chapter 2

Background

In this chapter, we review some essential prerequisites for our work. We begin with a summary of Wilsonian renormalization as a general notion of scale dependence in physics, along with definitions of recurring quantities such as beta function, fixed point, anomalous dimension, critical exponent and relevance/irrelevance. Armed with these concepts, we then focus on the running of the gauge coupling in quantum electrodynamics (QED). We see that at least according to perturbation theory, QED is inconsistent as a theory of interactions, since the gauge coupling appears to diverge at a finite scale known as the Landau pole.

Faced with this conundrum, we turn to the non-perturbative technique of functional renormalization, in particular the formulation by Wetterich. After a quick review of generating functionals in quantum field theories, we derive Wetterich's equation for the effective average action and comment on some pertinent concerns to further conceptual understanding.

We then finish with a revision of chiral symmetry breaking and the associated generation of mass, using the low-energy mesonic and baryonic degrees of freedom in QCD as a phenomenological example. This will motivate the formulation of our model in Chapter 3.

2.1 Wilsonian Renormalization

The renormalization group addresses a profound issue at the heart of physics; namely, how physical predictions could be made at our macroscopic scales, without first having obtained a microscopic theory of everything. The flow of a river is well described by the Navier-Stokes equation of fluid mechanics, without due consideration of the underlying molecular degrees of freedom by kinetic theory, the electronic wavefunctions by quantum mechanics, or ultimately, the open question of how the intricacies of quantum chromodynamics conspire to form nucleons bound together by the exchange of pions.

We begin with a review of Wilsonian renormalization, developed by Kenneth Wilson in order to solve a long-standing problem in condensed matter physics [4]. This is performed here in momentum space, though an alternative real-space formulation by Migdal and Kardanoff is commonly applied to lattice theories such as the well-known Ising model [5, 6, 7].

For simplicity, we consider a scalar field with the most general action in d dimensions:

$$S_\Lambda[\varphi] = \int d^d x \left[\frac{1}{2} \left(\partial_\mu \varphi\right)^2 + \sum_i \Lambda^{d-d_i} g_i \, \mathcal{O}_i(x) \right] , \tag{2.1}$$

where $\mathcal{O}_i(x)$ represent local operators of dimension d_i which may be consistent with desired symmetries of the system such as the discrete $\mathbb{Z}_2 : \varphi \to -\varphi$. For example, setting to zero all the coefficients g_i except for the quadratic and quartic terms would leave us with a massive φ^4 theory. Note that we have parametrized the action in terms of dimensionless (bare) couplings, by including suitable powers of the momentum cutoff Λ such that the action is dimensionless.

We can then construct the partition function in Euclidean spacetime, related to Minkowski spacetime by a Wick rotation $t \to -it$:

$$Z = \int_{|p|<\Lambda} \mathcal{D}\varphi \exp(-S_\Lambda[\varphi]), \tag{2.2}$$

where we regulate the theory by integrating only those degrees of freedom with momentum $|p| < \Lambda$, thus avoiding any ultraviolet (UV) divergences. Such a UV cutoff naturally arises in statistical mechanics, in an effective field theory (EFT) for the long-distance behaviour of a fundamentally discrete model at the atomic scale. For quantum field theories (QFTs), the cutoff Λ may represent a scale at which hitherto unknown physics emerges, far beyond the reach of current experimental probes. This may for example be at 10^{16} GeV for a Grand Unified Theory or 10^{19} GeV for quantum gravity [8]. Alternatively, we may be interested in sending the cutoff $\Lambda \to \infty$ in search of a well-defined continuum limit, which is known as the asymptotic freedom/safety scenario [9, 10].

To obtain a low energy effective field theory, we can perform the functional integral (2.2), but only over field fluctuations with momentum above a lower scale Λ'. Concretely, we decompose the field into fast modes $\varphi_>$ with support only over the shell $[\Lambda', \Lambda)$ in momentum space and slow modes $\varphi_<$ supported over $[0, \Lambda')$:

$$\varphi = \varphi_> + \varphi_<. \tag{2.3}$$

The partition function (2.2) then becomes

$$Z = \int \mathcal{D}\varphi_< \, \mathcal{D}\varphi_> \exp(-S_\Lambda[\varphi_> + \varphi_<]) := \int_{|p|<\Lambda'} \mathcal{D}\varphi_< \exp(-S_{\Lambda'}[\varphi_<]), \tag{2.4}$$

where we have defined a new effective action $S_{\Lambda'}[\varphi]$ at the lower scale Λ'. For a general action with non-Gaussian operators $\mathcal{O}_i$, the integrated fast modes φ mediate new interactions between the remaining slow modes. But since we started with the most general possible form of the action (2.1) at Λ, the effective action at Λ' must take the same form and differ only in the coupling values:

$$S_{\Lambda'}[\varphi_<] = \int d^d x \left[\frac{1}{2} Z_{\Lambda'} \left(\partial_\mu \varphi_<\right)^2 + \sum_i \Lambda'^{\,d-d_i} Z_{\Lambda'}^{n_i/2} \, g_i' \, \mathcal{O}_i(x) \right] , \tag{2.5}$$

where n_i represent the power of φ and its derivative contained in the monomial $\mathcal{O}_i$ and the *wavefunction renormalization* $Z_{\Lambda'}$ parametrizes quantum correction to the kinetic term. We can restore canonical normalization by rescaling

$$\varphi = Z_{\Lambda'}^{1/2} \varphi_<, \tag{2.6}$$

giving the effective action

$$S_{\Lambda'}[\varphi] = \int d^d x \left[\frac{1}{2} (\partial_\mu \varphi)^2 + \sum_i \Lambda'^{\,d-d_i} g_i' \, \mathcal{O}_i(x) \right]. \tag{2.7}$$

This integration of fast modes can be iterated, generating the *renormalization group* (RG) flow in an infinite-dimensional theory space of all possible couplings. By iteratively integrating over infinitesimally thin momentum shells, perturbative approximations can be employed with reduced violation of self-similarity in the RG flow, i.e. taking successive RG steps should amount to the same flow as one combined step [8]. Note that mathematically the renormalization group is actually a semigroup, as the elimination of small-wavelength fluctuations is not reversible and thus the existence of an inverse transformation is not guaranteed.

2.1.1 Beta Functions and Anomalous Dimensions

More quantitatively, the couplings $g_i(\Lambda)$ run in order to keep the partition function (2.2), and therefore the physics, unchanged. Defining an RG time as the logarithm of the cutoff Λ relative to some arbitrary scale μ:

$$t \coloneqq \log\left(\frac{\Lambda}{\mu}\right), \tag{2.8}$$

we obtain a *Gell-Mann-Low equation*

$$0 = \frac{\mathrm{d}}{\mathrm{d}t} Z = \left(\left.\frac{\partial}{\partial t}\right|_{g_i} + \sum_i \beta_i \frac{\partial}{\partial g_i} \right) Z, \tag{2.9}$$

where we have defined the *beta functions* as the rates at which the couplings run:

$$\beta_i(\{g_j\}) \coloneqq \frac{\partial g_i(\Lambda)}{\partial t} = (d_i - d) g_i + \text{quantum corrections}. \tag{2.10}$$

The first scaling term simply reflects the power-counting dimension of the (dimensionful) coupling, but this may be altered by quantum corrections generally involving all couplings g_j.

The Gell-Mann-Low equation (2.9) can be generalized to the n-point correlation functions

$$G_\Lambda^{(n)}(x_1, \ldots, x_n) = \frac{1}{Z} \int_\Lambda \mathcal{D}\varphi \, \varphi(x_1) \ldots \varphi(x_n) \exp\left[-S_\Lambda[\varphi]\right], \tag{2.11}$$

which are the vacuum expectation values of products of fields evaluated at different spacetime points. The scale dependence then enters through the wavefunction renormalization Z_Λ of the fields in (2.11):

$$Z_\Lambda^{-n/2}\, G_\Lambda^{(n)}(x_1,\ldots,x_n) = Z_{\Lambda'}^{-n/2}\, G_{\Lambda'}^{(n)}(x_1,\ldots,x_n). \tag{2.12}$$

Taking the scale derivative leads to the Gell-Mann-Low equation

$$0 = \left(\left.\frac{\partial}{\partial t}\right|_{g_i} + \sum_i \beta_i \frac{\partial}{\partial g_i} + n\gamma \right) G_\Lambda^{(n)}(x_1,\ldots,x_n), \tag{2.13}$$

where we have defined the *anomalous dimension*

$$\gamma = -\frac{1}{2}\frac{\partial \ln Z_\Lambda}{\partial t}. \tag{2.14}$$

In the next section 2.1.2, we will see the physical interpretation of this quantity.

2.1.2 Fixed Points, Critical Exponents and Universality

We now focus on special theories where the couplings have been tuned such that all the beta functions $\beta_i(\{g_j^*\}) = 0$ vanish. Such fixed points are left invariant under the RG flow, corresponding to scale-invariant theories where the correlation functions take a particularly simple form. In particular, the Gell-Mann-Low equation (2.13) simplifies to

$$\left(\Lambda\frac{\partial}{\partial \Lambda} + 2\gamma^* \right) G_\Lambda^{(2)}(x,y) = 0, \tag{2.15}$$

where $\gamma^* := \gamma(\{g_i^*\})$ is the anomalous dimension at the fixed point g_i^*. This implies a scale dependence of the form $G_\Lambda^{(2)} \sim \Lambda^{-2\gamma^*}$. Furthermore, dimensional analysis and Lorentz invariance imply that

$$G_\Lambda^{(2)}(x-y) = \Lambda^{d-2}\, g(\Lambda|x-y|, g_i^*) = \frac{f(g_i^*)\,\Lambda^{d-2}}{(\Lambda|x-y|)^{d-2+2\gamma^*}}. \tag{2.16}$$

The power-law scaling signifies a divergence of the correlation length (which would otherwise appear in the additional exponential decay of correlations), as well as a deviation from the classical scaling due to the anomalous dimension γ^*. In fact, under modest assumptions including unitarity and Poincare invariance [11], all known scale-invariant QFTs are further invariant under an enhanced group of angle-preserving conformal transformations. While a proof of this equivalence exists in $d = 2$ due to Zamolodchikov and Polchinski [12, 13], it remains a conjecture in $d = 4$ beyond perturbation theory. Nonetheless, in such *conformal field theories*, the n-point functions are completely constrained up to a set of parameters.

A trivial example of a fixed point is the *Gaussian fixed point*, where all couplings $g_i^* = 0$ vanish. The absence of interactions in this free theory generates no new terms upon integration of fast modes. In addition, there may be non-trivial fixed points where quantum corrections precisely cancel the canonical scaling in (2.10).

We can further linearize the RG flow in the vicinity of a fixed point:

$$\partial_t g_i = B_{ij}(g_j - g_j^*) + \mathcal{O}\left((g_i - g_i^*)^2\right), \tag{2.17}$$

where B_{ij} is the *stability matrix.* Its eigenvectors correspond to particular linear combinations of couplings which are not mixed by the linearized RG transformation. The corresponding (negatives of) eigenvalues are the *critical exponents* θ_i. As discussed in (2.10), we expect this to classically take the value of $\theta_i = d - d_i$ for an operator with power-counting dimension d_i. Quantum corrections such as the anomalous dimension γ_i further contribute to the actual scaling dimension Δ_i, such that $\theta_i = d - \Delta_i$. In this eigenbasis, (2.17) is then solved by the power law

$$\partial_t \delta g_i = -\theta_i\, \delta g_i \implies \delta g_i(\Lambda) \sim \Lambda^{-\theta_i}\, \delta g_{0i}, \tag{2.18}$$

where $\delta g_i = g_i - g_i^*$ is the deviation from the fixed point g_i^*. We can conclude that for a fixed spacetime dimension d, operators $\mathcal{O}_i$ with scaling dimensions $\Delta_i > d$ (negative critical exponents $\theta_i < 0$) are *irrelevant* to the long-range physics, as deviations along these directions are suppressed in the IR. As such, we need not consider arbitrarily complicated operators with many powers or derivatives of fields. In fact, the fixed point lies on an infinite-dimensional infrared (IR) *critical manifold/surface* consisting of all points which are attracted towards the fixed point in the IR. The irrelevant operators at each fixed point then span the corresponding tangent plane.

By contrast, operators with scaling dimensions $\Delta_i < d$ (positive critical exponents $\theta_i > 0$) are *relevant* as deformations in such directions, i.e. away from the critical manifold, drive the RG flow further away from the fixed point (Figure 2.1). For a fixed spacetime dimension, there are only finitely many such operators with sufficiently few powers or derivatives of fields. In the interest of asymptotic safety, the number of relevant directions corresponds to the number n_{phys} of physical parameters which must be fine-tuned so as to connect a particular long-range physical scenario with the UV fixed point in question. While a large n_{phys} accommodates a higher dimensional set of UV complete theories, this comes at the expense of predictability. On the other hand, irrelevant couplings can often[1] be eliminated from the physical description by a redefinition of the initial relevant couplings [7].

A QFT containing both relevant and irrelevant operators may happen to lie in the vicinity of a critical surface. The suppression of irrelevant operators and growth of relevant ones then focus the RG flow towards a *renormalized trajectory* emanating from a fixed point, largely independent of the initial conditions (Figure 2.1). This is the origin of *universality*, where seemingly unrelated phenomena exhibit the same power-law scaling close to *critical points*. For example, despite fundamental microscopic differences between the celebrated Ising model and the liquid-gas phase transition, they both belong to the same *universality class* [15], characterized by the critical exponents of their shared IR fixed point[2].

[1] However, there exist *dangerously irrelevant* systems where irrelevant couplings appear in a singular fashion in scaling relations, e.g. φ^4 theory above $d = 4$ [7].

[2] For completeness, we acknowledge that in addition to isolated fixed points, there exist RG flows with more exotic global topologies, for example including a one- or higher-dimensional continuum of fixed points (XY model in $d = 2$), recurring limit cycles (three-body bound states of $U(1)$ bosons and $SU(3)$ fermions) or even chaotic flows without fixed points [7].

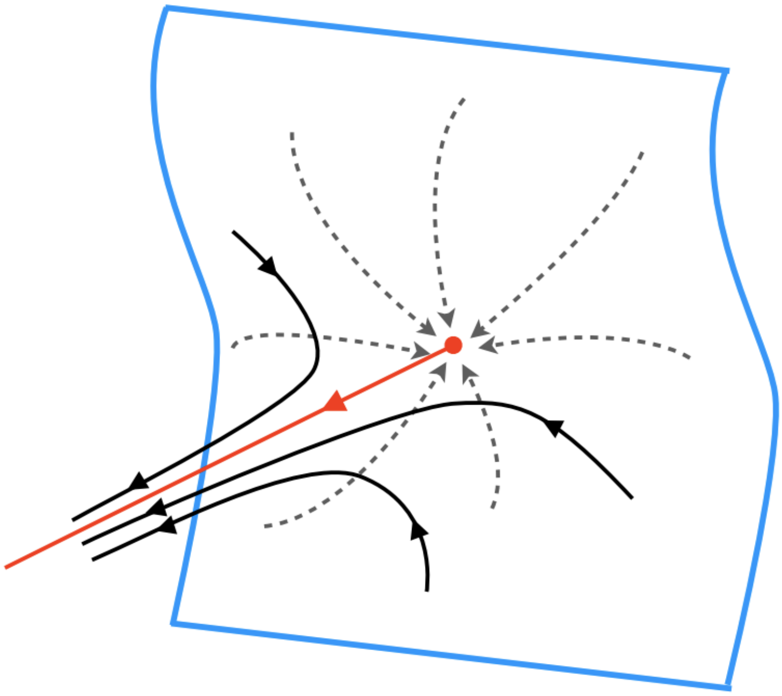

Figure 2.1: IR Critical manifold (blue) consisting of all RG trajectories (dashed) in theory space which are attracted towards the fixed point in the IR. Any deformation (black) from the critical surface results in focusing towards a renormalized trajectory (red). Thus, depending only on a handful of relevant couplings, all theories in the same universality class have the same IR limit. Image taken from [14].

The last case consists of marginal operators with $\Delta_i = d$ (vanishing critical exponents $\theta_i = 0$). Since the eigenvalues of the stability matrix then vanish, we must consider higher-order terms in the beta function (2.17), which give rise to weak logarithmic scale dependences. This allows classification as *marginally relevant/irrelevant*, with the same qualitative implications as the aforementioned relevant/irrelevant operators. As an example, we consider the Gaussian fixed point (where the anomalous dimension vanishes) for a scalar field φ with a discrete $\mathbb{Z}_2$ symmetry, which has mass dimension $(d-2)/2$ in spacetime dimension d. The mass term φ^2 remains relevant for all d. In $d = 4$, higher powers than φ^4 are irrelevant to the macroscopic physics. φ^4 becomes relevant for $d < 4$, but it's only at $d = 3$ that φ^6 becomes marginal.

While in $d = 4$ the quartic interaction of scalar fields and the gauge coupling in quantum electrodynamics (QED) are both dimensionless, one-loop calculations show that they are in fact marginally irrelevant [16]:

$$\beta_{\varphi^4}(\lambda) = \frac{3\lambda^2}{16\pi^2} \qquad\qquad \beta_{QED}(e) = \frac{e^3}{12\pi^2}. \tag{2.19}$$

The breakdown of classical scale invariance by quantum fluctuations in the screening vacua of massless φ^4 theory and QED are examples of *trace anomalies* [16].

2.1.3 Landau Pole

Before we discuss the ramifications of the QED beta function (2.19), we first consider the case of a single coupling (as in our single channel approximation in Section 3.2.2) and discuss possible behaviours of the perturbative beta function. To lowest order, this is determined by the sign of the coefficient a of the beta function $\beta(g) \sim a g^n$.

1. For $\beta(g) > 0$, the coupling $g(\Lambda)$ increases with scale Λ. Of course, this eventually runs into the large-coupling regime where perturbation theory breaks down. However, if g continues to grow under the non-perturbative beta function, it can diverge asymptotically as $\Lambda \to \infty$ or even at a finite value of Λ, which is known as a Landau pole. This phenomenon is further discussed below for the case of QED. In the IR, the coupling is attracted towards the Gaussian fixed point corresponding to a free theory.

2. For $\beta(g) < 0$, the coupling $g(\Lambda)$ instead decreases with scale Λ. The RG flow is repelled from the Gaussian fixed point in the UV and becomes non-perturbative in the IR. Such *asymptotic freedom* is a distinctive feature of Yang-Mills theories such as QCD.

3. If $\beta(g) = 0$ for all g, the theory is conformal and finite for all values of the coupling. An example is the highly symmetric $\mathcal{N} = 4$ Super-Yang-Mills theory, which features prominently in the AdS/CFT correspondence.

Considering higher-order terms, the beta function may change signs at non-trivial fixed points. For example, $\beta(g)$ may be positive to lowest order but then vanish at a non-trivial UV fixed point g^*, as shown in Figure 2.2(a). Alternatively, $\beta(g)$ may be negative for small g and vanish at a non-trivial IR fixed point (Figure 2.2(b)). This is observed in QED_3 as the gauge coupling becomes relevant, and in φ^4 theory as the Wilson-Fisher fixed point for $d < 4$. While the exact beta function may depend on the specific choice of regularization scheme, its slope at each fixed point represents a universal quantity, as the negative of a critical exponent.

Turning to QED, integration of (2.19) reveals that the gauge coupling e runs logarithmically at the one-loop level:

$$\frac{1}{e^2(\Lambda')} - \frac{1}{e^2(\Lambda)} = \frac{1}{6\pi^2} \ln \frac{\Lambda}{\Lambda'} \implies e^2(\Lambda) = \frac{6\pi^2}{\ln \Lambda_{\text{Landau}}/\Lambda}, \tag{2.20}$$

where as before the Landau pole Λ_{Landau} is the finite scale at which the gauge coupling diverges. To estimate the scale of the Landau pole, recall that the celebrated fine structure constant has been accurately measured at the scale of the electron mass $m_e = 511$ keV [1, 2]:

$$\alpha = \frac{e^2(m_e)}{4\pi} = \frac{1}{137} \implies \Lambda_{\text{Landau}} \approx 10^{286}\,\text{eV}. \tag{2.21}$$

Phenomenologically, this far exceeds the electroweak scale ~ 246 GeV where the electroweak $SU(2) \times U(1)_Y$ gauge group is spontaneously broken by the Higgs mechanism to the $U(1)_{\text{em}}$ symmetry of QED. This non-Abelian gauge theory modifies the QED beta function (2.19) before the purported Landau pole [17]. Similarly, the weak hypercharge

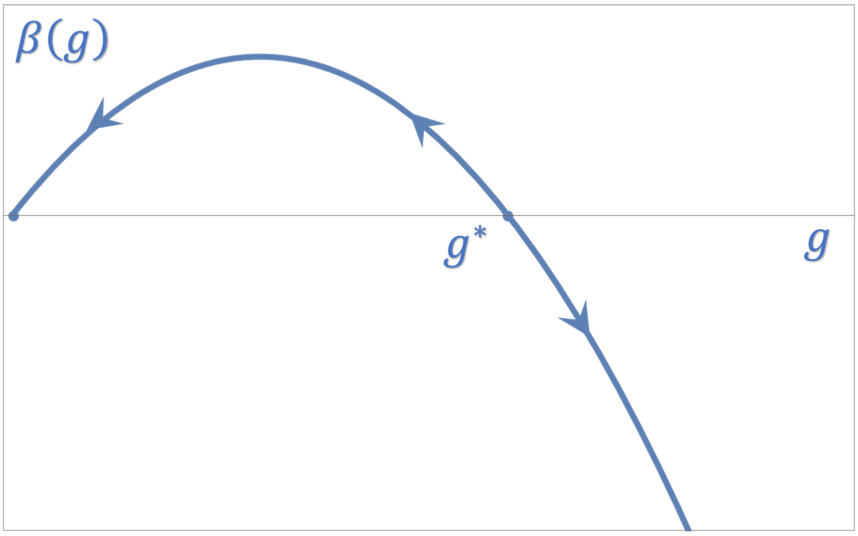

(a) Initially positive beta function $\beta(g)$ which vanishes at a UV fixed point.

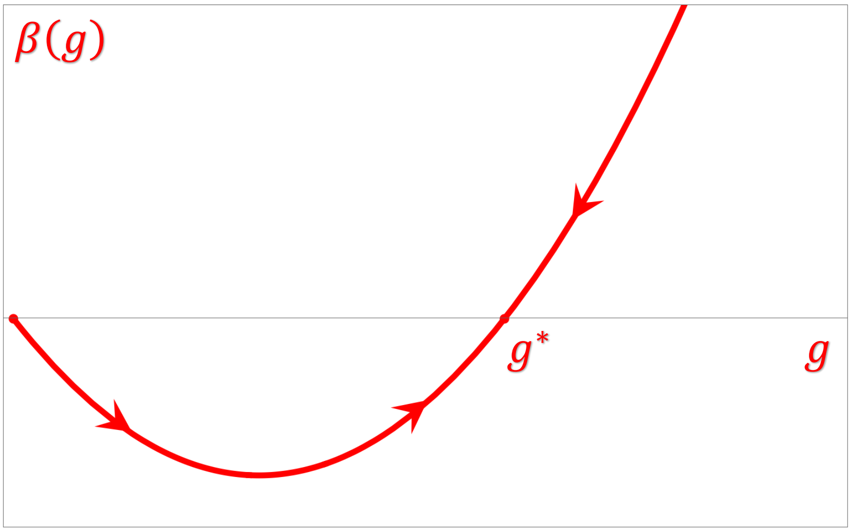

(b) Initially negative beta function $\beta(g)$ which vanishes at a IR fixed point.

Figure 2.2: Possible behaviors for the beta function when taking into account next-to-leading-order contributions in perturbation theory. The arrows show the direction of the RG flow towards the IR.

$U(1)_Y$ factor is expected to exhibit a Landau pole at 10^{40} GeV, which accommodates possible quantum gravitational physics at the Planck scale of 10^{19} GeV [3].

Based on this analysis of the perturbative beta function (2.19), it would seem that the Landau pole inconsistency of pure QED can only be avoided by considering a free theory in the IR (see Figure 2.3). This phenomenon is known as the (perturbative) triviality of QED. To clarify whether the Landau pole represents more than an artefact of perturbation theory, we review the non-perturbative techniques of the functional renormalization group.

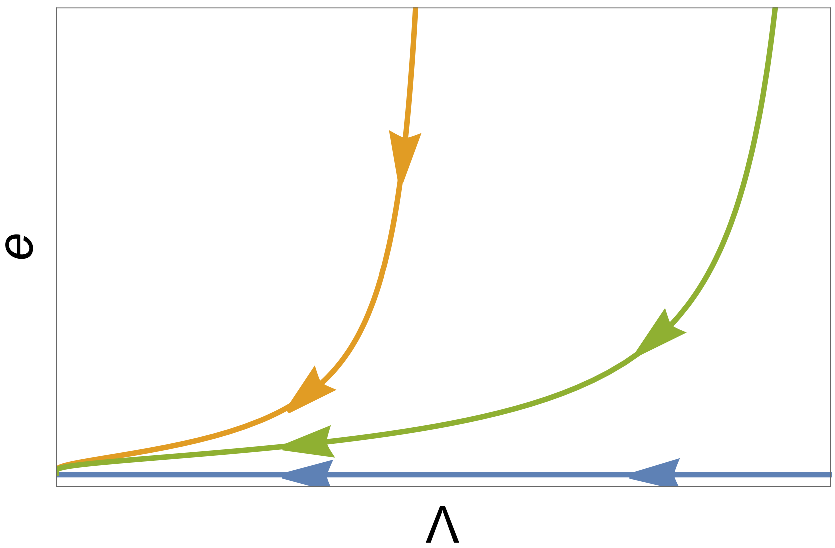

Figure 2.3: QED in $d = 4$ is perturbatively trivial. The perturbative beta function (2.19) predicts that the gauge coupling diverges at a finite Landau pole, as in (2.20). As such, perturbative QED admits a well-defined continuum limit only as a free theory with $e = 0$. Arrows indicate flows towards the Gaussian fixed point in the IR.

2.2 Functional Renormalization

There exist various implementations of the exact renormalization group (ERG), such as that due to Polchinski, which introduces a smooth UV cutoff to the Wilsonian action describing the slow modes yet to be integrated [8, 18, 19]. Here we focus on a mathematically equivalent formulation by Wetterich, which instead revolves around the 1PI effective action for the fast modes above a smooth IR cutoff. As such, we begin with a recapitulation of the functional formulation of QFT.

2.2.1 Generating Functionals

From the Wightman reconstruction theorem [20, 21], a QFT can be constructed from all the correlation functions or Green functions

$$\langle \varphi(x_1) \dots \varphi(x_n) \rangle = \frac{1}{Z} \int_\Lambda \mathcal{D}\varphi \, \varphi(x_1) \dots \varphi(x_n) \exp\left[-S[\varphi]\right], \tag{2.22}$$

as defined in (2.11). After the Wick rotation, the action plays an analogous role to the free energy in a statistical field theory, weighting the contribution of each field configuration in the functional integral $\int \mathcal{D}\varphi$.

We can further introduce a source field $J(x)$ to define the generating functional

$$Z[J] = \int \mathcal{D}\varphi \, \exp\left[-S[\varphi] + \int J\varphi\right] \equiv \exp\left[W[J]\right], \tag{2.23}$$

where $\int J\varphi = \int_x J(x)\varphi(x)$. In terms of the generating functional (2.23), all correlation functions can be computed by taking functional derivatives

$$\langle\varphi(x_1)\varphi(x_2)\dots\varphi(x_n)\rangle = \frac{1}{Z[0]}\frac{\delta^n}{\delta J(x_1)\dots\delta J(x_n)}Z[J]\Big|_{J=0}. \tag{2.24}$$

Similarly, the Schwinger functional $W[J] = \log Z[J]$ represents the generating functional of connected correlation functions. For example, the second derivative gives

$$\begin{aligned}\frac{\delta^2 W[J]}{\delta J(x)\delta J(y)}\bigg|_{J=0} &= \frac{1}{Z[0]}\int \mathcal{D}\varphi\,\varphi(x)\varphi(y)e^{-S[\varphi]} - \frac{1}{Z[0]^2}\int \mathcal{D}\varphi\,\varphi(x)e^{-S[\varphi]}\int \mathcal{D}\varphi\,\varphi(y)e^{-S[\varphi]} \\ &= \langle\varphi(x)\varphi(y)\rangle - \langle\varphi(x)\rangle\langle\varphi(y)\rangle \equiv G(x,y),\end{aligned} \tag{2.25}$$

which is the full non-perturbative propagator. Analogous calculations apply for the higher n-point connected functions.

In an analogy to statistical field theory, $\varphi(x)$ may represent the fluctuating spin field of an Ising ferromagnet and $J(x)$ an external magnetic field. The Schwinger functional $W[J] = \log Z[J]$ would be analogous to the Helmholtz free energy. A natural next step is then to perform a Legendre transform with respect to the source field $J(x)$ and define the *effective action*

$$\Gamma[\phi] \equiv \sup_J \left(\int J\phi - W[J]\right), \tag{2.26}$$

where the supremum ensures convexity of $\Gamma[\phi]$.

To interpret the new field ϕ, we note that at the supremum value of $J = J_{\text{sup}}[\phi]$,

$$\begin{aligned}&\frac{\delta}{\delta J(x)}\left(\int J\phi - W[J]\right) = 0 \\ \implies\ &\phi(x) = \frac{\delta W[J]}{\delta J(x)} = \frac{1}{Z[J]}\frac{\delta Z[J]}{\delta J(x)} \overset{(2.24)}{=} \langle\varphi(x)\rangle_J.\end{aligned} \tag{2.27}$$

Thus, the so-called classical field $\phi(x)$ is the expectation value of the fluctuating quantum field $\varphi(x)$ in the presence of the source field $J(x)$, analogous to the magnetization being the thermal average of the local spin field in the presence of an external magnetic field.

The utility of the effective action $\Gamma[\phi]$ can be seen be taking its functional derivative

$$\frac{\delta\Gamma[\phi]}{\delta\phi(x)} = J(x) + \int_y \left(\frac{\delta J(y)}{\delta\phi(x)}\phi(y) - \frac{\delta W[J]}{\delta J(y)}\frac{\delta J(y)}{\delta\phi(x)}\right) \overset{(2.27)}{=} J(x). \tag{2.28}$$

Setting $J(x) = 0$, we obtain the quantum equation of motion analogous to the classical principle of least action $\delta S/\delta\varphi = 0$. In particular, stationary points of the effective action correspond to vacuum states $\langle\varphi(x)\rangle$ in the absence of a source field. Much like $Z[J]$ and $W[J]$, $\Gamma[\phi]$ is a generating functional, but of one-particle-irreducible (1PI) correlation functions. These are represented by Feynman diagrams which cannot be disconnected into two non-trivial pieces by removing one line [16].

Substituting the equation of motion (2.28) into the definition (2.26) and performing a change of variable $\varphi \to \varphi + \phi$ under the functional integral, we obtain the expression

$$e^{-\Gamma[\phi]} = \int_\Lambda \mathcal{D}\varphi \, \exp\left(-S[\varphi + \phi] + \frac{\delta\Gamma[\phi]}{\delta\phi}\varphi\right) \tag{2.29}$$

for the effective action $\Gamma[\phi]$. Exact solutions of this nonlinear first-order functional differential equation are known only for special cases, thus necessitating approximation schemes. One approach proceeds by a vertex expansion of the effective action $\Gamma[\phi]$ in terms of 1PI vertices $\Gamma^{(n)}$:

$$\Gamma[\phi] = \sum_{i=0}^{\infty} \frac{1}{n!} \int d^D x_1 \dots d^D x_n \, \Gamma^{(n)}(x_1, \dots, x_n) \, \phi(x_1) \dots \phi(x_n). \tag{2.30}$$

Substitution of this series into equation (2.29) and equating the coefficients of corresponding monomials yields an infinite hierarchy of integro-differential equations known as *Dyson-Schwinger equations*. Approximate solutions by truncation have been found in the context of gauge theories [22, 23, 24].

2.2.2 Effective Average Action

Yet another approximation scheme involving the effective action (2.26) directly rather than the individual n-point functions $\Gamma^{(n)}$ is provided by the *functional renormalization group* (FRG), inspired by the Wilsonian idea of integrating over fluctuations in successive momentum shells rather than all at once [25, 26]. This is implemented by introducing an *effective average action* Γ_k which interpolates between the classical bare action S and the full quantum effective action Γ as we integrate over momentum shells centered at k:

$$\Gamma_{k\to\Lambda} = S + \text{const.} \qquad \Gamma_{k\to 0} = \Gamma. \tag{2.31}$$

To construct the effective average action Γ_k, we add an IR regulator term

$$\Delta S_k[\varphi] = \frac{1}{2} \int_p \varphi(-p) R_k(p) \varphi(p) \tag{2.32}$$

to the generating functional (2.23):

$$Z_k[J] = \int_\Lambda \mathcal{D}\varphi \, \exp\left[-S[\varphi] - \Delta S_k[\varphi] + \int J\varphi\right] \equiv \exp\left[W_k[J]\right]. \tag{2.33}$$

As a quadratic term in φ, the regulator (2.32) acts as a momentum-dependent mass term. In particular, the regulator function $R_k(p)$ should approach the limit

$$\lim_{p^2/k^2 \to 0} R_k(p) > 0 \tag{2.34}$$

such that IR fluctuations with momentum p much smaller than the IR cutoff k are screened. For example, the regulator may asymptotically adopt a constant value $R_k \to k^2$ and behave as a mass $m^2 \sim k^2$. To ensure that the boundary conditions (2.31) are satisfied, we require the limit

$$\lim_{k^2/p^2 \to 0} R_k(p) = 0 \tag{2.35}$$

as the cutoff $k \to 0$ is sent towards the IR. The vanishing regulator recovers the full generating functional $Z_{k\to 0}[J] = Z[J]$. In the opposite UV limit,

$$\lim_{k^2 \to \Lambda \to \infty} R_k(p) \to \infty \tag{2.36}$$

such that the only contribution to the functional integral (2.33) comes from the stationary point of the exponent, i.e. the classical field configuration. A plot of a typical regulator $R_k(p)$ satisfying these three conditions is shown in Figure 2.4. The form of the regulator is often expressed in terms of a dimensionless shape function $r(x)$ of dimensionless momentum:

$$\text{Boson: } R_k(p) = p^2 r_B(p^2/k^2) \qquad \text{Fermion: } R_k(p) = \not{p}\, r_F(p^2/k^2), \tag{2.37}$$

with a natural generalization to fermions which perserves chiral symmetry [27]. To compute

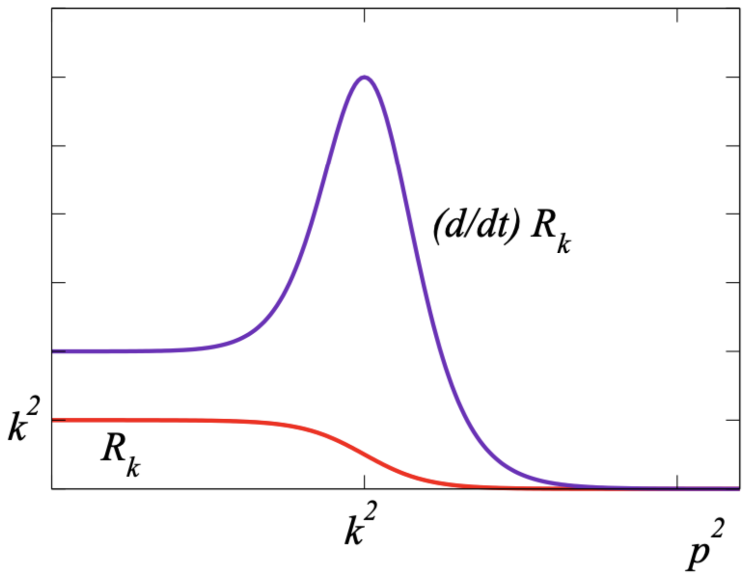

Figure 2.4: Shape of a typical regulator $R_k(p^2)$ (red), which screens IR fluctuations ($p^2 < k^2$) in a mass-like fashion. Its derivative $\partial_t R_k(p^2)$ (violet) is supported mainly in a momentum shell centred around the cutoff k^2. Image taken from [25].

the flow of the generating functional $W_k[J]$, we define an RG time as in (2.8):

$$t = \log\left(\frac{k}{\Lambda}\right). \tag{2.38}$$

Keeping the source J independent of k for the time being,

$$\begin{aligned}\partial_t W_k[J]|_J &= -\frac{1}{2Z_k[J]}\int_\Lambda \mathcal{D}\varphi \int_p \varphi(-p)\partial_t R_k(p)\varphi(p) \exp\left[-S[\varphi] - \Delta S_k[\varphi] + \int J\varphi\right] \\ &= -\frac{1}{2}\int_p \partial_t R_k(p)\, G_k(p) - \partial_t \Delta S_k[\phi], \end{aligned} \tag{2.39}$$

where the first term would pick up a minus sign in the fermionic case from commuting the Grassman-valued fields. Analogous to (2.25),

$$G_k(p) = \frac{\delta^2 W_k[J]}{\delta J(p)\delta J(-p)} = \langle\varphi(p)\varphi(-p)\rangle - \langle\varphi(p)\rangle\langle\varphi(-p)\rangle \tag{2.40}$$

denotes the full connected propagator in the presence of the cutoff k.

We now define the effective average action Γ_k as the modified Legendre transform

$$\Gamma_k[\phi] \equiv \sup_J \left(\int J\phi - W_k[J]\right) - \Delta S_k[\phi], \tag{2.41}$$

where any non-convexity introduced by the regulator $\Delta S_k[\phi]$ must vanish as $k \to 0$. As in (2.27) in the absence of the regulator,

$$\phi(x) = \frac{\delta W_k[J]}{\delta J(x)} = \langle\varphi(x)\rangle_J \tag{2.42}$$

and so the classical field ϕ remains as the expectation value of the quantum field φ in the presence of the now k-dependent source J. But the quantum equation of motion (2.28) is modified to

$$\frac{\delta\Gamma[\phi]}{\delta\phi(x)} + (R_k\phi)(x) = J(x). \tag{2.43}$$

The analogue of equation (2.29) becomes

$$e^{-\Gamma_k[\phi]} = \int_\Lambda \mathcal{D}\varphi \,\exp\left(-S[\varphi+\phi] - \Delta S_k[\varphi] + \frac{\delta\Gamma_k[\phi]}{\delta\phi}\varphi\right). \tag{2.44}$$

For $k \to \infty$, the divergent regulator tends toward the delta functional $\delta[\varphi]$ and suppresses all fluctuations in the functional integral, explicitly showing that the desired boundary conditions (2.31) for the effective average action $\Gamma_k[\phi]$ are fulfilled.

2.2.3 Wetterich Equation

Taking the functional derivative of (2.43) yields the operator equation

$$\frac{\delta^2\Gamma[\phi]}{\delta\phi(x)\delta\phi(y)} + R_k(x,y) = \frac{\delta J(x)}{\delta\phi(y)}, \tag{2.45}$$

where for the case of Grassman-valued fermionic fields, the two functional derivatives are to act from opposite sides. On the other hand, differentiating (2.42) gives an expression for the inverse:

$$\frac{\delta\phi(y)}{\delta J(x')} = \frac{\delta^2 W_k[J]}{\delta J(x')\delta J(y)} \equiv G_k(x'-y). \tag{2.46}$$

Composing equations (2.45) and (2.46) implies

$$\delta(x-x') = \frac{\delta J(x)}{\delta J(x')} = \int_y \frac{\delta J(x)}{\delta\phi(y)}\frac{\delta\phi(y)}{\delta J(x')} = \int_y \left(\Gamma_k^{(2)}[\phi] + R_k\right)(x,y) G_k(y-x'), \tag{2.47}$$

where we denote the functional derivatives of the effective average action

$$\Gamma_k^{(n)}[\phi](x_1,\dots,x_n) = \frac{\delta^n \Gamma_k[\phi]}{\delta\phi(x_1)\dots\delta\phi(x_n)}. \tag{2.48}$$

In operator notation, we can write the inverse propagator as

$$G_k^{-1} = \Gamma_k^{(2)} + R_k. \tag{2.49}$$

With these results, we now derive the *Wetterich equation* for the effective average action [28]. Taking ϕ to be a k-independent field, the supremum value of the source $J \equiv J_{\sup}[\phi]$ in definition (2.41) must then depend on k:

$$\begin{aligned}
\partial_t \Gamma_k[\phi] &= -\partial_t W_k[J]|_\phi + \int (\partial_t J)\,\phi - \partial_t \Delta S_k[\phi] \\
&= -\partial_t W_k[J]|_J - \partial_t \Delta S_k[\phi] \\
&\overset{(2.39)}{=} \frac{1}{2}\int_p \partial_t R_k(p)\, G_k(p) \\
&\overset{(2.49)}{=} \frac{1}{2}\mathrm{Tr}\left[\partial_t R_k \left(\Gamma_k^{(2)}[\phi] + R_k\right)^{-1}\right].
\end{aligned} \tag{2.50}$$

In a theory with more complicated field structures, we would take a supertrace STr over real or momentum space as well as any Lorentz or internal indices such as Dirac or flavor, with an extra minus sign in the fermionic sector. Due to the quadratic form of the regulator (2.32), the Wetterich equation has a one-loop structure in the exact propagator [29], as shown in Figure 2.5. This avoids the technical difficulties associated with overlapping loop integrals in perturbation theory [16] or the Dyson-Schwinger equations.

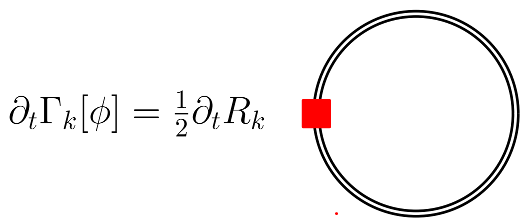

Figure 2.5: One-loop form of the Wetterich equation, consisting of the full propagator $G_k(p)$ and the derivative insertion $\partial_t R_k$.

While R_k serves as an IR regulator in the denominator of (2.50), its inserted derivative $\partial_t R_k$ acts as a UV regulator, since a typical regulator is mainly supported over a momentum shell at $p^2 = k^2$ (Figure 2.4). Though the UV cutoff Λ appeared in the functional definitions (2.33) and (2.44), the flow equations themselves are oblivious to the presence of Λ. While we have derived the Wetterich equation from the more familiar functional formalism of QFT, it is equally justified to define the theory by the bare action and its flow towards the IR, subject to symmetry constraints [25]. This is the perspective we will adopt in Chapter 3. In light of this, we can search for UV completions by sending $k \to \infty$ without regard for Λ. The absence of Λ also ensures that the self-similarity of the RG flow is preserved, even when truncated in a derivative expansion (a common approximation to be discussed later in this section) [8].

As shown in Figure 2.6, the arbitrary choice of regulator may affect the RG trajectory, but the boundary conditions (2.31) ensure that the endpoints remain the same. We should also note that in gauge theories, the appearance of the IR cutoff k inevitably violates gauge invariance. Such complications can be sidestepped by introducing a non-dynamical background field such that the theory is invariant under the enlarged group of gauge transformations and only removing the auxiliary field at the end of the computation [25].

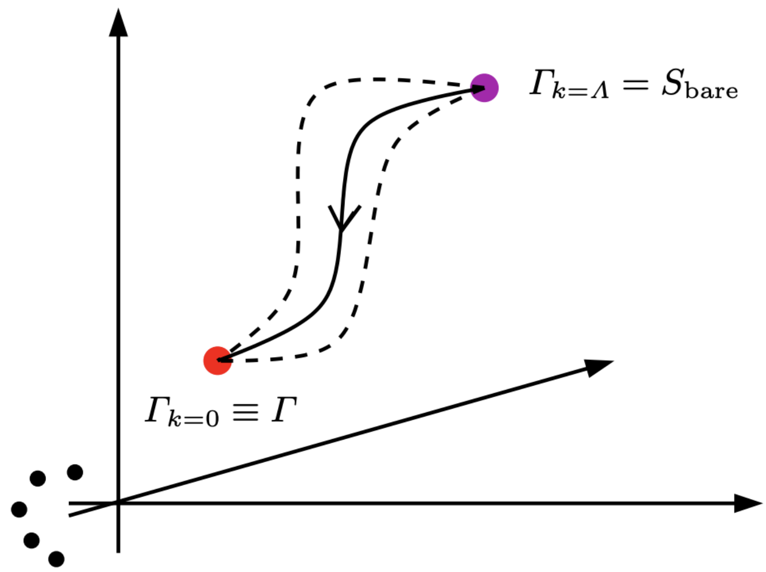

Figure 2.6: The specific RG trajectory in theory space depends on the choice of regulator, but the endpoints do not, since the boundary conditions (2.31) fix them to equal the bare action (violet) in the UV and the full effective action (red) in the IR. Image taken from [25].

As a further sanity check, perturbation theory at the leading-order can be recovered by a loop expansion of the effective average action

$$\Gamma_k = S + \hbar \Gamma_k^{\text{1-loop}} + \mathcal{O}(\hbar^2). \tag{2.51}$$

To leading order, the Wetterich equation (2.50) then becomes

$$\partial_t \Gamma_k^{\text{1-loop}} = \frac{1}{2} \mathrm{STr} \left[\partial_t R_k \left(S^{(2)} + R_k \right)^{-1} \right] = \frac{1}{2} \partial_t \left[\mathrm{STr} \ln \left(S^{(2)} + R_k \right) \right]. \tag{2.52}$$

Taking the limit $k \to 0$ where (2.35) applies, we obtain the usual one-loop effective action

$$\Gamma = S + \frac{\hbar}{2} \operatorname{STr} \ln S^{(2)} + \text{const.} \tag{2.53}$$

Compared to (2.29), the Wetterich equation is unburdened by the additional complication of a functional integral. Nevertheless, the solution of this functional differential equation is mathematically nontrivial as it corresponds to an infinite tower of coupled nonlinear partial differential equations [30]. The strength of functional RG techniques thereby lies in the diversity of systematic approximation schemes. One possibility is to perform a vertex expansion as in (2.30) and obtain flow equations for the 1PI vertices $\Gamma_k^{(n)}$ as they interpolate between the bare and fully dressed vertices, somewhat resembling the Schwinger-Dyson equations [25].

The alternative approach which we will employ is to expand the effective average action in terms of operators with increasing derivative order or canonical dimension. The infinite hierarchy of equations can then be closed by a systematic and consistent truncation which retains all terms of a given order. The choice of a suitable truncation is generally informed only by an understanding of the relevant physical degrees of freedom, though truncation errors need to be estimated. While this can be achieved by a somewhat involved examination of higher-order terms, a convenient check is provided by the spurious regulator dependence introduced by the truncation.

Furthermore, we ought to choose *optimized* regulators such that the RG flow takes the "shortest" path in theory space and converges most rapidly towards the true, scheme-independent values of physical observables [31, 32, 33, 34, 35]. In particular, they can be chosen to maximize the mass gap C of the full inverse propagator, defined as

$$\min_{p^2 \geq 0} \left(\frac{\delta^2 \Gamma_k}{\delta\phi(p)\delta\phi(-p)} + R_k(p) \right) \equiv C k^2. \tag{2.54}$$

This ensures effective IR regularization of singular zero modes and optimizes the regularity of the RG flow kernel, thus enhancing robustness against approximations [36, 37].

2.3 Chiral Symmetry Breaking

We are now ready to apply the techniques of functional RG to asymptotic safety of QED, but as one final piece of preparation, let us review the phenomenon of chiral symmetry breaking and the associated dynamic generation of mass. Consider the QED action for N_f flavors of massless Dirac fermions ψ^a minimally coupled to a $U(1)$ gauge field A_μ:

$$S = \int_x \bar{\psi}^a i \not{D}[A] \psi^a + \frac{1}{4} F_{\mu\nu} F^{\mu\nu}, \tag{2.55}$$

where $a = 1, \ldots, N_f$ labels the fermion flavors and is implicitly summed over. $D_\mu[A] = \partial_\mu - ieA_\mu$ is the gauge covariant derivative. Our following discussion also applies to non-Abelian gauge theories such as *quantum chromodynamics* (QCD), where the fermions carry an extra color index transforming in the fundamental representation of an $SU(3)$ gauge group and A_μ represents some element of the corresponding Lie algebra.

In the chiral representation which exists only in even spacetime dimensions (explicitly given in Appendix 6), we can decompose the fermionic term in terms of left-handed and right-handed Weyl spinors ψ_L^a and ψ_R^a, respectively:

$$\bar{\psi}^a \not{D}[A]\psi^a = i\psi_R^{a\dagger}\sigma_\mu D^\mu \psi_R^a + i\psi_L^{a\dagger}\bar{\sigma}_\mu D^\mu \psi_L^a, \tag{2.56}$$

where the Pauli matrices are packaged into the convenient notation $\sigma^\mu = (1, \sigma^i)$, $\bar{\sigma}^\mu = (1, -\sigma^i)$. Here we have used the Euclidean Dirac matrices, though the discussion proceeds similarly for Minkowski spacetime. We see that the action (2.55) is classically invariant under a global $U(N_f)_L \times U(N_f)_R$ symmetry, which allows independent unitary transformations of the two chiralities in flavor space:

$$U(N_f)_L : \psi_L^a \mapsto L^{ab}\psi_L^b, \qquad U(N_f)_R : \psi_R^a \mapsto R^{ab}\psi_R^b. \tag{2.57}$$

We can factorize this symmetry group and discuss the fate of each part upon quantization:

$$U(N_f)_L \times U(N_f)_R = U(1)_V \times U(1)_A \times SU(N_f)_L \times SU(N_f)_R, \tag{2.58}$$

The Abelian $U(1)_V$ vector symmetry consists of overall phase rotations of both handedness

$$U(1)_V : \psi^a \mapsto e^{i\alpha}\psi^a, \qquad \text{Noether current: } j_\mu = \bar{\psi}^a \gamma_\mu \psi^a. \tag{2.59}$$

This preserved symmetry gives rise to the conservation of fermions of either handedness, known as baryon number in the context of QCD. The other Abelian $U(1)_A$ axial symmetry transforms the two chiralities with opposite phases

$$U(1)_A : \psi^a \mapsto e^{i\beta\gamma_5}\psi^a, \qquad \text{Noether current: } j_{5\mu} = \bar{\psi}^a \gamma_\mu \gamma_5 \psi^a. \tag{2.60}$$

While this would result in conservation of left- and right-handed fermions separately, the axial symmetry suffers the *Adler-Bell-Jackiw anomaly* in the presence of a gauge field [38, 39], as it is only a symmetry of the classical action (2.55), but not of the measure in the functional integral.

Phenomenologically, the remaining non-Abelian chiral symmetry $SU(N_f)_L \times SU(N_f)_R$ is explicitly broken by the non-zero quark masses of QCD. Nonetheless, it may survive as an approximate symmetry when only considering the u, d and perhaps s quarks, which have relatively small masses compared to the QCD scale of ~ 300 MeV [40]. However, the Lagrangian (2.55) would then be invariant under axial flavor transformations

$$\psi^a \mapsto e^{i\alpha^A (T^A)^{ab}\gamma_5}\psi^b, \qquad \text{Noether current: } J_{5\mu}^A = \bar{\psi}^a \gamma_\mu \gamma_5 \left(T^A\right)^{ab} \psi^b, \tag{2.61}$$

where T^A are the generators of $SU(N_f)$ labelled by the index $A = 1, \ldots, N_f^2 - 1$ running up to the dimensionality $N_f^2 - 1$ of the Lie algebra. The corresponding pseudoscalar Noether charges, when acting upon single-particle states[3] constructed from a chirally invariant

[3]For simplicity, let us ignore confinement here.

vacuum,

$$Q_5^A = \int d^3x J_{50}^A \implies Q_5^A \left|M, s, +, a\right\rangle = \left(T^A\right)^{ab} \left|M, s, -, b\right\rangle \tag{2.62}$$

would be expected to produce hadronic doublets of (approximately) equal masses and spins, but opposite parities.

The general absence of such parity doublets can be explained by spontaneous *chiral symmetry breaking* (χSB) due to the formation of a *chiral condensate* in the non-perturbative regime of a gauge theory [40]. Analogous to the formation of Cooper pairs in superconductors, the condensate corresponds to a nonzero vacuum expectation value of the composite operator

$$\langle \bar{\psi}_L^a \psi_R^b \rangle = -\sigma \delta^{ab}, \tag{2.63}$$

where $\sigma \sim \Lambda_{\text{QCD}}^3$ is a parameter of mass dimension three, anticipated to scale with the cube of the QCD scale. This implies that the ground state no longer satisfies the full $SU(N_f)_L \times SU(N_f)_R$ global symmetry of the Lagrangian (2.55). Indeed, under the transformation (2.57) but with $L, R \in SU(N_f)$,

$$\langle \bar{\psi}_L^a \psi_R^b \rangle \mapsto -\sigma \left(RL^\dagger\right)^{ba}, \tag{2.64}$$

which remains invariant only if $L = R$. This leaves us only with the diagonal subgroup of flavour symmetries

$$SU(N_f)_L \times SU(N_f)_R \to SU(N_f)_V. \tag{2.65}$$

According to *Goldstone's theorem*, each of the spontaneously broken $N_f^2 - 1$ continuous symmetry gives rise to a massless *Goldstone boson*, corresponding to an excitation along the degenerate manifold of vacua [41, 42]. In QCD, the (pseudo-)Goldstone bosons correspond to the $SU(3)_V$ octet of pseudoscalar mesons composed of the three lightest quarks[4]. These mesons are light compared to the proton, but not massless due to explicit breaking of flavour symmetry by the different quark masses and couplings to the EM sector. With a relatively small mass difference of ~ 2 MeV compared to the QCD scale, the $SU(2)_V$ isospin symmetry of the u and d quarks accounts for the pions as the lightest mesons [40]. Relations within the mass spectrum can be computed by a low-energy chiral perturbation theory.

In addition, there exist bound states of $N_c = 3$ quarks called baryons. With masses of the order of the QCD scale Λ_{QCD} (much heavier than the current quark masses), baryons are nonetheless stable as the lightest particles charged under $U(1)_V$. They can in fact be viewed as *Skyrmions* with non-trivial winding numbers in chiral perturbation theory, where they are also organized into approximate multiplets of $SU(3)_V$.

The formation of a chiral condensate has been observed in lattice simulations, but in the absence of a complete analytic explanation, a commonly studied model for χSB is the *Nambu-Jonas-Lasinio* (NJL) model [43], which we review in Section 3.2.

[4]The broken $U(1)_A$ axial symmetry also manifests in the relatively large mass of the η' meson.

Chapter 3

Model

Having reviewed the perturbative trviality of textbook QED, in this chapter we discuss one possible resolution by the Pauli operator. As this spin-field coupling term is perturbatively non-renormalizable, functional renormalization techniques have been applied to investigate asymptotic safety scenarios, one of which exhibits long-range physics consistent with experimental observations.

To investigate if such UV completions are consistent with the light fermions of the Standard Model, we also introduce the Nambu-Jona-Lasinio (NJL) model, which is known as an effective four-fermion model for chiral symmetry breaking in QCD, but can also be induced by Abelian gauge interactions, While this symmetry is already explicitly broken by the Pauli term, divergences in the NJL couplings still indicate dynamical generation of Planck scale masses.

3.1 Pauli Term

Pure QED consists of a $U(1)$ gauge field A_μ minimally coupled to a Dirac fermion ψ, whose partial derivatives ∂_μ are replaced by gauge covariant derivatives $D_\mu[A] = \partial_\mu - ieA_\mu$. Physically, this describes a coupling between the gauge field and fermion charge. As discussed in Sections 2.1.2 and 2.1.3, the $\bar{\psi}\not{A}\psi$ operator, of dimension-4 in $d = 4$, is marginally irrelevant as per the perturbative beta function (2.19), which predicts a Landau pole inconsistency for any non-trivial theory with interactions. Of course, this may simply signal the expected breakdown of perturbation theory in the regime of large gauge coupling e, but lattice simulations [44, 45] and non-perturbative functional methods [46] further substantiate the triviality of pure QED, though the exact mechanism inhibiting a UV-complete theory is somewhat different from a naive Landau pole.

Various resolutions have been proposed; for example, based on the introduction of additional fields [47, 48, 49, 50], enhancement of the $U(1)$ symmetry [51, 52] or even the inclusion of quantum gravitational fluctuations [53, 54, 55, 56]. One possibility retaining only fermionic and photonic degrees of freedom is that the Landau pole emerges only as an artifact of pure QED as the leading order approximation of an effective field theory (EFT), which may further contain an infinite number of irrelevant local interactions, as long as they are consistent with underlying symmetries [57]. A next-to-leading order contribution is the *Pauli term* $\bar{\psi}\sigma_{\mu\nu}F^{\mu\nu}\psi$, which completes the truncation of the effective action to lowest derivative-order (1st order for fermions and 2nd order for photons) and to operators of dimension-5.

While the Pauli term is a perturbatively non-renormalizable dimension-5 operator, this

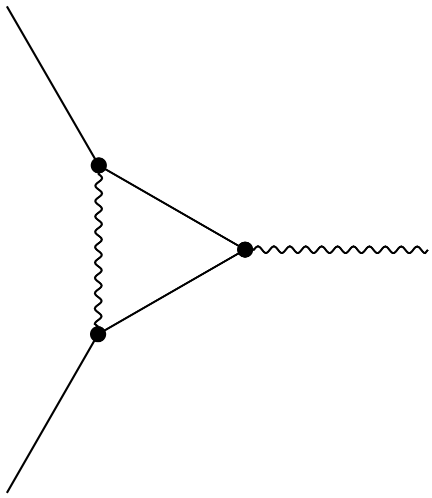

Figure 3.1: One-loop correction to the QED vertex function, giving rise to an anomalous magnetic moment deviating from the Dirac prediction of $g = 2$.

proximity to the theory space of textbook QED suggests possible RG relevance in a strong coupling regime, where quantum fluctuations can counteract the canonical scaling. Functional RG techniques have recently been used by Gies and Ziebell to show that the extended theory space spanned by the Pauli coupling includes additional non-trivial fixed points which enable an asymptotic safety scenario for QED as observed at low energies [3].

Recall that the commutator $\sigma_{\mu\nu} = i\left[\sigma_\mu, \sigma_\nu\right]/2$ furnishes a representation of the $SO(4)$ rotational symmetry group of Euclidean spacetime, generalizing the non-relativistic Pauli spin matrices. The Pauli term couples these to the electromagnetic field tensor $F_{\mu\nu} = \partial_{[\mu} A_{\nu]}$. Such a term describes the famous anomalous magnetic moment of the electron due to the contributions of diagrams such as in Figure 3.1 [58].

Here we include the Pauli term explicitly in the bare action, defined with a UV cutoff Λ due to the perturbative non-renormalizability of the Pauli coupling:

$$S = \int d^4x \left[\bar{\psi}^a i\not{D}[A]\psi^a + \frac{1}{4} F_{\mu\nu}F^{\mu\nu} - i\bar{m}\bar{\psi}^a\psi^a + i\bar{\kappa}\bar{\psi}^a\sigma_{\mu\nu}F^{\mu\nu}\psi^a \right], \tag{3.1}$$

where $D_\mu[A] = \partial_\mu - i\bar{e}A_\mu$ is the gauge covariant derivative and $\bar{m}$, $\bar{\kappa}$, $\bar{e}$ denote the bare mass and couplings. The factors of i in the mass and Pauli terms ensure reflection positivity, which allows for analytic continuation back to a QFT on a Lorentzian manifold by the Osterwalder-Schrader theorem [59].

While the action (3.1) retains a local $U(1)$ gauge symmetry, global chiral symmetry is broken by both the mass and Pauli terms. While the mass is traditionally ignored as a source of chiral symmetry breaking (χSB) in the *deep Euclidean region* where the renormalized mass m is negligible in comparison to any other momentum scale, the explicit breaking of chiral symmetry by the Pauli term necessitates a more equitable treatment of both mass and Pauli coupling, which is enabled by the formalism of functional RG. Here we summarize some relevant results as reported in [3], as well as from our earlier analysis of the flavor N_f dependence of the RG flow [60].

The average effective action Γ_k, which flows from the bare action (3.1) upon integration of modes with momentum k as discussed in Section 2.2.2, reads

$$\Gamma_k = \int d^4x \left[\bar{\psi}^a \left(iZ_\psi \partial\!\!\!/ + \bar{e} A\!\!\!/ - i\bar{m} + i\bar{\kappa}\sigma_{\mu\nu}F^{\mu\nu} \right) \psi^a + \frac{1}{4} Z_A F_{\mu\nu} F^{\mu\nu} + \frac{Z_A}{2\xi} (\partial_\mu A^\mu)^2 \right], \quad (3.2)$$

where Z_ψ and Z_A are the wavefunction renormalizations for the fermions and photon respectively and ξ is the gauge fixing parameter, which we set to $\xi = 0$ in the Landau gauge as a fixed point of the RG flow [61, 62]. Subleading terms omitted in this truncation may include higher derivatives such as $\bar{\psi} D\!\!\!/ D\!\!\!/ \psi$ (dimension-5) and $F_{\mu\nu} \Box F^{\mu\nu}$ (dimension-6), or the dimension-6 four-fermion operators which form the focus of this study.

In the search for scale-invariant fixed points, it is convenient to define the renormalized dimensionless parameters

$$e = \frac{\bar{e}}{Z_\psi \sqrt{Z_A}}, \qquad \kappa = \frac{k\bar{\kappa}}{Z_\psi \sqrt{Z_A}}, \qquad m = \frac{\bar{m}}{Z_\psi k}, \quad (3.3)$$

and anomalous dimensions

$$\eta_\psi = -\partial_t \ln Z_\psi \qquad \eta_A = -\partial_t \ln Z_A. \quad (3.4)$$

The corresponding beta functions (22), (23), (24) and anomalous dimensions (25), (26) as obtained from the Wetterich equation are given in the Appendix 6 [3].

For the case of $N_f = 1$, two interacting fixed points $\mathcal{B}$ and $\mathcal{C}$ can be observed in addition to the Gaussian fixed point $\mathcal{A}$, with their properties listed in Table 3.1. The fixed points occur with various multiplicities since the action (3.2) is invariant under two $\mathbb{Z}_2$ symmetries: charge conjugation, as well as the discrete axial rotation

$$\psi \to e^{i\frac{\pi}{2}\gamma_5}\psi \qquad \bar{\psi} \to \bar{\psi} e^{i\frac{\pi}{2}\gamma_5} \qquad \bar{\kappa} \to -\bar{\kappa} \qquad \bar{m} \to -\bar{m}, \quad (3.5)$$

a relic of the broken continuous chiral symmetry. As such, for each fixed point (e^*, κ^*, m^*), there exist further fixed points

$$(-e^*, -\kappa^*, m^*), (e^*, -\kappa^*, -m^*), (-e^*, \kappa^*, -m^*), \quad (3.6)$$

obtained by simultaneous sign-flips of e and κ or κ and m, all representing the same universality class. Table 3.1 also lists their critical exponents and corresponding eigendirections in terms of components along the e, κ and m basis in theory space. The number n_{phys} of (marginally) relevant directions corresponds to physical parameters which must be fine-tuned to determine the long-range physics of the theory. As an estimate of the validity of our truncated derivative expansion of the effective action (3.2), the anomalous dimensions η_ψ and η_A parametrizing the running of the kinetic terms are expected to remain small. Only those fixed points satisfying this consistency criterion have been retained. Figure 3.2 shows the phase diagram in the (κ, m) plane at $e = 0$, where the gauge coupling beta function (22) vanishes, as well as the (κ, e) plane at $m = 0$.

As expected from the discussions of Section 2.1.2, the anomalous dimensions vanish at the Gaussian fixed point $\mathcal{A}$ and the critical exponents are as expected from power-

Table 3.1: Fixed points of QED with Pauli coupling in $d = 4$ and $N_f = 1$.

	$(e^*,\, \kappa^*,\, m^*)$	Multiplicity	$\left(\eta_\psi^*,\, \eta_A^*\right)$	n_{phys}	Critical Exponents	Eigendirections
$\mathcal{A}$	$\begin{pmatrix}0\\0\\0\end{pmatrix}$	–	$(0, 0)$	1	$(1, 0, -1)$	$\begin{pmatrix}0\\0\\1\end{pmatrix} \begin{pmatrix}1\\0\\0\end{pmatrix} \begin{pmatrix}0\\1\\0\end{pmatrix}$
$\mathcal{B}$	$\begin{pmatrix}0\\5.09\\0.328\end{pmatrix}$	$\mathbb{Z}_2 \times \mathbb{Z}_2$	$(-1.4, 0.53)$	2	$(3.10, 2.13, -0.813)$	$\begin{pmatrix}0\\-1\\0.04\end{pmatrix} \begin{pmatrix}0.4\\0.9\\0.02\end{pmatrix} \begin{pmatrix}0\\-1\\-0.1\end{pmatrix}$
$\mathcal{C}$	$\begin{pmatrix}0\\3.82\\0\end{pmatrix}$	$\mathbb{Z}_2$	$(-1, 0)$	3	$(2.25, 1.79, 0.413)$	$\begin{pmatrix}0\\1\\0\end{pmatrix} \begin{pmatrix}1.0\\0\\0.3\end{pmatrix} \begin{pmatrix}0\\0\\1\end{pmatrix}$

counting. The mass m is the only RG relevant direction with critical exponent $\theta_m = 1$. As in perturbation theory, the gauge coupling is marginally irrelevant ($\theta_e = 0$) and the Pauli coupling irrelevant $\theta_\kappa = -1$.

As for the non-trivial fixed points, these lie outside the theory subspace of usual QED with finite values of κ^*. Fixed point $\mathcal{B}$ also features a finite (dimensionless) mass m^* and just one irrelevant direction lying within the (κ, m) plane at $e = 0$. By tuning two parameters, for example the IR value of the gauge coupling in accordance with $\alpha \simeq 1/137$ and the initial UV scale in terms of the physical fermion mass, the long-range Pauli coupling is then a firm prediction of the universality class. Two UV-complete trajectories can be constructed from fixed point $\mathcal{B}$ and its $\mathbb{Z}_2$ reflection under charge conjugation, but the associated anomalous magnetic moments

$$a_e = -\frac{4}{e}\kappa m\bigg|_{k=0} = \begin{Bmatrix}-18.55\\14.01\end{Bmatrix} \gg \frac{g-2}{2} = \frac{\alpha}{2\pi} + \mathcal{O}(\alpha^2) \approx 0.00116 \tag{3.7}$$

are orders of magnitude larger than the physical value, dominating even the Dirac contribution of $g = 2$ to the g-factor. This contradiction with one of the most precise measurements in physics clearly rules out physical QED from belonging to the universality of fixed point $\mathcal{B}$, despite offering an asymptotically free gauge coupling.

On the other hand, fixed point $\mathcal{C}$ is entirely IR repulsive, with the anomalous dimensions $\eta_\psi^* = -1, \eta_A^* = 0$ responsible for the (marginal) relevance of the Pauli coupling even before considering further quantum fluctuations. With three relevant directions, the basin of attraction of $\mathcal{C}$ must contain some three-dimensional neighbourhood of the fixed point. The $\mathbb{Z}_2$ reflection of $\mathcal{C}$ has in fact been connected to a range of long-range values including those of physical QED, with the transition from perturbative to asymptotically safe regime occurring at a scale much larger than the electron mass, but below the electroweak scale:

$$\Lambda_c \approx 23.67\,\text{GeV}. \tag{3.8}$$

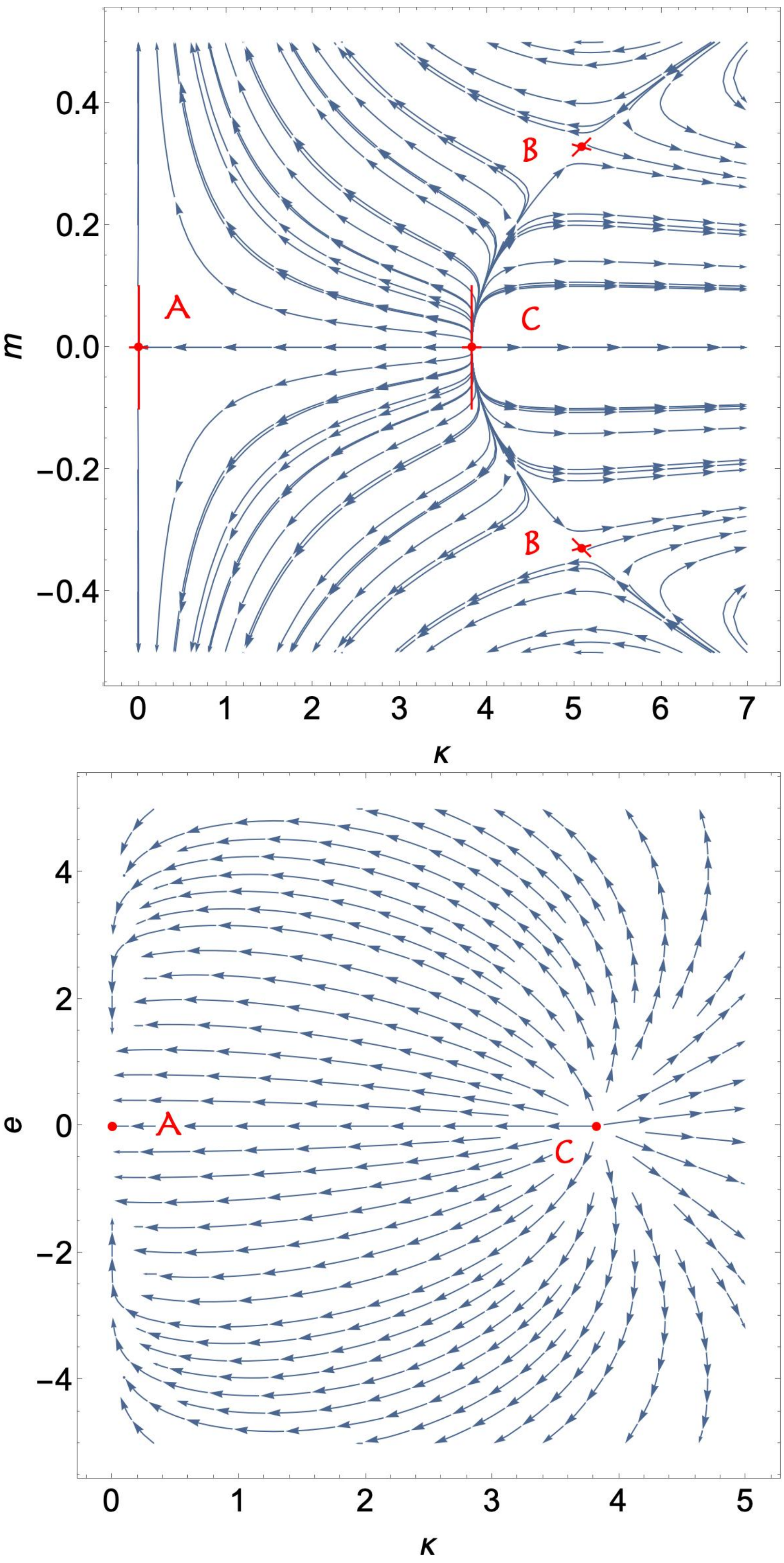

Figure 3.2: Renormalization group flow for QED with Pauli term in $d = 4$ spacetime dimensions and with $N_f = 1$ fermion flavor. The Gaussian fixed point $\mathcal{A}$ and non-Gaussian fixed points $\mathcal{B}$ and $\mathcal{C}$ are labelled as red crosses indicating their respective eigendirections. The arrows point in the directions of flow towards the IR.

As seen in Figure 3.2, separatrices lead from the UV fixed point $\mathcal{C}$ to the IR fixed points $\mathcal{A}$ and $\mathcal{B}$. All other trajectories emanating from $\mathcal{B}$ and $\mathcal{C}$ towards smaller Pauli coupling

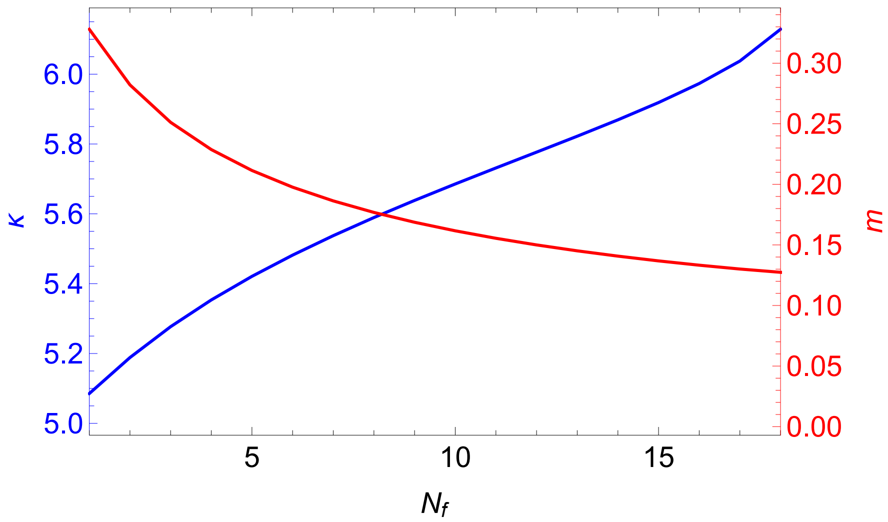

Figure 3.3: Variation of the Pauli coupling κ^* and mass m^* at fixed point $\mathcal{B}$ with increasing flavor number.

κ flow toward the formal fixed point at $|m| \to \infty$ of non-propagating fermions and free photons ($e = \kappa = 0$). Since m represents the dimensionless mass, the physical mass approaches a finite IR value as massive modes decouple from the RG flow.

Our subsequent studies showed that in $d = 4$, the fixed point $\mathcal{C}$ and its critical exponents do not depend on flavor number N_f [60]. For vanishing gauge coupling e and mass m in $d = 4$, the beta function of the Pauli coupling (23) reduces to

$$\partial_t \kappa|_{e,m=0} = (1 + \eta_\psi)\kappa, \qquad \eta_\psi = -\frac{3}{5\pi^2} \frac{\kappa^2}{1 - \frac{3}{40\pi^2}\kappa^2}; \tag{3.9}$$

namely, the fermion anomalous dimension η_ψ^* at fixed point $\mathcal{C}$ must take exactly the value required to render the Pauli coupling marginally relevant, for all N_f. On the contrary, for fixed point $\mathcal{B}$ with finite mass, κ^* increases and m^* decreases with increasing N_f, as shown in Figure 3.3. The simultaneous increase in anomalous dimensions casts doubt on the reliability of our conclusions, but within the current approximation, a quantum phase transition seems to occur at the critical flavor number $N_f \simeq 18.50$[1] Fixed point $\mathcal{B}$ collides with another fixed point coming from even larger coupling values, bifurcating into the complex plane. This other unphysical fixed point fails our consistency condition of small anomalous dimensions at $N_f = 1$.

[1]In contrast to their classical counterparts, quantum phase transitions occur by varying some non-thermal parameter at $T = 0$, where critical behavior is governed by quantum (rather than thermal) fluctuations [63].

3.2 Nambu-Jona-Lasinio Model

The aim of our present studies is to investigate the consistency of the non-Gaussian fixed points $\mathcal{B}$ and $\mathcal{C}$, by extending our truncation to include dimension-6 four-fermion operators. Such interactions may be rendered relevant by quantum fluctuations and trigger dynamic generation of fermion mass in contradistinction to the small values observed in the Standard Model.

Four-fermion interactions are of interest in various physical systems. Perhaps most famous is Fermi's theory of beta decay as a local four-fermion interaction with a (V-A) structure (see (3.15) for clarification of the notation). This non-renormalizable theory is now understood as a low-energy EFT obtained after integrating out the highly massive gauge bosons of the weak interaction. Self-interacting fermions also feature in the exactly solvable Thirring (vector channel) and Gross-Neveu (scalar channel) models [64, 65, 66, 67]. Despite its simplicity[2], the non-trivial phase structure of the Gross-Neveu model describes the Peierls-Froehlich model and relativistic ferromagnetic superconductors in condensed matter physics [69]. In $1+1$ dimensions, the perturbatively renormalizable coupling is asymptotically free. Moreover, the Gross-Neveu model contains a discrete chiral symmetry which may be spontaneously broken, resulting in mass generation and formation of bound states [70].

In this work, we focus on the *Nambu-Jona-Lasinio*-type (NJL) channels, which admit an enhanced continuous chiral symmetry. Inspired by the successful theory of superconductivity by Bardeen, Cooper and Schrieffer [71, 72, 73], the NJL model was devised as a description of two-body interactions between nucleons. Despite later being supplanted by QCD, it remains useful as a mathematically tractable EFT of strongly interacting fermions which captures some essential symmetries of QCD. Thus, the NJL model facilitates studies of chiral symmetry breaking and the associated dynamic generation of fermion masses. By fitting the model to empirical values of masses and decay constants, two- and three-flavor variants of the model describe with reasonable accuracy the meson spectrum introduced in Section 2.3 and provide qualitative insights into the effects of external influences such as temperature and chemical potential [43]. The generation of NJL-type interactions from QCD in the course of the RG flow has now been studied from first principles [74, 75, 76].

For one fermion flavor in spacetime dimension $d = 4$, the effective action takes the form

$$\Gamma_{\mathrm{NJL}}[\psi, \bar{\psi}] = \int d^4x \left\{ iZ_\psi \bar{\psi} \partial\!\!\!/ \psi + \frac{1}{2}\bar{\lambda}_\sigma \left[\left(\bar{\psi}\psi\right)^2 - \left(\bar{\psi}\gamma_5\psi\right)^2 \right] \right\}, \tag{3.10}$$

where higher-order derivative terms can be dropped in the leading order of a derivative expansion, as long as the anomalous dimension $\eta_\psi = -\partial_t \ln Z_\psi$ is small. Such four-fermion interactions may be due to fundamental fermionic nonlinearities, but here we will adopt the perspective that such terms are generated by UV gauge boson fluctuations in the course of the RG flow.

Note that in $d = 4$, fermionic fields have mass dimension $3/2$ and thus any four-fermion coupling has dimension -2, implying that the NJL model is perturbatively non-renormalizable.

[2]The finite temperature phase diagram can even be analytically computed in the large N_f limit [68].

Thus, the model must be defined along with a choice of regularization scheme based on desired physical properties and symmetries [43]. Here we impose a UV cutoff in Euclidean spacetime, though other possibilities include a non-covariant three-momentum cutoff, proper-time and Pauli-Villars regularization.

3.2.1 Chiral Symmetry and Fierz Transformations

As with the QED action (2.55), the NJL action (3.10) is clearly invariant under the $U(1)_V$ vector symmetry

$$\psi \mapsto e^{i\alpha}\psi, \qquad \bar{\psi} \mapsto \bar{\psi}e^{-i\alpha}, \tag{3.11}$$

as well as the $U(1)_A$ axial symmetry

$$\psi \mapsto e^{i\beta\gamma_5}\psi, \qquad \bar{\psi} \mapsto \bar{\psi}e^{i\beta\gamma_5} \tag{3.12}$$

in the absence of an explicit mass term. To see this, we rewrite the NJL channel in terms of Weyl spinors transforming with opposite phases: $\psi_L \mapsto e^{-i\beta}\psi_L$, $\psi_R \mapsto e^{i\beta}\psi_R$. In the chiral representation of the Euclidean Dirac matrices given in Appendix 6,

$$\begin{aligned}\left(\bar{\psi}\psi\right)^2 - \left(\bar{\psi}\gamma_5\psi\right)^2 &= \left(\psi_R^\dagger\psi_L + \psi_L^\dagger\psi_R\right)^2 - \left(-\psi_R^\dagger\psi_L + \psi_L^\dagger\psi_R\right)^2 \\ &= 4\left(\psi_R^\dagger\psi_L\right)\left(\psi_L^\dagger\psi_R\right).\end{aligned} \tag{3.13}$$

Thus, the linear combination $\left(\bar{\psi}\psi\right)^2 - \left(\bar{\psi}\gamma_5\psi\right)^2$ is invariant under the axial rotation (3.12), even though each individual term is not.

However, the NJL action (3.10) is by no means complete, as local four-field operators can be algebraically reordered by the *Fierz transformations* [77].

$$\left(\bar{\psi}_1 A\psi_2\right)\left(\bar{\psi}_3 B\psi_4\right) = \left(\bar{\psi}_1 C\psi_4\right)\left(\bar{\psi}_3 D\psi_2\right). \tag{3.14}$$

For the case of one fermion flavour ψ, A, B, C and D are simply elements of the Euclidean Clifford algebra $Cl_{4,0}(\mathbb{C})$, which we can expand in a complete basis Γ_a, normalized by $\mathrm{Tr}\{\Gamma_a\Gamma_b\} = 4\delta_{ab}$. We further choose basis elements which yield irreducible representations of the $SO(4)$ symmetry group of Euclidean spacetime:

$$\Gamma^{\mathrm{S}} = \mathbb{I}_4 \qquad \Gamma^{\mathrm{V}} = \gamma_\mu \qquad \Gamma^{\mathrm{T}} = \frac{i}{2}\left[\gamma_\mu, \gamma_\nu\right] \qquad \Gamma^{\mathrm{A}} = i\gamma_\mu\gamma_5 \qquad \Gamma^{\mathrm{P}} = \gamma_5, \tag{3.15}$$

with the corresponding Dirac bilinears transforming as a scalar, vector, tensor, axial vector and pseudoscalar, respectively. Note that factors of i have been included as necessary to render all basis elements Hermitian. Here we work with an irreducible representation of the Dirac algebra, with dimension $d_\gamma = 2^{\lfloor d/2 \rfloor} = 4$. The completeness of this basis is evident as the $1+4+6+4+1$ basis elements account for the 16 independent entries of a 4×4 matrix A. In such a basis, we can write the Fierz transformations as

$$\left(\bar{\psi}_1\Gamma_a\psi_2\right)\left(\bar{\psi}_3\Gamma_b\psi_4\right) = C_{ab}{}^{cd}\left(\bar{\psi}_1\Gamma_c\psi_4\right)\left(\bar{\psi}_3\Gamma_d\psi_2\right), \tag{3.16}$$

with repeated indices summed over implicitly. The coefficients ${C_{ab}}^{cd}$ can be found using the orthonormality of the basis (3.15):

$$(\Gamma_a)_{ij}\,(\Gamma_b)_{kl} = {C_{ab}}^{cd}\,(\Gamma_c)_{il}\,(\Gamma_d)_{kj} \implies {C_{ab}}^{cd} = \frac{1}{16}\,\mathrm{Tr}\left[\Gamma_a\Gamma_d\Gamma_b\Gamma_c\right]. \tag{3.17}$$

In fact, to obtain a scalar Lagrangian invariant under $SO(4)$, we need not consider all possible pairs of basis matrices $\left(\bar{\psi}_1\Gamma_a\psi_2\right)\left(\bar{\psi}_3\Gamma_b\psi_4\right)$, but rather just invariants

$$\left(\bar{\psi}_1\Gamma^{\mathcal{A}}_a\psi_2\right)\left(\bar{\psi}_3\Gamma^{\mathcal{A}a}\psi_4\right), \tag{3.18}$$

where $a = 1, \dots, \dim\mathcal{A}$ now runs only over the elements in an irreducible representation $\mathcal{A} = \mathrm{S}, \mathrm{V}, \mathrm{T}, \mathrm{A}, \mathrm{P}$ as enumerated in the basis (3.15). For ease of notation, we adopt the shorthand

$$(\mathcal{A}) = \left(\bar{\psi}\Gamma^{\mathcal{A}}_a\psi\right)\left(\bar{\psi}\Gamma^{\mathcal{A}a}\psi\right), \tag{3.19}$$

such that NJL channel is written as $(\mathrm{S}-\mathrm{P})$. Of such four-fermion operators, any other chirally invariant channel must be constructed from the vector (V) channel and the axial vector (A) channel, since γ_5 anti-commutes with all gamma matrices γ_μ.

However, the Fierz transformation (3.17) shows that these three channels are in fact not independent. In particular, the NJL channel can be rewritten as

$$(\mathrm{S}-\mathrm{P}) = -\frac{1}{2}\,(\mathrm{V}+\mathrm{A}). \tag{3.20}$$

Thus, for one fermion flavour, the space of chirally symmetric four-fermion couplings is two-dimensional, spanned by a basis $(\mathrm{V}\pm\mathrm{A})$.[3] The Fierz-complete action

$$\Gamma[\psi,\bar{\psi}] = \int d^4x\left\{iZ_\psi\bar{\psi}\partial\!\!\!/\psi + \frac{1}{2}\bar{\lambda}_+\,(\mathrm{V}+\mathrm{A}) + \frac{1}{2}\bar{\lambda}_-\,(\mathrm{V}-\mathrm{A})\right\}. \tag{3.21}$$

removes any ambiguity in the representation of four-fermion channels that are consistent with the $U(1)$ chiral symmetry. The action must then be closed under the RG flow, with a non-trivial $\bar{\lambda}_-$ possibly generated even starting with a pure NJL model with just $\bar{\lambda}_+$.

As a leading order approximation, we further ignore any momentum dependence in the couplings:

$$\bar{\lambda}(p_1,p_2,p_3) = \bar{\lambda}(0,0,0) + \mathcal{O}\left(\frac{|p_i|}{k}\right). \tag{3.22}$$

While this point-like limit can herald the onset of spontaneous chiral symmetry breaking (see Section 3.2.2), a drawback is that it cannot predict the mass spectrum in the chirally broken phase, as bound states (e.g. mesons in QCD) appear as momentum poles in the couplings. Such momentum dependence may be conveniently described by a *Hubbard-*

[3]For a single-channel approximation, writing $(\mathrm{V}+\mathrm{A}) = -2(\mathrm{S}-\mathrm{P})$ somewhat simplifies computation of the beta function by one gamma matrix per four-fermion vertex. But for a Fierz-complete analysis, taking the basis $(\mathrm{V}+\mathrm{A})$ allows for a similar treatment of both channels for much of the calculations.

Stratonovich transformation, which introduces bosonic fields to represent possible bound states $\langle \phi \rangle \sim \langle \bar{\psi}\psi \rangle$ of the fermions [70]. The four-fermion coupling is resolved to be mediated by the condensate bosons, which are Yukawa-coupled to the fermions [70]. The point-like limit is then a decent approximation when the exchanged bosons are heavy, i.e. in the chirally symmetric phase.

3.2.2 Renormalization Group Flow for $N_f = 1$

As we derive from the Wetterich equation (2.50) in Chapter 4, the beta functions for the renormalized dimensionless couplings

$$\lambda_{\pm} = (Z_{\psi})^{-2} \, k^2 \bar{\lambda}_{\pm} \tag{3.23}$$

are given by

$$\partial_t \lambda_+ = (2 + 2\eta_{\psi})\lambda_+ + 8v_4 \, l_4^{(\mathrm{F})}(0,0) \left(3\lambda_+^2 + 4\lambda_+\lambda_-\right) \tag{3.24}$$

$$\partial_t \lambda_- = (2 + 2\eta_{\psi})\lambda_- + 8v_4 \, l_4^{(\mathrm{F})}(0,0)\lambda_+^2, \tag{3.25}$$

where $v_4 = 1/\left(32\pi^2\right)$. For consistency, the flow equations (3.24) and (3.25) can be compared to those given in [70] for the basis $(\mathrm{S}-\mathrm{P}), -(\mathrm{V})$, related by the transformation $\lambda_\sigma = 2\left(\lambda_- - \lambda_+\right), \lambda_{\mathrm{V}} = -2\lambda_-$.

The threshold function $l_4^{(\mathrm{F})}(0,0)$, as defined in Appendix 6, imposes the IR and UV regularization in the Wetterich formulation of FRG (see Section 2.2.3) and thereby quantifies the contribution of the 1PI Feynman diagram shown in Figure 3.4(a) to the four-fermion couplings, as successive momentum shell are integrated over. While threshold functions encapsulate the freedom to choose the regularization scheme without altering predictions for physical observables, we use the optimized regulators introduced in Section 2.2.3, with rapid convergence properties. Due to the one-loop structure of the Wetterich equation, higher-order femion self-interactions do not contribute to the RG flow of our four-fermion interactions, at least in the point-like approximation[4].

As for the anomalous dimension η_ψ associated with the running of the kinetic term, this is expected to receive contributions from the 1PI Feynman diagram of Figure 3.4(b). However, in our point-like limit (3.22), momentum conservation requires that the loop momentum q be independent of the incoming/outgoing momentum p. As a result, η_ψ vanishes and the wavefunction renormalization can be set to a constant $Z_\psi = 1$. This is no longer true if we resolve the momentum dependence of the couplings in a partially bosonized formulation [70].

[4] In a partially bosonized formulation, 8-fermion interactions, as parametrized by quartic interactions of the condensate bosons, do contribute to the RG flow of four-fermion couplings. Deviations from the purely fermionic formulation become especially pronounced in the chirally broken phase due to excitations of massless Goldstone bosons [70].

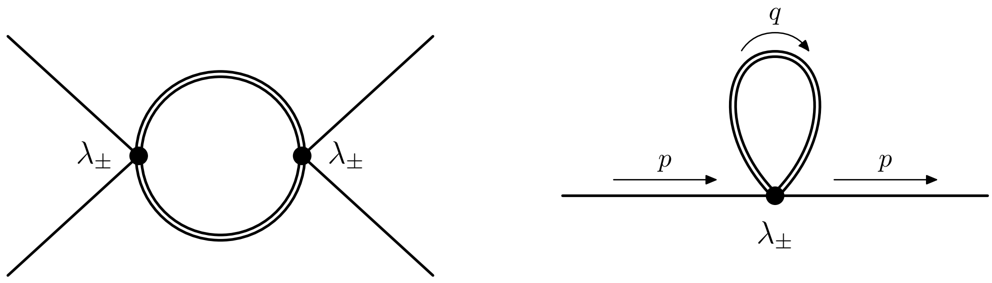

(a) (b)

Figure 3.4: a) 1PI Feynman diagram representing quantum self-corrections which contribute to the RG flow of the four-fermion couplings $\lambda_\pm$, as described by the quadratic terms in the beta functions (3.24) and (3.25). The double lines represent the full propagator. b) 1PI Feynman diagram representing modifications to the propagator, thereby contributing to the running of the wavefunction renormalization Z_ψ. In the point-like limit, the loop momentum q must be independent of the incoming/outgoing momentum p due to momentum conservation, which leads to a vanishing anomalous dimension $\eta_\psi = -\partial_t \ln Z_\psi$.

Single-Channel Model

To simplify the analysis of the beta functions, we first consider a single-channel approximation. Since (for one fermion flavour) the beta function (3.25) of λ_- only receives quantum correction from the $(\mathrm{V}+\mathrm{A})$ channel, we set $\lambda_- = 0$. The remaining beta function then reduces to

$$\partial_t \lambda_+ = 2\lambda_+ + 24 v_4\, l_4^{(\mathrm{F})}(0,0)\lambda_+^2, \tag{3.26}$$

with a Gaussian fixed point $\lambda_+^{\mathrm{Gauss}} = 0$ as well as a non-trivial UV fixed point[5]

$$\lambda_+^* = -\frac{4}{3}\zeta = -\frac{16\pi^2}{3}, \tag{3.27}$$

where for ease of comparison with later results, we have defined the scheme-dependent quantity

$$\zeta \equiv \frac{1}{16 v_4\, l_4^{(\mathrm{F})}(0,0)}, \tag{3.28}$$

and in the last step we evaluated the optimized regulator $l_4^{(\mathrm{F})}(0,0) = 1/2$ as tabulated in Appendix 6. This beta function is analogous to that shown in Figure 2.2(a). As observed in Figure 3.5, we can affect a quantum phase transition by tuning the UV value λ_+^Λ of the coupling. For $\lambda_+^\Lambda > \lambda_+^*$, the subsequent RG flow is attracted towards the Gaussian fixed point and the theory becomes free in the IR while preserving chiral symmetry. On the contrary, with $\lambda_+^\Lambda < \lambda_+^*$, the flow is repelled away from the interacting fixed point λ_+^* and λ_+ decreases rapidly. In fact, the flow equation (3.26) can be solved analytically as

$$\lambda_+(k) = \lambda_+^\Lambda \left[\left(\frac{\Lambda}{k}\right)^\theta \left(1 - \frac{\lambda_+^\Lambda}{\lambda_+^*}\right) + \frac{\lambda_+^\Lambda}{\lambda_+^*} \right]^{-1} \tag{3.29}$$

[5]It has been shown that this non-Gaussian fixed point is an artefact of the point-like approximation with a finite UV cutoff λ in $d = 4$ [70].

where θ is a universal critical exponent

$$\theta = -\frac{\partial\left(\partial_t \lambda_+\right)}{\partial \lambda_+}\Big|_{\lambda_+^*} = 2, \tag{3.30}$$

whose value does not depend on the choice of regulator. From this solution, we see that the NJL coupling λ_+ diverges at a finite scale[6]

$$k_{\mathrm{SB}} = \Lambda \left(1 - \frac{\lambda_+^*}{\lambda_+^\Lambda}\right)^{1/\theta} \theta(\lambda_+^* - \lambda_+^\Lambda). \tag{3.31}$$

From a bosonized formulation of the model (3.21), we can interpret the divergent coupling as an indicator that the ground state of the theory no longer respects chiral symmetry, as the Ginzburg-Landau-type effective potential of the condensate develops a non-trivial minimum [70]. Thus, the non-Gaussian fixed point (3.27) behaves as a quantum critical point, separating two qualitatively disjunct regimes.

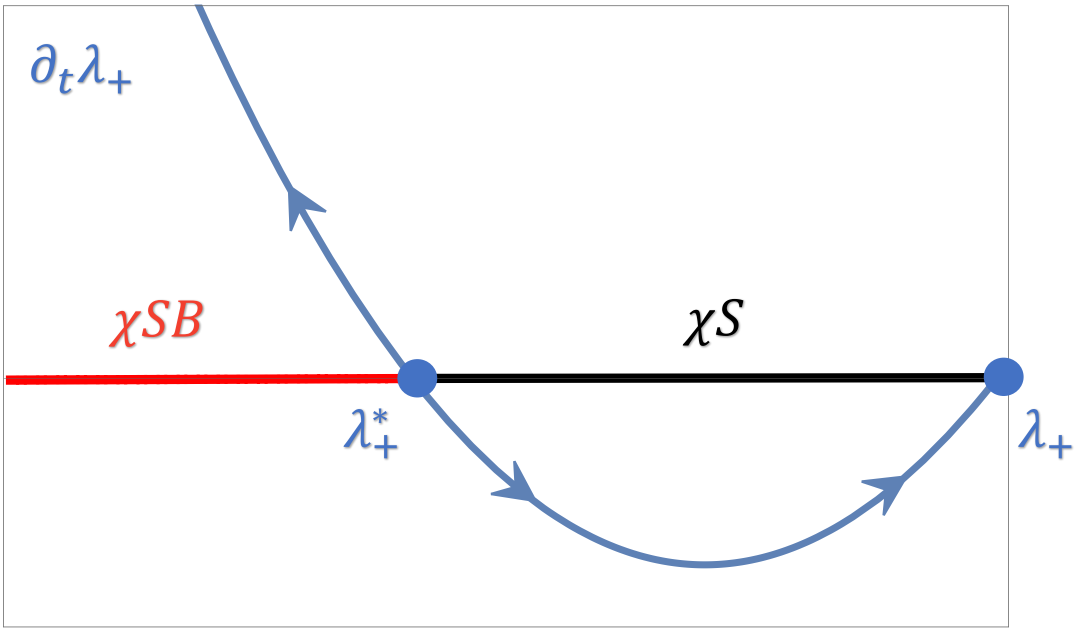

Figure 3.5: Phase diagram for the single-channel NJL model. If we tune the UV value of the four-fermion coupling $\lambda_+^\Lambda > \lambda_+^*$ above the critical value λ_+^* given by the non-trivial fixed point, the RG flow drives the theory towards asymptotic freedom in the IR. On the other hand, a UV value $\lambda_+^\Lambda < \lambda_+^*$ below the fixed point results in a rapid divergence of the coupling, which heralds the spontaneous breakdown of chiral symmetry. This constitutes a quantum phase transition between a chiral-symmetric (χS, black) and chiral-symmetry-broken (χSB) phase.

[6]This in fact defines the scale for any observable $\mathcal{O} \sim k_{\mathrm{SB}}^{d_{\mathcal{O}}}$ with dimension $d_{\mathcal{O}}$ in the chirally broken phase [70].

Fierz-Complete Basis

Returning to the full Fierz-complete beta functions (3.24) and (3.25), we now observe the scheme-dependent fixed points tabulated in Table 3.2, along with their universal critical exponents and eigendirections. As in (2.17) and (3.30), these are defined by diagonalizing the stability matrix

$$B_{ij} = \frac{\partial\left(\partial_t \lambda_i\right)}{\partial \lambda_j}\bigg|_{\lambda^*}. \tag{3.32}$$

Table 3.2: Fixed points of four-fermion interactions with $N_f = 1$.

	$(\lambda_+^*, \lambda_-^*)$	Critical Exponents	Eigendirections
$\mathcal{F}_1^{\text{Gauss}}$	$\begin{pmatrix}0\\0\end{pmatrix}$	$(-2, -2)$	$\begin{pmatrix}0\\1\end{pmatrix}\begin{pmatrix}1\\0\end{pmatrix}$
$\mathcal{F}_2$	$\begin{pmatrix}-\zeta\\-\zeta/4\end{pmatrix}$	$(2, -5/2)$	$\begin{pmatrix}2\\1\end{pmatrix}\begin{pmatrix}1/4\\-1\end{pmatrix}$
$\mathcal{F}_3$	$\begin{pmatrix}4\zeta\\-4\zeta\end{pmatrix}$	$(2, -10)$	$\begin{pmatrix}1\\-2\end{pmatrix}\begin{pmatrix}1\\1\end{pmatrix}$

All interacting fixed points feature one IR attractive and one IR repulsive direction, with $\mathcal{F}_2$ approximated by the single-channel non-trivial fixed point (3.27). As shown in Figure 3.6 (drawn for optimized regulators for which $\zeta = 4\pi^2$), the two-dimensional theory space is divided into regions by separatrices (red curves) flowing between fixed points (blue points), which generalize the role of the critical coupling (3.27) in the single-channel approximation.

For example, by tuning the UV values $(\lambda_+^\Lambda, \lambda_-^\Lambda)$ to lie within the Ia, Ib, IIIa or IIIb domains, chiral symmetry is broken when the four-fermion couplings diverge at a finite scale k_{SB} as in (3.31). However, theories within the Ia/b universality class are attracted towards a different IR fixed point (at infinity)

$$\mathcal{F}_2^\infty = \lim_{\alpha\to\infty} F_2 = \lim_{\alpha\to\infty} \left(-\alpha\zeta, \alpha\zeta/4\right) \tag{3.33}$$

than those in the IIIa/b universality class:

$$\mathcal{F}_3^\infty = \lim_{\alpha\to\infty} F_3 = \lim_{\alpha\to\infty} \left(4\alpha\zeta, -4\alpha\zeta\right). \tag{3.34}$$

Though both universality classes feature a ground state with some broken symmetry, differences in their low-energy phenomenologies would have to be resolved by a partially bosonized formulation [70]. On the contrary, theories in the II and IV regions belong to the basin of attraction of the Gaussian fixed point $\mathcal{F}_1^{\text{Gauss}}$ and therefore become free in the IR.

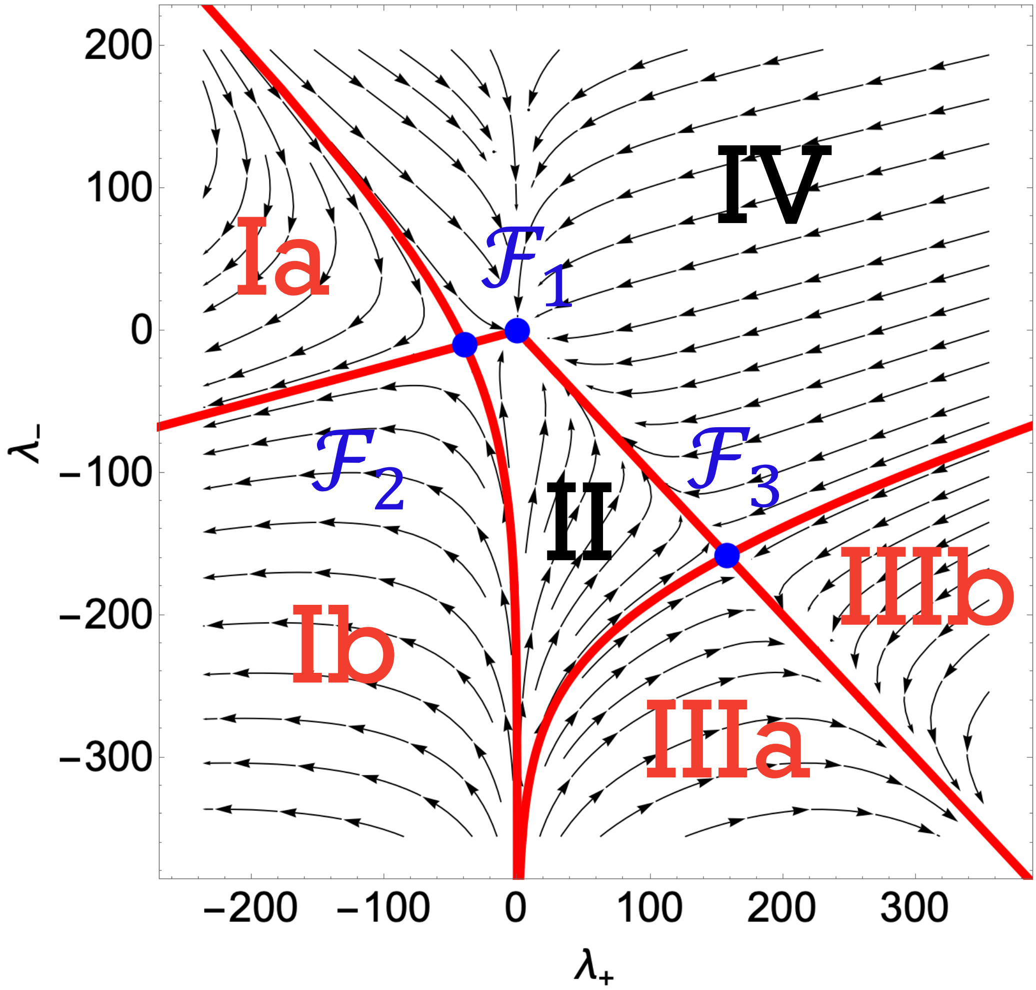

Figure 3.6: Phase diagram of a Fierz-complete NJL model with a single fermion flavor. The separatrices (red curves) flowing between fixed points $\mathcal{F}_i$ (blue dots) divide the theory space into disjunct domains based on UV and IR properties. Theories belonging to phases II and IV (labelled in black) preserve chiral symmetry and become asymptotically free. Theories in phases I and III (labelled in red) break chiral symmetry in the ground state, though they may still differ in the IR.

We note once more that for the current $N_f = 1$ model, the RG flows of $\lambda_\pm$ are coupled such that there exists no pure NJL-like trajectory with $\lambda_- \equiv 0$, while $\lambda_+ \equiv 0$ corresponds to a trivial trajectory with a constant dimensionful $\bar{\lambda}_-$. This absence of quantum self-corrections to λ_- in the beta function (3.25) gives rise to only three fixed points with finite couplings. In the many-flavor model discussed in the next Section 3.2.3, the fixed point at infinity, whose UV-critical manifold includes the Ib and IIIa regimes, becomes finite.

3.2.3 Renormalization Group Flow for $N_f > 1$

A natural deformation of our action (3.21) is to introduce $N_f > 1$ flavors ψ^a satisfying a chiral $SU(N_f)_L \otimes SU(N_f)_R$ symmetry, which we recall from Section 2.3 to be the symmetry of QED/QCD in the limit of massless fermions. Of course, there now exist more possible contractions into fermion bilinears. Starting with the smaller symmetry group of $SU(N_f)$, these can be classified as flavor singlets

$$(\mathrm{S}-\mathrm{P}) \equiv \left(\bar{\psi}^a\psi^a\right)^2 - \left(\bar{\psi}^a\gamma_5\psi^a\right)^2 \tag{3.35}$$

$$(\mathrm{V}\pm\mathrm{A}) \equiv \left(\bar{\psi}^a\gamma_\mu\psi^a\right)^2 \mp \left(\bar{\psi}^a\gamma_\mu\gamma_5\psi^a\right)^2, \tag{3.36}$$

where the flavor indices are pairwise contracted within the same fermion bilinear, or alternatively as flavor non-singlets

$$(\mathrm{S}-\mathrm{P})_{\mathrm{N}} \equiv \left(\bar{\psi}^a\psi^b\right)^2 - \left(\bar{\psi}^a\gamma_5\psi^b\right)^2 \tag{3.37}$$

$$(\mathrm{V}\pm\mathrm{A})_{\mathrm{N}} = \left(\bar{\psi}^a\gamma_\mu\psi^b\right)^2 \mp \left(\bar{\psi}^a\gamma_\mu\gamma_5\psi^b\right)^2, \tag{3.38}$$

where the flavor indices are contracted non-trivially between the different bilinears, as in $\left(\bar{\psi}^a\psi^b\right)^2 \equiv \left(\bar{\psi}^a\psi^b\right)\left(\bar{\psi}^b\psi^a\right)$. In the point-like limit, we can independently perform a Fierz transformation with respect to the flavor indices as well as the Dirac indices:

$$(\mathrm{S}-\mathrm{P}) = -\frac{1}{2}\,(\mathrm{V}+\mathrm{A})_{\mathrm{N}} \tag{3.39}$$

$$(\mathrm{V}-\mathrm{A}) = (\mathrm{V}-\mathrm{A})_{\mathrm{N}} \tag{3.40}$$

$$(\mathrm{V}+\mathrm{A}) = -2\,(\mathrm{S}-\mathrm{P})_{\mathrm{N}}\,. \tag{3.41}$$

Such relations allow us to consider only the three flavor singlets as independent four-fermion operators. To see the additional restrictions in the case of $SU(N_f)_L \times SU(N_f)_R$, we express the channels in terms of Weyl spinors. As in (3.13),

$$(\mathrm{S}-\mathrm{P}) = \left(\psi_R^{a\dagger}\,\psi_L^a + \psi_L^{a\dagger}\,\psi_R^a\right)^2 - \left(\psi_R^{a\dagger}\,\psi_L^a - \psi_L^{a\dagger}\,\psi_R^a\right)^2 \tag{3.42}$$

$$= 4\left(\psi_R^{a\dagger}\,\psi_L^a\right)\left(\psi_L^{b\dagger}\,\psi_R^b\right), \tag{3.43}$$

which is not invariant under separate chiral transformations of the left- and right-handed fermions:

$$SU(N_f)_L : \psi_L^a \mapsto L^{ab}\psi_L^b, \qquad SU(N_f)_R : \psi_R^a \mapsto R^{ab}\psi_R^b. \tag{3.44}$$

Likewise, we can express the $(\mathrm{V}\pm\mathrm{A})$ channels using the chiral representation (3):

$$(\mathrm{V}+\mathrm{A}) = i\left(\psi_L^{a\dagger}\bar{\sigma}_\mu\psi_L^a + \psi_R^{a\dagger}\sigma_\mu\psi_R^a\right)^2 - i\left(-\psi_L^{a\dagger}\bar{\sigma}_\mu\psi_L^a + \psi_R^{a\dagger}\sigma_\mu\psi_R^a\right)^2 \tag{3.45}$$

$$= 4i\left(\psi_L^{a\dagger}\bar{\sigma}_\mu\psi_L^a\right)\left(\psi_R^{b\dagger}\sigma_\mu\psi_R^b\right) \tag{3.46}$$

$$(\mathrm{V}-\mathrm{A}) = 2i\left(\psi_L^{a\dagger}\bar{\sigma}_\mu\psi_L^a\right)^2 + 2i\left(\psi_L^{a\dagger}\bar{\sigma}_\mu\psi_L^a\right)^2,$$

which remain as the only two independent channels consistent with an $SU(N_f)_L \times SU(N_f)_R$ symmetry.

As we derive in Chapter 4, the flow equations for this Fierz-complete basis read

$$\partial_t \lambda_+ = (2+2\eta_\psi)\lambda_+ + 4v_4\, l_4^{(\mathrm{F})}(0,0)\left[6\lambda_+^2 + (d_\gamma N_f + 4)\,\lambda_+\lambda_-\right] \tag{3.47}$$

$$\partial_t \lambda_- = (2+2\eta_\psi)\lambda_- + 2v_4\, l_4^{(\mathrm{F})}(0,0)\left[(d_\gamma N_f - 4)\,\lambda_-^2 + d_\gamma N_f \lambda_+^2\right]. \tag{3.48}$$

Note that the flavor dependence drops out in the single-channel approximation $\lambda_- = 0$, as we will explain in the next Chapter 4. We see that for $N_f > 1$, the λ_-^2 term in the beta function (3.48) no longer vanishes, giving rise to an additional IR-repulsive fixed point $\mathcal{F}_4$ which comes from infinity at $N_f = 1$:

Table 3.3: Fixed points of four-fermion interactions with N_f flavors.

	$(\lambda_+^*, \lambda_-^*)$	Critical Exponents	Eigendirections
$\mathcal{F}_1^{\text{Gauss}}$	$\begin{pmatrix}0\\0\end{pmatrix}$	$(-2,-2)$	$\begin{pmatrix}0\\1\end{pmatrix}\begin{pmatrix}1\\0\end{pmatrix}$
$\mathcal{F}_2$	$\begin{pmatrix}-\frac{4\zeta(N_f+3)}{2N_f^2+5N_f+9}\\-\frac{4\zeta N_f}{2N_f^2+5N_f+9}\end{pmatrix}$	$\left(2,-2-\frac{8N_f}{2N_f^2+5N_f+9}\right)$	$\begin{pmatrix}1+\frac{2}{N_f+1}\\1\end{pmatrix}\begin{pmatrix}1-\frac{3}{N_f+3}\\-1\end{pmatrix}$
$\mathcal{F}_3$	$\begin{pmatrix}\frac{4\zeta}{2N_f-1}\\-\frac{4\zeta}{2N_f-1}\end{pmatrix}$	$\left(2,-2-\frac{8}{2N_f-1}\right)$	$\begin{pmatrix}1-\frac{1}{N_f+1}\\-1\end{pmatrix}\begin{pmatrix}1\\1\end{pmatrix}$
$\mathcal{F}_4$	$\begin{pmatrix}0\\-\frac{4\zeta}{N_f-1}\end{pmatrix}$	$\left(2,2+\frac{8}{N_f-1}\right)$	$\begin{pmatrix}0\\1\end{pmatrix}\begin{pmatrix}1\\0\end{pmatrix}$

As such, the phase diagram for $N_f > 1$ flavors is qualitatively identical to that shown in Figure 3.7 for $N_f = 2$, with chirally symmetric phases II and IV flowing towards the attractive Gaussian fixed point $\mathcal{F}_1$. Fixed point $\mathcal{F}_4$ is purely repulsive; $\mathcal{F}_2$ and $\mathcal{F}_3$ each have one attractive and one repulsive direction[7].

[7]An interesting limit is that of $N_f \to \infty$. At leading order in $1/N_f$, the rescaled fixed-point couplings $N_f \mathcal{F}_i$ approach a constant limit [70].

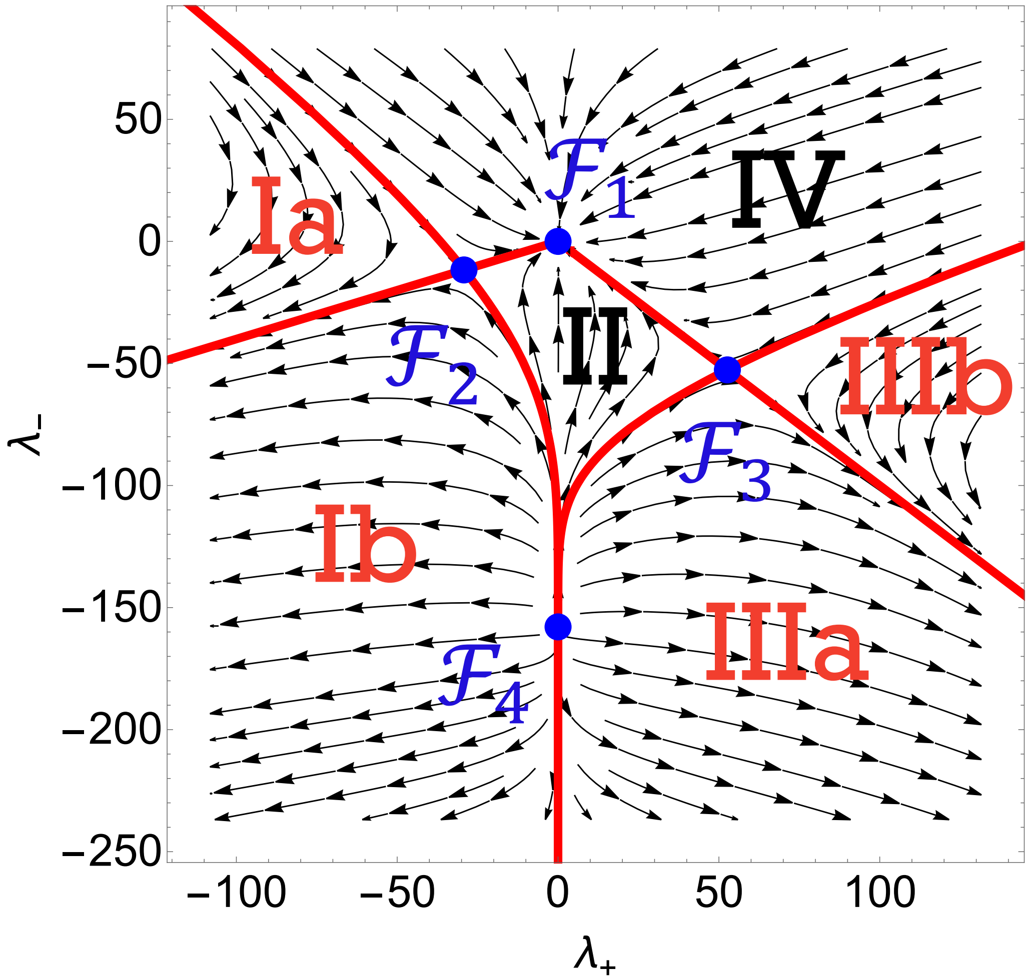

Figure 3.7: Phase diagram of a Fierz-complete NJL model with $N_f = 2$ flavors. The separatrices (red curves) flowing between fixed points $\mathcal{F}_i$ (blue dots) divide the theory space into disjunct domains based on UV and IR properties. Theories belonging to phases II and IV (labelled in black) preserve chiral symmetry and become asymptotically free. Theories in phases I and III (labelled in red) break chiral symmetry in the ground state, though they may still differ in the IR.

Chapter 4

Calculation

Having laid the groundwork in Chapters 2 and 3, we are ready to confront the central problem of this thesis: to investigate the relevance of four-fermion interactions in the asymptotic safety scenarios provided by adding the Pauli term to textbook QED. If these dimension-6 operators do turn out to be RG-relevant at the UV fixed points $\mathcal{B}$ or $\mathcal{C}$, it would indicate the potential dynamical generation of fermion masses on the order of some UV scale, say the Planck scale. This would be much larger than the phenomenological values due to the Higgs mechanism, in contrast to observation. In this chapter, we derive the flow equations for the basis of four-fermion interactions identified in Section 3.2.3, which are considered to be induced by photonic fluctuations.

4.1 Computation of $\Gamma^{(2)}$

We consider an Abelian-gauged NJL model of N_f Dirac flavors with an $SU(N_f)_L \otimes SU(N_f)_R$ chiral symmetry. This is explicitly broken by an additional Pauli term, but we assume that we can neglect the additional four-fermion terms generated by the RG flow and focus on the theory subspace spanned by the (V $\pm$ A) flavor singlet channels. This is motivated by the fact that explicit symmetry breaking terms in the Standard Model vanish or at least are extremely small; hence such terms in our model should also be insignificant so as to be compatible with observation.

The corresponding effective action is given by

$$\begin{aligned}\Gamma_k[\Phi] = \int_x \Big\{ &\bar{\psi}^a \left(i Z_\psi \partial\!\!\!/ + \bar{e} A\!\!\!/ + i\bar{\kappa}\sigma_{\mu\nu}F^{\mu\nu} \right) \psi^a + \frac{Z_A}{4} F_{\mu\nu}F^{\mu\nu} + \frac{Z_A}{2\alpha} \left(\partial_\mu A^\mu \right)^2 \\ &+ \frac{1}{2}\bar{\lambda}_+ \left(\mathrm{V} + \mathrm{A} \right) + \frac{1}{2}\bar{\lambda}_- \left(\mathrm{V} - \mathrm{A} \right) \Big\},\end{aligned} \tag{4.1}$$

where we have grouped the fermionic and bosonic fields into the collective field

$$\Phi \equiv \begin{pmatrix} A_\mu(p) \\ \psi^a(p) \\ \bar{\psi}^{a^T}(-p) \end{pmatrix}, \qquad \Phi^T \equiv \Big(A_\mu(-p), \psi^{a^T}(-p), \bar{\psi}^a(p) \Big) \tag{4.2}$$

Here the adjoints of the complex Dirac spinors count as independent degrees of freedom.

With the Fourier conventions

$$A_\mu(x) = \int \frac{d^4p}{(2\pi)^4} A_\mu(p) e^{ip\cdot x}, \ \psi^a(x) = \int \frac{d^4p}{(2\pi)^4} \psi^a(p) e^{ip\cdot x}, \ \bar\psi^a(x) = \int \frac{d^4p}{(2\pi)^4} \bar\psi^a(p) e^{-ip\cdot x}, \tag{4.3}$$

we can rewrite the action in momentum space,

$$\begin{aligned} \Gamma_k[\Phi] = &\int_p \left\{ -Z_\psi \bar\psi^a(p) \not{p}\, \psi^a(p) + \frac{Z_A}{2} \left(p^2 \left|A_\mu(p)\right|^2 + \left(\frac{1}{\alpha} - 1\right) \left|p^\mu A_\mu(p)\right|^2 \right) \right\} \\ &+ \int_{p_1, p_2} \bar\psi^a(p_1 + p_2) \left(\bar e \gamma^\mu + 2\bar\kappa p_{2\nu}\, \sigma^{\mu\nu}\right) \psi^a(p_1) A_\mu(p_2) \\ &+ \int_{p_1, p_2, p_3} \sum_\pm \frac{\bar\lambda_\pm}{2} \left[\bar\psi^a(p_1)\gamma_\mu \psi^a(p_2) \bar\psi^b(p_3) \gamma^\mu \psi^b(p_1 - p_2 + p_3) \mp (\gamma_\mu \to \gamma_\mu\gamma_5) \right], \end{aligned} \tag{4.4}$$

where one of the momentum integrals has been eliminated by the locality of the field operators and we have used the reality of the gauge field $A^\mu(-p) = A^{\mu^*}(p)$.

To compute the beta functions of the four-fermion couplings, it is convenient to express the Wetterich equation (2.50) as

$$\partial_t \Gamma_k = \frac{1}{2} \mathrm{STr}\, \tilde\partial_t \ln \left(\Gamma_k^{(1,1)} + R_k \right), \tag{4.5}$$

in an analogous form to the perturbative equation (2.52). Here the supertrace STr is defined as in Section 2.2.3 and the formal derivative $\tilde\partial_t$ acts only on the scale dependence of the regulator R_k. We denote the $(m+n)$-point functions of the effective average action as

$$\Gamma_k^{(m,n)}[\Phi] \equiv \underbrace{\frac{\overrightarrow{\delta}}{\delta\Phi^T} \cdots \frac{\overrightarrow{\delta}}{\delta\Phi^T}}_{\text{m-times}} \Gamma_k[\Phi] \underbrace{\frac{\overleftarrow{\delta}}{\delta\Phi} \cdots \frac{\overleftarrow{\delta}}{\delta\Phi}}_{\text{n-times}}, \tag{4.6}$$

which takes into account the Grassmann nature of the fermionic fields and their derivatives. To derive the beta functions, it suffices to consider spatially homogeneous background fields[1], which are represented in momentum space by

$$\psi^a(p) = \psi^a (2\pi)^4 \delta^{(4)}(p), \quad \bar\psi^a(p) = \bar\psi^a (2\pi)^4 \delta^{(4)}(p) \tag{4.7}$$

[1]To compute the anomalous dimension, we would instead consider a plane wave background $\psi^a(p) = \psi^a(2\pi)^4\delta^{(4)}(p - Q)$.

The second functional derivative then becomes the field-space matrix

$$
\Gamma_k^{(1,1)}[\Phi] \tag{4.8}
$$

$$
= \begin{pmatrix} Z_A\, p^2 \left(P_\perp^{\mu\nu}(p) + \frac{1}{\alpha} P_\parallel^{\mu\nu}(p)\right) & \bar{\psi}^b \left(\bar{e}\gamma^\mu + 2\bar{\kappa} p_\rho\, \sigma^{\rho\mu}\right) & -\psi^{b^T} \left(\bar{e}\gamma^{\mu^T} + 2\bar{\kappa} p_\rho\, \sigma^{\rho\mu^T}\right) \\ \left(-\bar{e}\gamma^{\nu^T} + 2\bar{\kappa} p_\rho\, \sigma^{\rho\nu^T}\right) \bar{\psi}^{a^T} & F_{11}^{ab} & -Z_\psi \not{p}^T \delta^{ab} + F_{12}^{ab} \\ \left(\bar{e}\gamma^\nu - 2\bar{\kappa} p_\rho\, \sigma^{\rho\nu}\right) \psi^a & -Z_\psi \not{p}\, \delta^{ab} + F_{21}^{ab} & F_{22}^{ab} \end{pmatrix} \delta_{p,\,p'},
$$

where the delta function $\delta_{p,p'} = (2\pi)^4 \delta(p - p')$ indicates that the two-point function $\Gamma_k^{(1,1)}[\Phi]$ is diagonal in momentum space for constant background fields.

In the bosonic sector, the transversal and longitudinal projectors are respectively defined as

$$
P_\perp^{\mu\nu}(p) = g^{\mu\nu} - \frac{p^\mu p^\nu}{p^2}, \qquad P_\parallel^{\mu\nu}(p) = \frac{p^\mu p^\nu}{p^2}. \tag{4.9}
$$

Meanwhile, the fermionic entries are given by

$$
F_{11}^{ab} = -\sum_\pm \bar{\lambda}_\pm \left\{ \gamma_\rho^T \bar{\psi}^{a^T} \bar{\psi}^b \gamma^\rho \mp \gamma^{5^T} \gamma_\rho^T \bar{\psi}^{a^T} \bar{\psi}^b \gamma^\rho \gamma^5 \right\} \tag{4.10}
$$

$$
F_{21}^{ab} = \sum_\pm \bar{\lambda}_\pm \left\{ \gamma_\rho \left[\psi^a \bar{\psi}^b \pm \gamma^5 \psi^a \bar{\psi}^b \gamma^5\right] \gamma^\rho + \delta^{ab} \gamma_\rho \left[\left(\bar{\psi}^c \gamma^\rho \psi^c\right) \mp \gamma^5 \left(\bar{\psi}^c \gamma^\rho \gamma^5 \psi^c\right)\right] \right\} \tag{4.11}
$$

$$
F_{12}^{ab} = -F_{21}^{ba^T}, F_{22}^{ab} = F_{11}^{ab} \quad \text{with} \quad \bar{\psi}^{a^T} \to \psi^a, \bar{\psi}^b \to \psi^{b^T}, \tag{4.12}
$$

where we have dropped any terms involving gauge field A_μ since we consider only the flows of the four-fermion couplings. Note that the transposition of Grassmann-valued spinors such as $\left(\psi^a \bar{\psi}^b\right)^T = -\bar{\psi}^{b^T} \psi^{a^T}$ incurs a minus sign. Whereas (4.10) describes four-fermion vertices with two outgoing external fermions of flavors a and b, (4.11) represents vertices with one incoming and one outgoing external fermion, with the first term allowing for a change in the flavor carried by the loop ($b \to a$) and the second corresponding to an unchanged loop flavor $a = b$ before and after the vertex.

Note that the momentum dependence of the Pauli vertex leads to a sign difference from the corresponding minimal coupling term when taking fermionic functional derivatives from the left (corresponding to entries in the first column of (4.8)). The antisymmetry of the field strength tensor $F_{\mu\nu}$ results in relatively large numerical prefactors in the beta function.

To form the inverse propagator, we use the chirally symmetric regulators introduced in (2.37):

$$R_k(p,p') = \begin{pmatrix} Z_A\, p^2\, r_B(p)\, g^{\mu\nu} & 0 & 0 \\ 0 & 0 & -Z_\psi\, r_F(p)\, \not{p}^T \delta^{ab} \\ 0 & -Z_\psi\, r_F(p)\, \not{p}\, \delta^{ab} & 0 \end{pmatrix} \delta_{p,p'}. \quad (4.13)$$

We then decompose the inverse regularized propagtor into a field-independent (inverse) propagator matrix $\mathcal{P}_k$ and a field-dependent fluctuation matrix $\mathcal{F}_k$:

$$\Gamma_k^{(1,1)} + R_k = \mathcal{P}_k + \mathcal{F}_k[\Phi], \quad (4.14)$$

in terms of which equation (4.5) can be Taylor expanded:

$$\partial_t \Gamma_k = \frac{1}{2}\mathrm{STr}\left\{ \tilde{\partial}_t \left(\frac{1}{\mathcal{P}_k}\mathcal{F}_k \right) \right\} - \frac{1}{4}\mathrm{STr}\left\{ \tilde{\partial}_t \left(\frac{1}{\mathcal{P}_k}\mathcal{F}_k \right)^2 \right\} + \frac{1}{6}\mathrm{STr}\left\{ \tilde{\partial}_t \left(\frac{1}{\mathcal{P}_k}\mathcal{F}_k \right)^3 \right\} + \ldots, \quad (4.15)$$

where we have dropped a field-independent constant $\sim \mathrm{STr}\, \tilde{\partial}_t \ln \mathcal{P}_k$. Our propagator matrix reads

$$\frac{1}{\mathcal{P}_k} = \begin{pmatrix} \frac{1}{P_B} P^\perp_{\mu\nu} & 0 & 0 \\ 0 & 0 & -\frac{1}{\sqrt{p^2 P_F}}\, \not{p} \\ 0 & -\frac{1}{\sqrt{p^2 P_F}}\, \not{p}^T & 0 \end{pmatrix} \delta_{p,p'}, \quad (4.16)$$

where we have gauge fixed after the inversion, setting $\alpha = 0$ in the Landau gauge as a fixed point of the RG flow [61, 62]. Here we have defined the regularized momenta

$$P_B = p^2 \left(1 + r_B(p)\right), \qquad P_F = p^2 \left(1 + r_F(p)\right)^2. \quad (4.17)$$

The corresponding fluctuation matrix is given by

$$\mathcal{F}_k = \begin{pmatrix} 0 & \bar{\psi}^b \left(\bar{e}\gamma^\mu + 2\bar{\kappa} p_\rho\, \sigma^{\rho\mu}\right) & -\psi^{b^T} \left(\bar{e}\gamma^{\mu^T} + 2\bar{\kappa} p_\rho\, \sigma^{\rho\mu^T}\right) \\ \left(-\bar{e}\gamma^{\nu^T} + 2\bar{\kappa} p_\rho\, \sigma^{\rho\nu^T}\right) \bar{\psi}^{a^T} & F_{11}^{ab} & F_{12}^{ab} \\ \left(\bar{e}\gamma^\nu - 2\bar{\kappa} p_\rho\, \sigma^{\rho\nu}\right) \psi^a & F_{21}^{ab} & F_{22}^{ab} \end{pmatrix} \delta_{p,\,p'}, \tag{4.18}$$

which includes all the dressed vertices of the theory after amputating two legs. Multiplying powers of the propagator (4.16) and fluctuation (4.18) matrices and taking the supertrace as in (4.15), we sum over all diagrams which are one-loop in the full propagator and of arbitrarily high perturbative-loop order [29]. At first order in the expansion (4.15) of the one-loop structure, the trace over momentum space vanishes due to a linear integrand in p:

$$\frac{1}{\mathcal{P}_k}\mathcal{F}_k \tag{4.19}$$

$$= \begin{pmatrix} 0 & \frac{1}{P_B} P^\perp_{\mu\nu} \bar{\psi}^b \left(\bar{e}\gamma^\mu + 2\bar{\kappa} p_\rho\, \sigma^{\rho\mu}\right) & -\frac{1}{P_B} P^\perp_{\mu\nu} \psi^{b^T} \left(\bar{e}\gamma^{\mu^T} + 2\bar{\kappa} p_\rho\, \sigma^{\rho\mu^T}\right) \\ \frac{1}{\sqrt{p^2 P_F}} \not{p} \left(-\bar{e}\gamma^\nu + 2\bar{\kappa} p_\rho\, \sigma^{\rho\nu}\right) \psi^a & -\frac{1}{\sqrt{p^2 P_F}} \not{p}\, F_{21}^{ab} & -\frac{1}{\sqrt{p^2 P_F}} \not{p}\, F_{22}^{ab} \\ \frac{1}{\sqrt{p^2 P_F}} \not{p}^T \left(\bar{e}\gamma^{\nu^T} - 2\bar{\kappa} p_\rho\, \sigma^{\rho\nu^T}\right) \bar{\psi}^{a^T} & -\frac{1}{\sqrt{p^2 P_F}} \not{p}^T F_{11}^{ab} & -\frac{1}{\sqrt{p^2 P_F}} \not{p}^T F_{12}^{ab} \end{pmatrix} \delta_{p,\,p'}.$$

4.2 Terms of $\mathcal{O}(\bar{\lambda}^2)$

Going to second order in the expansion (4.15), we obtain

$$
\left(\frac{1}{\mathcal{P}_k}\mathcal{F}_k\right)^2 \tag{4.20}
$$

$$
= \left(\begin{array}{cc}
\begin{array}{c}
\frac{1}{\sqrt{p^2 P_F} P_B} P^{\perp}_{\mu\nu}\, \bar{\psi}^a \Big[\bar{e}^2 \left(\gamma^\alpha \not{p} \gamma^\mu - \mu \leftrightarrow \alpha\right) \\
+2\bar{e}\bar{\kappa} p_\rho \left(\gamma^\mu \not{p}\, \sigma^{\rho\alpha} - \sigma^{\rho\mu} \not{p}\, \gamma^\alpha + \mu \leftrightarrow \alpha\right) \\
+4\bar{\kappa}^2 p_\rho p_\sigma \left(\sigma^{\rho\mu} \not{p}\, \sigma^{\sigma\alpha} - \mu \leftrightarrow \alpha\right)\Big]\psi^a
\end{array} & \\
\begin{array}{c}
\frac{1}{p^2 P_F}\Big[\bar{e}\not{p}\left(F^{ab}_{21} \not{p}\, \gamma^\nu \psi^b - F^{ab}_{22} \not{p}^T \gamma^{\nu^T} \bar{\psi}^{b^T}\right) \\
+2\bar{\kappa} p_\rho \not{p}\left(-F^{ab}_{21} \not{p}\, \sigma^{\rho\nu}\psi^b + F^{ab}_{22} \not{p}^T \sigma^{\rho\nu^T} \bar{\psi}^{b^T}\right)\Big]
\end{array} &
\begin{array}{c}
\frac{1}{p^2 P_F}\left(\not{p} F^{ac}_{21} \not{p} F^{cb}_{21} + \not{p} F^{ac}_{22} \not{p}^T F^{cb}_{11}\right) \\
+\mathcal{O}\left(\bar{e}^2, \bar{e}\bar{\kappa}, \bar{\kappa}^2\right)
\end{array} \\
\mathcal{O}\left(\bar{e}\bar{\lambda}\right) &
\begin{array}{c}
\mathcal{O}\left(\bar{\lambda}^2\right) \\
\mathcal{O}\left(\bar{e}^2\right) \\
\mathcal{O}\left(\bar{e}\bar{\kappa}\right) \\
\mathcal{O}\left(\bar{\kappa}^2\right)
\end{array}
\end{array}\right) \delta_{p,\,p'},
$$

where we have abbreviated terms giving identical contributions to those written explicitly. The terms associated with the interchange of Lorentz indices $\mu \leftrightarrow \alpha$ are obtained by transposition of fermion bilinears $\left(\psi^T \bar{\psi}^T\right) = \left(\psi^T \bar{\psi}^T\right)^T = -\bar{\psi}\psi$. Once again, note the relative minus signs carried by the Pauli coupling terms.

We can further simplify the top left entry by projecting the product of Dirac matrices onto the basis (3.15) of the Clifford algebra. In particular, for the Euclidean conventions where $\gamma^5 = \gamma^1\gamma^2\gamma^3\gamma^4$ (see Appendix 6),

$$
\gamma^\mu\gamma^\nu\gamma^\rho = g^{\mu\nu}\gamma^\rho + g^{\rho\nu}\gamma^\mu - g^{\rho\mu}\gamma^\nu - \epsilon^{\rho\mu\nu\sigma}\gamma_\sigma\gamma^5 \tag{4.21}
$$

$$
\begin{aligned}
\gamma^\mu\gamma^\nu\gamma^\rho\gamma^\sigma = {} & g^{\rho\nu}g^{\sigma\mu} - g^{\rho\mu}g^{\sigma\nu} + g^{\rho\sigma}g^{\mu\nu} + \epsilon^{\rho\sigma\mu\nu}\gamma^5 \\
& - ig^{\mu\nu}\sigma^{\rho\sigma} - ig^{\sigma\nu}\sigma^{\rho\mu} + ig^{\rho\nu}\sigma^{\sigma\mu} + ig^{\sigma\mu}\sigma^{\rho\nu} - ig^{\rho\mu}\sigma^{\sigma\nu} - ig^{\rho\sigma}\sigma^{\mu\nu}
\end{aligned} \tag{4.22}
$$

$$
\begin{aligned}
\gamma^\mu\gamma^\nu\gamma^\rho\gamma^\sigma\gamma^\alpha = {} & g^{\mu\sigma}g^{\nu\rho}\gamma^\alpha - g^{\mu\rho}g^{\nu\sigma}\gamma^\alpha + g^{\mu\nu}g^{\rho\sigma}\gamma^\alpha + g^{\alpha\sigma}g^{\nu\rho}\gamma^\mu - g^{\alpha\rho}g^{\nu\sigma}\gamma^\mu + g^{\alpha\nu}g^{\rho\sigma}\gamma^\mu \\
& - g^{\alpha\sigma}g^{\mu\rho}\gamma^\nu + g^{\alpha\rho}g^{\mu\sigma}\gamma^\nu - g^{\alpha\mu}g^{\rho\sigma}\gamma^\nu + g^{\alpha\sigma}g^{\mu\nu}\gamma^\rho - g^{\alpha\nu}g^{\mu\sigma}\gamma^\rho + g^{\alpha\mu}g^{\nu\sigma}\gamma^\rho \\
& - g^{\alpha\rho}g^{\mu\nu}\gamma^\sigma + g^{\alpha\nu}g^{\mu\rho}\gamma^\sigma - g^{\alpha\mu}g^{\nu\rho}\gamma^\sigma + \epsilon^{\alpha\mu\rho\sigma}\gamma^\nu\gamma^5 - \epsilon^{\alpha\nu\rho\sigma}\gamma^\mu\gamma^5 \\
& - \epsilon^{\alpha\rho\sigma\beta}g^{\mu\nu}\gamma_\beta\gamma^5 + \epsilon^{\mu\nu\sigma\beta}g^{\alpha\rho}\gamma_\beta\gamma^5 - \epsilon^{\mu\nu\rho\beta}g^{\alpha\sigma}\gamma_\beta\gamma^5 - \epsilon^{\alpha\mu\nu\beta}g^{\rho\sigma}\gamma_\beta\gamma^5.
\end{aligned} \tag{4.23}
$$

To obtain these from the corresponding Minkowski relations (where $\gamma_5 = i\gamma^0\gamma^1\gamma^2\gamma^3$), we can perform the substitution $(\gamma_5)_M \to i\,(\gamma_5)_E$. Since the trace of an odd product of gamma matrices vanishes, identities (4.21) and (4.23) involve only the vector and axial vector terms, which both give rise to chirally symmetric four-fermion channels. On the other hand, identity (4.22) for an even product generates chiral-symmetry-breaking channels outside the two-dimensional NJL subspace. With a caveat regarding Fierz ambiguity (further discussed in the next section 4.3), we choose to discard such terms.

The matrix (4.20) then simplifies to

$$
\left(\frac{1}{\mathcal{P}_k}\mathcal{F}_k\right)^2 \tag{4.24}
$$

$$
= \left(\begin{array}{ccc}
\begin{array}{c} -\frac{2}{\sqrt{p^2 P_F} P_B} P^{\perp}_{\mu\nu}\left(\bar{e}^2 - 4\bar{\kappa}^2 p^2\right) \\ \epsilon^{\alpha\mu\rho\sigma} p_\sigma \left(\bar{\psi}^a \gamma_\rho \gamma_5 \psi^a\right) \end{array} & & \\
\begin{array}{c} \frac{2}{p^2 P_F}\Big[\bar{e}\not{p}\left(-F^{ab}_{21}\not{p}\,\gamma^\nu \psi^b + F^{ab}_{22}\not{p}^T \gamma^{\nu^T}\bar{\psi}^{b^T}\right) \\ +2\bar{\kappa} p_\rho \not{p}\left(F^{ab}_{21}\not{p}\,\sigma^{\rho\nu}\psi^b - F^{ab}_{22}\not{p}^T\sigma^{\rho\nu^T}\bar{\psi}^{b^T}\right)\Big] \end{array} & \begin{array}{c} \frac{1}{p^2 P_F}\left(\not{p}F^{ac}_{21}\not{p}F^{cb}_{21} + \not{p}F^{ac}_{22}\not{p}^T F^{cb}_{11}\right) \\ +\mathcal{O}\left(\bar{e}^2, \bar{e}\bar{\kappa}, \bar{\kappa}^2\right) \end{array} & \\
\mathcal{O}\left(\bar{e}\bar{\lambda}, \bar{\kappa}\bar{\lambda}\right) & & \begin{array}{c} \mathcal{O}\left(\bar{\lambda}^2\right) \\ \mathcal{O}\left(\bar{e}^2\right) \\ \mathcal{O}\left(\bar{e}\bar{\kappa}\right) \\ \mathcal{O}\left(\bar{\kappa}^2\right) \end{array}
\end{array}\right)\delta_{p,\,p'},
$$

Focusing on the fermionic sector and taking into account identical contributions from the two diagonal elements,

$$
-\frac{1}{4}\mathrm{STr}\left\{\tilde{\partial}_t\left(\frac{1}{\mathcal{P}_k}\mathcal{F}_k\right)^2\right\}\Bigg|_{\bar{\lambda}^2} \tag{4.25}
$$

$$
= \frac{1}{2}\Omega\int_p \frac{1}{p^2}\,\tilde{\partial}_t\left(\frac{1}{P_F}\right)\mathrm{tr}\left(\not{p}\,F^{ab}_{21}\not{p}\,F^{ba}_{21} + \not{p}\,F^{ab}_{22}\not{p}^T F^{ba}_{11}\right)
$$

$$
= -\frac{1}{2}\Omega\,\left(\bar{\lambda}_-^2, \bar{\lambda}_+^2, 2\bar{\lambda}_+\bar{\lambda}_-\right)\cdot\int_p \frac{1}{p^2}\,\tilde{\partial}_t\left(\frac{1}{P_F}\right) \tag{4.26}
$$

$$
\Bigg\{\begin{pmatrix}2\\2\\0\end{pmatrix}\left(\bar{\psi}^a\gamma_\mu\not{p}\,\gamma_\nu\psi^a - \mu\leftrightarrow\nu\right)\left(\bar{\psi}^b\gamma^\nu\not{p}\,\gamma^\mu\psi^b\right) + \begin{pmatrix}2\\-2\\0\end{pmatrix}\left(\gamma_\nu\to\gamma_\nu\gamma^5\right)
$$

$$
+\begin{pmatrix}4\\0\\2\end{pmatrix}\left(\bar{\psi}^a\gamma_\mu\not{p}\,\gamma_\nu\not{p}\,\gamma^\mu\psi^a\right)\left(\bar{\psi}^b\gamma^\nu\psi^b\right) + \begin{pmatrix}4\\0\\-2\end{pmatrix}\left(\gamma_\nu\to\gamma_\nu\gamma^5\right)
$$

$$
+ N_f\,\mathrm{tr}\left(\not{p}\,\gamma_\mu\not{p}\,\gamma_\nu\right)\left[\begin{pmatrix}-1\\-1\\-1\end{pmatrix}\left(\bar{\psi}^a\gamma^\mu\psi^a\right)\left(\bar{\psi}^b\gamma^\nu\psi^b\right) + \begin{pmatrix}-1\\-1\\1\end{pmatrix}\left(\gamma_{\mu,\nu}\to\gamma_{\mu,\nu}\gamma^5\right)\right]\Bigg\}
$$

$$
= \Omega k^2 v_4\, l_4^{(\mathrm{F})}(0,0)\big\{\bar{\lambda}_-^2\left(d_\gamma N_f - 4\right)(\mathrm{V}-\mathrm{A}) + \bar{\lambda}_+^2\left[12\,(\mathrm{V}+\mathrm{A}) + d_\gamma N_f\,(\mathrm{V}-\mathrm{A})\right]
$$

$$
+ 2\bar{\lambda}_+\bar{\lambda}_-\left(d_\gamma N_f + 4\right)(\mathrm{V}+\mathrm{A})\big\}, \tag{4.27}
$$

where $\Omega = (2\pi)^4\,\delta^4(0)$ represents the spacetime volume arising from the integration over p' and tr indicates a Dirac trace. In the second line, we use that γ^5 anticommutes with all gamma matrices ($\{\gamma^\mu, \gamma^5\} = 0$) and is traceless ($\operatorname{tr}\gamma^5 = 0$). In the third line (4.26), we apply identities (4.21) and (4.23) to the product of gamma matrices and take the Dirac trace of (4.22), keeping the dimension $d_\gamma = \operatorname{tr}\big(I_{d_\gamma}\big)$ of the representation general. The momentum integrals are simplified by spherical symmetry to

$$\int_p p^\mu p^\nu f(p^2) = \frac{1}{4} g^{\mu\nu} \int_p p^2 f(p^2), \tag{4.28}$$

the normalization of which can be confirmed by contraction with $g_{\mu\nu}$. Another useful relation for dealing with the Levi-Civita symbols that arise from (4.21) and (4.23) is

$$\epsilon^{\mu\nu\rho\sigma} \epsilon_{\mu\nu\rho}{}^{\alpha} = 6 g^{\sigma\alpha}. \tag{4.29}$$

The definitions for all threshold functions in this chapter are given in Appendix 6.

The result (4.27) agrees with the findings of [70] and [78], upon taking the appropriate no-color limit. The various terms on line (4.26) can be interpreted in terms of the 1PI diagrams of Figure 4.1. Here the fermion lines have been color-coded by their flavors a/b, while the black fermion loop in diagram 4.1(c) indicates a sum over all possible flavors circulating therein. Note that such diagrams (proportional to N_f) with two λ_+ vertices do not contribute to the RG flow of λ_+ in (4.27), such that the single-channel approximation $\lambda_- = 0$ exhibits no flavor dependence. Furthermore, the λ_-^2 diagrams 4.1(a) and 4.1(b) are exactly cancelled by diagram 4.1(c) for $N_f = 1$, such that there is no self-correction term in the beta function of λ_-. This has important ramifications for the NJL fixed point structure discussed in Chapter 5.

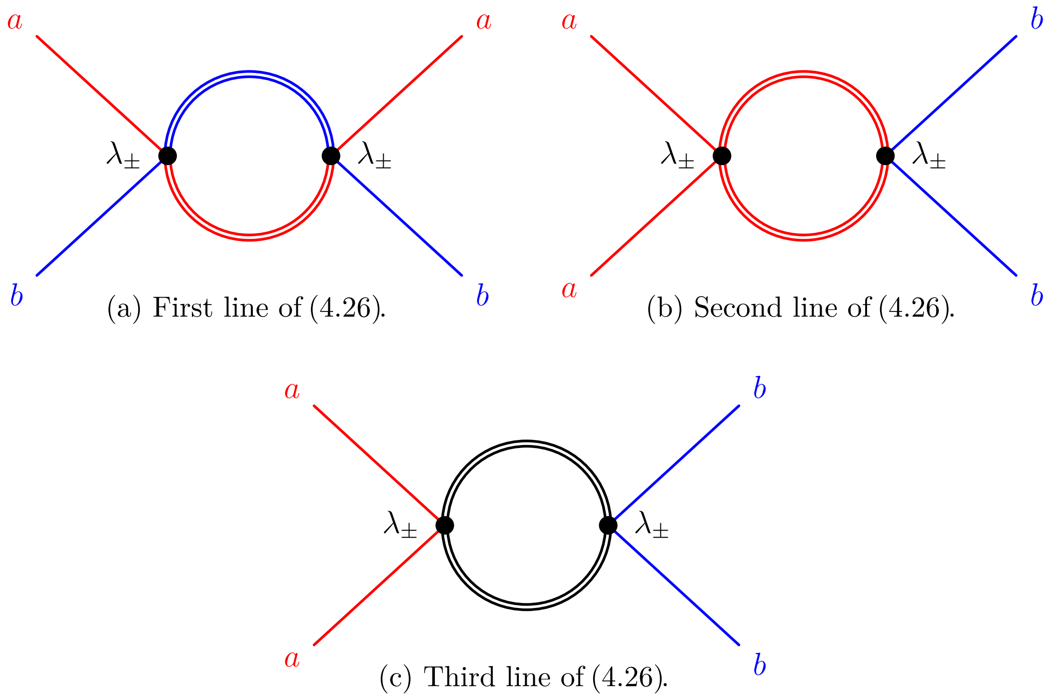

(a) First line of (4.26).

(b) Second line of (4.26).

(c) Third line of (4.26).

Figure 4.1: 1PI Feynman diagrams representing the terms of (4.26). The fermion lines are color-coded based on their flavors, with double lines representing full propagators and black lines indicating a sum over all flavors.

4.3 Terms of $\mathcal{O}(\bar{e}^2\bar{\lambda}, \bar{\kappa}^2\bar{\lambda})$

Turning now to the third order terms of the expansion (4.15),

$$\left(\frac{1}{\mathcal{P}_k}\mathcal{F}_k\right)^3 \tag{4.30}$$

$$= \begin{pmatrix} \begin{array}{l} \frac{2}{p^2 P_F P_B} P^\perp_{\mu\nu}\, \bar{\psi}^a \Big[\bar{e}^2 \gamma^\mu \, \not{p} \left(F^{ab}_{21} \not{p}\, \gamma^\alpha \psi^b - F_{22} \not{p}^T \gamma^{\alpha^T} \bar{\psi}^{b^T} \right) \\ -4\bar{\kappa}^2\, p_\rho p_\sigma\, \sigma^{\rho\mu} \not{p} \left(F^{ab}_{21} \not{p}\, \sigma^{\sigma\alpha} \psi^b - F^{ab}_{22} \not{p}^T\, \sigma^{\sigma\alpha^T} \bar{\psi}^{b^T} \right) \Big] \end{array} & & \\ & \begin{array}{c} \mathcal{O}(\bar{e}^2\bar{\lambda}) \\ \mathcal{O}(\bar{\kappa}^2\bar{\lambda}) \end{array} & \\ & & \begin{array}{c} \mathcal{O}(\bar{e}^2\bar{\lambda}) \\ \mathcal{O}(\bar{\kappa}^2\bar{\lambda}) \end{array} \end{pmatrix} \delta_{p,p'},$$

where the factor of 2 in the top left entry accounts for the identical contributions from terms of $\mathcal{O}\left(\bar{e}\bar{\lambda}, \bar{\kappa}\bar{\lambda}\right)$ in the first column of (4.24).

Likewise, the diagonal entries of the fermionic sector contribute identically to the supertrace upon transposition, giving another overall factor of 3:

$$
\begin{aligned}
&\frac{1}{6}\mathrm{STr}\left\{\tilde{\partial}_t\left(\frac{1}{\mathcal{P}_k}\mathcal{F}_k\right)^3\right\}\Bigg|_{\bar{e}^2\bar{\lambda}} \\
&= \Omega\,\bar{e}^2\int_p \frac{1}{p^2}\,\tilde{\partial}_t\left(\frac{1}{P_F P_B}\right) P^{\perp}_{\mu\nu}\,\bar{\psi}^a\gamma^\mu \not{p}\left(F^{ab}_{21}\not{p}\,\gamma^\nu\psi^b - F^{ab}_{22}\not{p}^T\gamma^{\nu^T}\bar{\psi}^{b^T}\right) \\
&= \Omega\,\bar{e}^2\int_p \frac{1}{p^2}\,\tilde{\partial}_t\left(\frac{1}{P_F P_B}\right) P^{\perp}_{\mu\nu}\left(\bar{\lambda}_-,\bar{\lambda}_+\right)\cdot \\
&\quad\left\{\begin{pmatrix}1\\1\end{pmatrix}\left[\left(\bar{\psi}^a\gamma^\mu\not{p}\,\gamma^\rho\psi^a - \mu\leftrightarrow\rho\right)\left(\bar{\psi}^b\gamma_\rho\not{p}\,\gamma^\nu\psi^b\right) + \left(\bar{\psi}^a\gamma^\mu\not{p}\,\gamma^\rho\not{p}\,\gamma^\nu\psi^a\right)\left(\bar{\psi}^b\gamma_\rho\psi^b\right)\right]\right. \\
&\quad\left. + \begin{pmatrix}1\\-1\end{pmatrix}\left(\gamma_\rho\to\gamma_\rho\gamma^5\right)\right\} \\
&= 12\,\Omega\,v_4\,l_4^{(\mathrm{B,F})}(0,0)\left[\bar{e}^2\bar{\lambda}_-(\mathrm{V}-\mathrm{A}) - \bar{e}^2\bar{\lambda}_+(\mathrm{V}+\mathrm{A})\right],
\end{aligned}
\tag{4.31}
$$

The terms due to the gauge coupling agree with the analysis of four-fermion interactions with an additional $SU(N_c)$ gauge symmetry in [78], up to a factor of two that has been accounted for.

$$
\begin{aligned}
&\frac{1}{6}\mathrm{STr}\left\{\tilde{\partial}_t\left(\frac{1}{\mathcal{P}_k}\mathcal{F}_k\right)^3\right\}\Bigg|_{\bar{\kappa}^2\bar{\lambda}} \\
&= -4\Omega\,\bar{\kappa}^2\int_p \frac{p_\rho\,p_\sigma}{p^2}\tilde{\partial}_t\left(\frac{1}{P_F P_B}\right) P^{\perp}_{\mu\nu}\,\bar{\psi}^a\sigma^{\rho\mu}\not{p}\left(F^{ab}_{21}\not{p}\,\sigma^{\sigma\nu}\psi^b - F^{ab}_{22}\not{p}^T\sigma^{\sigma\nu^T}\bar{\psi}^{b^T}\right) \\
&= -4\Omega\,\bar{\kappa}^2\int_p \frac{p_\rho\,p_\sigma}{p^2}\tilde{\partial}_t\left(\frac{1}{P_F P_B}\right) P^{\perp}_{\mu\nu}\left(\bar{\lambda}_-,\bar{\lambda}_+\right)\cdot \\
&\quad\left\{\begin{pmatrix}1\\1\end{pmatrix}\left[\left(\bar{\psi}^a\sigma^{\sigma\mu}\not{p}\,\gamma^\alpha\psi^a\right)\left(\bar{\psi}^b\gamma_\alpha\not{p}\,\sigma^{\rho\nu}\psi^b - \gamma_\alpha\leftrightarrow\sigma^{\rho\nu}\right) + \left(\bar{\psi}^a\sigma^{\sigma\mu}\not{p}\,\gamma^\alpha\not{p}\,\sigma^{\rho\nu}\psi^a\right)\left(\bar{\psi}^b\gamma_\alpha\psi^b\right)\right]\right. \\
&\quad\left. + \begin{pmatrix}1\\-1\end{pmatrix}\left[\left(\gamma_\alpha\to\gamma_\alpha\gamma^5\right)\right]\right\} \\
&= -24\,\Omega\,k^2\,v_4\,l_4^{(1,\mathrm{B,F})}(0,0)\left[\bar{\kappa}^2\bar{\lambda}_-(\mathrm{V}+\mathrm{A}) + \bar{\kappa}^2\bar{\lambda}_+(\mathrm{V}-\mathrm{A})\right] + \text{discarded (S)},
\end{aligned}
\tag{4.32}
$$

where in addition to the relations of the previous Section 4.2, we also use that $P^{\perp}_{\mu\nu}$ is a symmetric projector of trace 3:

$$
P^{\perp}_{\mu\nu} = P^{\perp}_{\nu\mu}, \qquad p^\mu P^{\perp}_{\mu\nu} = 0, \qquad g^{\mu\nu}P^{\perp}_{\mu\nu} = 3. \tag{4.33}
$$

This vanishes upon contraction with the antisymmetric Levi-Civita symbol ($P^{\perp}_{\mu\nu}\epsilon^{\mu\nu\rho\sigma} = 0$).

Moreover, under the momentum integrals, we can make the replacement

$$P^{\perp}_{\mu\nu}\, q_\alpha q_\beta\, \epsilon^{\mu\rho\gamma\alpha} \epsilon^{\nu}{}_{\rho}{}^{\delta\beta} \rightarrow q_\alpha q_\beta\, \epsilon^{\mu\rho\gamma\alpha} \epsilon_{\mu\rho}{}^{\delta\beta}, \tag{4.34}$$

as the momentum-dependent part of the projector $P^{\perp}_{\mu\nu}$ would lead to a quartic term $q_\mu q_\nu q_\alpha q_\beta$ in momentum. The generalization of identity (4.28) leads to all possible contractions of the four indices μ, ν, α, β in the two Levi-Civita symbols, which cancel each other.

Note that there are no $\bar{e}\bar{\kappa}\bar{\lambda}$ terms as their integrands are odd in momentum. Since chiral symmetry is explicitly broken by the Pauli term, channels outside our two-dimensional NJL subspace are generated in (4.32). To further comment on such terms, we consider the 1PI Feynman diagrams described by these cubic terms (Figure 4.2). In particular, Figure 4.2(a) depicts the exchange of a Pauli-coupled photon between different flavors. The even number of Dirac matrices on each fermion line generates the scalar Gross-Neveu $\left(\bar{\psi}^a \psi^a\right)\left(\bar{\psi}^b \psi^b\right)$ scalar channel, violating chiral symmetry.

On the contrary, the chiral-invariant exchange of a Pauli-coupled photon between the same flavor contributes non-diagonally to the RG flow in the (V $\pm$ A) basis, such that λ_+ in Figure 4.2(b) contributes solely to the RG flow of λ_-, and vice versa. This is because the γ_5 at the four-fermion vertex anticommutes with each of the three gamma matrices from the propagator and the Pauli vertex further along the fermion line. This coupling between the flows of $\lambda_\pm$ is thus not captured in the single-channel model $\lambda_- = 0$.

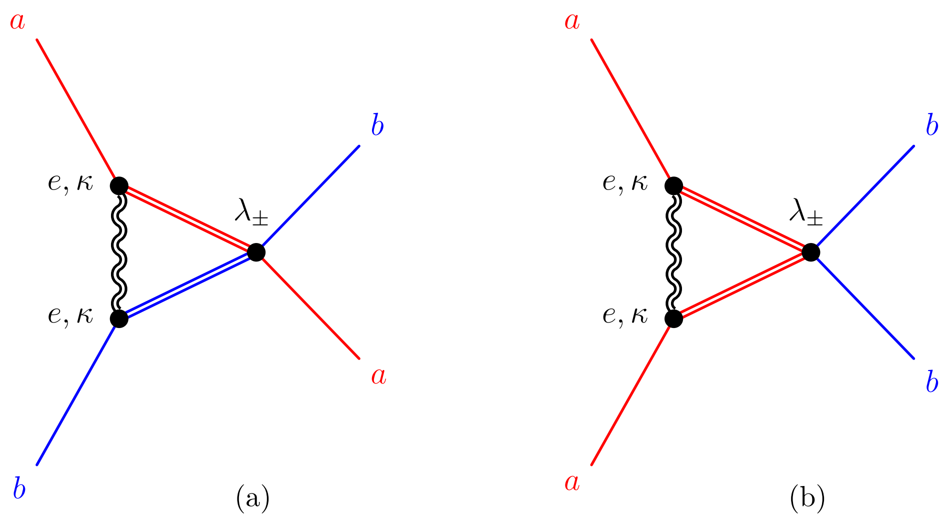

Figure 4.2: 1PI Feynman diagrams representing the cubic terms in the expansion (4.15) of the one-loop Wetterich equation, with the double lines representing full propagators. Diagrams 4.2(a)/4.2(b), depicting the exchange of a photon between different/identical flavors, respectively violates/respects chiral symmetry, in agreement with the number of Dirac matrices along each fermion line. Moreover, diagram (b) couples the RG flows of $\lambda_\pm$, such that λ_+ in this diagram contributes exclusively to the RG flow of λ_-, and vice versa.

In the absence of a Fierz-complete basis in the larger space of all four-fermion interactions (chirally invariant or not), the choice of terms to retain or discard is somewhat arbitrary. For example, we can decompose the scalar channel as

$$
(\mathrm{S}) = (\mathrm{S} + \gamma \mathrm{V} \pm \gamma \mathrm{A}) - \gamma\,(\mathrm{V} \pm \mathrm{A})\,, \tag{4.35}
$$

for any arbitrary $\gamma \in \mathbb{R}$. In the face of this Fierz ambiguity, we adopt a "maximal subtraction" prescription and simply discard any contributions which do not reside entirely within the two-dimensional NJL theory subspace. This prescription is unambiguous as it preserves the chirally invariant subspace.

4.4 Terms of $\mathcal{O}\left(\bar{e}^4, \bar{e}^2\bar{\kappa}^2, \bar{\kappa}^4\right)$

As for the quartic terms of the expansion (4.15),

$$
\left(\frac{1}{\mathcal{P}_k}\mathcal{F}_k\right)^4 \tag{4.36}
$$

$$
= \begin{pmatrix}
\begin{array}{l} \frac{4}{p^2 P_F P_B^2} P^{\perp}_{\mu\nu} P^{\perp}_{\alpha\beta} \left(\bar{e}^4 - 8\bar{e}^2\bar{\kappa}^2 p^2 + 16\bar{\kappa}^4 (p^2)^2\right) \\ \epsilon^{\alpha\mu\rho\sigma}\epsilon^{\epsilon\beta\gamma\delta} p_\sigma p_\delta \left(\bar{\psi}^a\gamma_\rho\gamma_5\psi^a\right)\left(\bar{\psi}^b\gamma_\gamma\gamma_5\psi^b\right) \end{array} & & \\
 & \begin{array}{c} \mathcal{O}\left(\bar{e}^4\right) \\ \mathcal{O}\left(\bar{e}^2\bar{\kappa}^2\right) \\ \mathcal{O}\left(\bar{\kappa}^4\right) \end{array} & \\
 & & \begin{array}{c} \mathcal{O}\left(\bar{e}^4\right) \\ \mathcal{O}\left(\bar{e}^2\bar{\kappa}^2\right) \\ \mathcal{O}\left(\bar{\kappa}^4\right) \end{array}
\end{pmatrix} \delta_{p,p'}\,,
$$

where the abbreviated fermionic elements collectively give the same term as the bosonic entry upon transposition, resulting in an overall factor of 2 in the supertrace:

$$
\begin{aligned}
&-\frac{1}{8}\mathrm{STr}\left\{\tilde{\partial}_t\left(\frac{1}{\mathcal{P}_k}\mathcal{F}_k\right)^4\right\}\Bigg|_{\bar{e}^4,\,\bar{e}^2\bar{\kappa}^2,\,\bar{\kappa}^4} \qquad (4.37)\\
&= \Omega\int_p \left(\bar{e}^4 - 8\bar{e}^2\bar{\kappa}^2 p^2 + 16\bar{\kappa}^4 (p^2)^2\right)\frac{p_\sigma p_\delta}{p^2}\tilde{\partial}_t\left(\frac{1}{P_F P_B^2}\right) P^{\perp}_{\mu\nu} P^{\perp}_{\alpha\beta}\\
&\qquad \epsilon^{\mu\alpha\rho\sigma}\epsilon^{\nu\beta\gamma\delta}\left(\bar{\psi}^a\gamma_\rho\gamma_5\psi^a\right)\left(\bar{\psi}^b\gamma_\gamma\gamma_5\psi^b\right)\\
&= 3\Omega\, k^{-2}\, v_4\, l_4^{(\mathrm{B}^2,\,\mathrm{F})}(0,0)\,\bar{e}^4 - 24\Omega\, v_4\, l_4^{(1,\,\mathrm{B}^2,\,\mathrm{F})}(0,0)\,\bar{e}^2\bar{\kappa}^2 + 48\Omega\, k^2\, v_4\, l_4^{(2,\,\mathrm{B}^2,\,\mathrm{F})}(0,0)\,\bar{\kappa}^4\\
&\qquad \left[(\mathrm{V}+\mathrm{A}) - (\mathrm{V}-\mathrm{A})\right].
\end{aligned}
$$

Along with the relations of the previous sections 4.2 and 4.3, we use a generalization of the argument behind (4.34), such that only the momentum-independent terms of the two projectors give rise to non-vanishing contributions upon contraction with the Levi-Civita symbols.

The terms of this order correspond to the *box diagrams* of Figure 4.3, which only survive upon momentum integration for even powers of $\bar{e}$ and $\bar{\kappa}$. The Gross-Neveu channel dropped in (4.24) is generated by the even number of Dirac matrices associated with one gauge and one Pauli vertex on the same fermion line. No other chirally asymmetric channels are induced, as all other placements of an even number of gauge and Pauli vertices results in an odd number of Dirac matrices on each line.

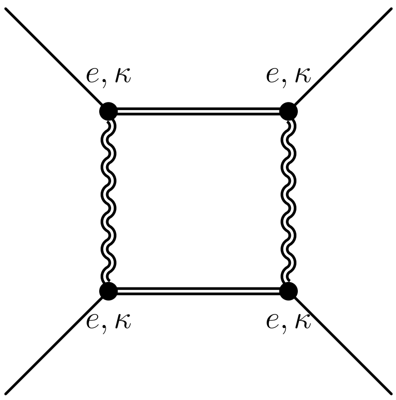

Figure 4.3: 1PI Feynman diagrams representing the quartic terms in the expansion (4.15) of the one-loop Wetterich equation, with the double lines representing full propagators. The chiral-symmetry-breaking Gross-Neveu channel is generated by diagrams with one gauge and one Pauli vertex on each fermion line, associated with four Dirac matrices.

Through such box diagrams, four-fermion interactions may be generated even if the couplings λ are set to vanish in the UV. Combined with the 1PI diagram 4.2 (absent in the single-channel approximation), all ladder and crossed-ladder diagrams are resummed [79, 80].

4.5 Four-Fermion Couplings Flow Equations

Meanwhile, substitution of the homogeneous background fields (4.7) simplifies the four-fermion terms in the left-hand side of the Wetterich equation (4.15) to

$$\partial_t \Gamma_k = \frac{1}{2}\Omega \sum_{\pm} \partial_t \lambda_{\pm} (\mathrm{V} \pm \mathrm{A}). \tag{4.38}$$

Equating this to terms from (4.25), (4.31), (4.32) and (4.37) and defining the renormalized dimensionless couplings

$$\lambda_{\pm} = \frac{k^2 \bar{\lambda}_{\pm}}{Z_{\psi}^2}, \qquad e = \frac{\bar{e}}{Z_{\psi}\sqrt{Z_A}}, \qquad \kappa = \frac{k\bar{\kappa}}{Z_{\psi}\sqrt{Z_A}}, \tag{4.39}$$

the beta functions of the four-fermion couplings are given by

$$\begin{aligned}\partial_t \lambda_{+} = &(2 + 2\eta_{\psi})\, \lambda_{+} + 4v_4\, l_4^{(\mathrm{F})}(0,0) \left[6\lambda_{+}^2 + (d_{\gamma} N_f + 4)\, \lambda_{+}\lambda_{-}\right] \\ &- 24v_4\, l_4^{(\mathrm{B,F})}(0,0)\, e^2 \lambda_{+} - 48v_4\, l_4^{(1,\mathrm{B,F})}(0,0)\, \kappa^2 \lambda_{-} \\ &+ 6v_4\, l_4^{(\mathrm{B}^2,\mathrm{F})}(0,0)\, e^4 - 48v_4\, l_4^{(1,\mathrm{B}^2,\mathrm{F})}(0,0)\, e^2\kappa^2 + 96v_4\, l_4^{(2,\mathrm{B}^2,\mathrm{F})}(0,0)\, \kappa^4,\end{aligned} \tag{4.40}$$

$$\begin{aligned}\partial_t \lambda_{-} = &(2 + 2\eta_{\psi})\lambda_{-} + 2v_4\, l_4^{(\mathrm{F})}(0,0) \left[(d_{\gamma} N_f - 4)\, \lambda_{-}^2 + d_{\gamma} N_f \lambda_{+}^2\right] \\ &+ 24v_4\, l_4^{(\mathrm{B,F})}(0,0)\, e^2 \lambda_{-} - 48v_4\, l_4^{(1,\mathrm{B,F})}(0,0)\, \kappa^2 \lambda_{+} \\ &- 6v_4\, l_4^{(\mathrm{B}^2,\mathrm{F})}(0,0)\, e^4 + 48v_4\, l_4^{(1,\mathrm{B}^2,\mathrm{F})}(0,0)\, e^2\kappa^2 - 96v_4\, l_4^{(2,\mathrm{B}^2,\mathrm{F})}(0,0)\, \kappa^4.\end{aligned} \tag{4.41}$$

We will analyse the implications of these flow equations in the next chapter 5.

Chapter 5

Analysis

Having derived the flow equations (4.40) and (4.41), we now consider the RG flow of the NJL sector in the vicinities of the Pauli-induced UV fixed points $\mathcal{B}$ and $\mathcal{C}$ (see Table 3.1), in which an asymptotically safe trajectory remains for infinite RG time. We thus neglect the flow in the gauge/Pauli sectors, though (e^*, κ^*, m^*) may still be tuned by varying the number of fermion flavors N_f (at least at fixed point $\mathcal{B}$). This analysis provides first indications as to whether such asymptotic safety scenarios for QED are compatible with the light fermions of the Standard Model. We will also be interested in how the number of physical parameters for each universality class $\mathcal{B}/\mathcal{C}$ is altered by the inclusion of the dimension-6 NJL operators.

5.1 Single-Channel Model

For simplicity, we start again with a single-channel approximation, setting $\lambda_- = 0$ and investigating the fate of the fixed point structure illustrated in Figure 3.5. We first focus on the non-Gaussian fixed point $\mathcal{C}(e^* = 0, \kappa^* = 3.82, m^* = 0)$, which can be connected to phenomenological values of the fine-structure constant and anomalous magnetic moment of the electron (see Section 3.1). The following analysis applies also to the $\mathbb{Z}_2$ reflection of $\mathcal{C}$, since the beta function (4.40) is even in κ.

In the neighborhood of $\mathcal{C}$, we can neglect the fermion mass and assume that the asymptotically safe trajectory remains within the massless regime for a large range of scales, as have been constructed in [3]. The Pauli term is then the only source of explicit chiral symmetry breaking. As we saw in Chapter 4, this generates an additional Gross-Neveu channel outside the two-dimensional NJL theory subspace, which would otherwise be consistent with an $SU(N_f)_L \times SU(N_f)_R$ symmetry. For this analysis, we assume such terms to remain irrelevant and concentrate only on the possibility of mass generation by the NJL channels.

For the vanishing gauge coupling $e^* = 0$ at $\mathcal{C}$, (4.40) simplifies to

$$\partial_t \lambda_+ = (2 + 2\eta_\psi^*)\,\lambda_+ + 24 v_4\, l_4^{(\mathrm{F})}(0,0)\lambda_+^2 + 96 v_4\, l_4^{(2,\,\mathrm{B}^2,\,\mathrm{F})}(0,0)\,\kappa^{*4}. \tag{5.1}$$

With the non-diagonal contribution of diagram 4.2(b) to the RG flow in the (V ± A) basis, the finite Pauli coupling manifests only in the term associated with the box diagram 4.3. As would also be the case for a nonvanishing gauge coupling e^*, the net effect is a constant upward shift of the convex beta function, allowing for the possibility of a fixed-point collision and annihilation in a saddle-node bifurcation (Figure 5.1). As alluded to in Section 3.2.2, it has been shown by bosonization that a divergent λ_+ corresponds to the formation of a chiral condensate $\langle \bar{\psi}\psi \rangle$, with scalar and pseudoscalar (pionic) excitations evocative of low-energy QCD phenomenology.

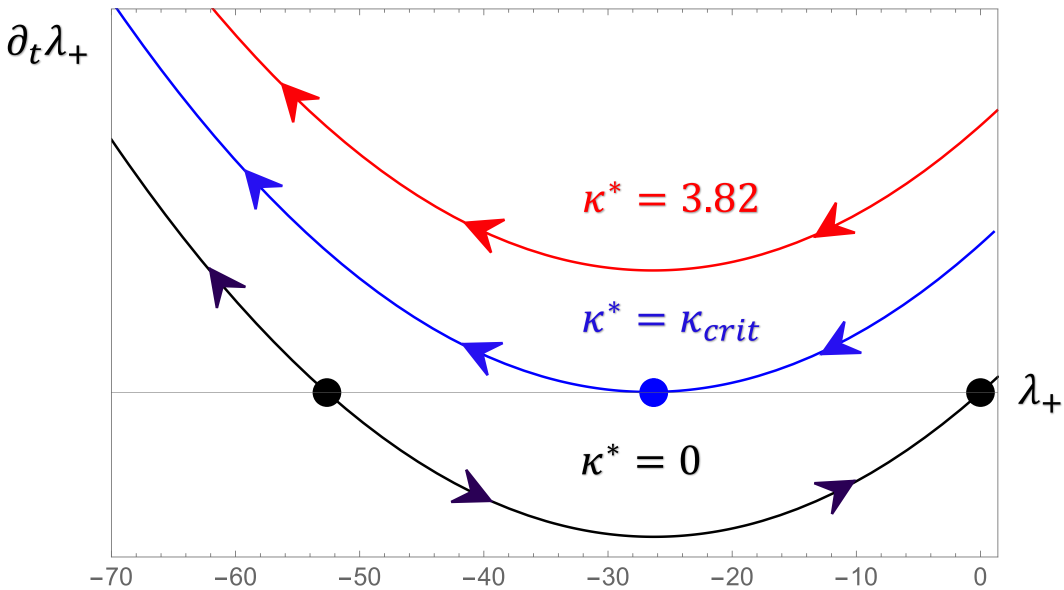

Figure 5.1: The two fixed points (black dots) of the (V + A) channel annihilate at a critical value $\kappa_{\mathrm{crit}} \approx 3.28$ of the Pauli coupling (blue dot). Above this value, the NJL operator becomes relevant, signaling dynamical generation of mass at the scale where the coupling diverges.

5.1.1 Vanishing Anomalous Dimension

In the leading order, we neglect the anomalous dimension $\eta_\psi = -\partial_t \ln Z_\psi$. The beta function (5.1) then exhibits two fixed points as long as

$$1 - 2304 v_4^2\, \kappa^{*4}\, l_4^{(\mathrm{F})}(0,0)\, l_4^{(2,\,\mathrm{B}^2,\,\mathrm{F})}(0,0) > 0 \qquad \Longrightarrow \qquad |\kappa^*| < \kappa_{\mathrm{crit}} = \sqrt[4]{\frac{32}{27}}\pi \approx 3.28, \quad (5.2)$$

where we have evaluated the optimized regulators as enumerated in Appendix 6. This condition is evidently not satisfied at fixed point $\mathcal{C}\,(\kappa^* = 3.82)$. In the absence of an IR attractor, the NJL channel becomes relevant regardless of the initial UV value. As discussed in Section 3.2.2, mass is dynamically generated at the scale where the four-fermion coupling λ_+ diverges, in contradistinction to the small fermion masses observed in the Standard Model. Since the single-channel beta function is independent of flavor number N_f, as is the fixed point $\mathcal{C}$, the conclusion is the same for all values of N_f.

As for fixed point $\mathcal{B}$, we can explore its consistency by including a finite fermion mass m^* in the regulators of the beta function (5.1). Neglecting that this additional source of χSB generates additional terms in the beta function, the only role of the mass is then to decouple the fermions from the RG flow, such that stronger interactions are required to induce criticality. In terms of Figure 5.1, the finite m^* reduces the shift of the beta function due to the Pauli coupling κ^* and decreases the curvature of the parabola such that the two fixed points are spaced further apart, possibly avoiding bifurcation at $\mathcal{B}$. The condition analogous to (5.2) for the irrelevance of the NJL operator reads

$$4 - \frac{9(2m^{*2}+3)\kappa^{*4}}{8\pi^4\,(m^{*2}+1)^4} > 0, \qquad (5.3)$$

which is not satisfied by the fixed point $\mathcal{B}(\kappa^* = 5.09, m^* = 0.328)$. For larger N_f, this is further exacerbated as the Pauli coupling κ^* grows and the suppressive effect of m^* decreases. Therefore, at least at leading order in the single-channel approximation, both UV fixed points $\mathcal{B}$ and $\mathcal{C}$ trigger dynamical mass generation close to the initial UV scale.

5.1.2 Non-Vanishing Anomalous Dimension

Beyond the leading order, we take into account the anomalous dimension $\eta_\psi^* = -1$ at fixed point $\mathcal{C}$, which would result in a marginally relevant Pauli coupling as required by (3.9) (though the 1PI diagrams associated with each threshold function generate further quantum fluctuations and result in relevance). With no contributions from four-fermion terms in the point-like limit (see Figure 3.4(b)), the same value of $\eta_\psi^* = -1$ significantly alters the structure of the beta function (5.1). In particular, the vanishing scaling term (linear in λ_+) renders the NJL coupling marginal at the (only) Gaussian fixed point, highly susceptible to fluctuations due to the Pauli term. We see that any finite coupling κ^* removes the IR (saddle-node) fixed point and renders the channel relevant, again culminating in dynamical mass generation.

In the vicinity of fixed point $\mathcal{B}$, the even larger (negative) anomalous dimension $\eta_\psi^* = -1.38$ renders λ_+ relevant at the NJL Gaussian fixed point, such that the RG flow develops a non-trivial IR fixed point. Regardless of whether we take into account higher-order resummations through the appearance of anomalous dimensions $\eta_{\psi,\,A}^*$ in the regulators, the fixed point is annihilated at the large Pauli coupling $\kappa^* = 5.09$ at $\mathcal{B}$. This same observation applies to $N_f > 1$. While the growth in η_A^* with increasing N_f tends to result in a smaller coefficient of the Pauli term in (5.1), this is offset by increases in κ^* and η_ψ^*, as well as a decrease in the dimensionless mass m^*. Thus, our conclusions regarding the viability of fixed points $\mathcal{B}$ and $\mathcal{C}$ remain unchanged from the leading order.

5.2 Two-Channel Model

While the conclusions of the previous Section 5.1 may seem inauspicious for the premise of Pauli-induced asymptotic safety scenarios, we highlight two pecularities of the single-channel model. Firstly, it is independent of flavor number N_f, since diagram 4.1(c) does not contribute to self-correction terms $\sim \lambda_+^2$ in the beta function (4.40). By extending the truncation to include also the $(\mathrm{V}-\mathrm{A})$ channel, the flavor number serves as an additional parameter in the search for consistent asymptotic safety scenarios.

Moreover, by setting $\lambda_- = 0$, the role of diagram 4.2(b) in coupling the RG flows of $\lambda_\pm$ is overlooked and the only effect of a finite Pauli coupling is to bring the NJL fixed points closer together towards bifurcation. This is only exacerbated with the anomalous dimension $\eta_\psi = -1$ rendering the NJL couplings perturbatively marginal and the ensuing instability of fixed points against further quantum fluctuations. However, from the beta functions for both $(\mathrm{V}\pm\mathrm{A})$ channels (for the irreducible representation of the Dirac algebra with $d_\gamma = 4$)

$$\begin{aligned}\partial_t\lambda_+ = {} & (2+2\eta_\psi)\,\lambda_+ + 8v_4\, l_4^{(\mathrm{F})}(0,0)\left[3\lambda_+^2 + 2\,(N_f+1)\,\lambda_+\lambda_-\right] \\ & - 48v_4\, l_4^{(1,\,\mathrm{B},\,\mathrm{F})}(0,0)\,\kappa^{*2}\lambda_- + 96v_4\, l_4^{(2,\,\mathrm{B}^2,\,\mathrm{F})}(0,0)\,\kappa^{*4},\end{aligned} \tag{5.4}$$

$$\begin{aligned}\partial_t\lambda_- = {} & (2+2\eta_\psi)\lambda_- + 8v_4\, l_4^{(\mathrm{F})}(0,0)\left[(N_f-1)\,\lambda_-^2 + N_f\lambda_+^2\right] \\ & - 48v_4\, l_4^{(1,\,\mathrm{B},\,\mathrm{F})}(0,0)\,\kappa^{*2}\lambda_+ - 96v_4\, l_4^{(2,\,\mathrm{B}^2,\,\mathrm{F})}(0,0)\,\kappa^{*4},\end{aligned} \tag{5.5}$$

we observe that by allowing for mutual feedback within the two-dimensional flow of $\lambda_\pm$, a linear term $\sim \kappa^{*2}\lambda_\mp$ is restored in the presence of a finite Pauli coupling κ^*. Such terms (represented by diagram 4.2(b)) enable the resummation of all ladder and crossed-ladder diagrams and turn out to play an essential role in preventing fixed point annihilations. As for the gauge coupling e, the box diagram terms $\sim \kappa^{*4}$ contribute with opposite signs to the flows of $\lambda_\pm$.

5.2.1 Vanishing Anomalous Dimension

Single Fermion Flavor at $\mathcal{C}$

To appreciate the consequence of a finite Pauli coupling κ^* as opposed to gauge coupling e^*, we first consider the leading order approximation $\eta_\psi = 0$ at fixed point $\mathcal{C}$. The missing quadratic λ_-^2 term from the λ_- beta function (5.5) for $N_f = 1$ allows for simple substitution into the λ_+ beta function, resulting in the cubic equation

$$\frac{1}{32\pi^4}\lambda_+^3 - \left(\frac{5\kappa^{*2}}{16\pi^4} + \frac{3}{8\pi^2}\right)\lambda_+^2 - \left(\frac{\kappa^{*4}}{16\pi^4} + 2\right)\lambda_+ + \frac{9\kappa^{*6}}{8\pi^4} - \frac{9\kappa^{*4}}{4\pi^2} = 0, \tag{5.6}$$

with three fixed points

$$\begin{aligned}
\mathcal{F}_1^{\text{Gauss}} &= \left(8\pi^2 + 4\kappa^{*2} - \sqrt{34\kappa^{*4} + 64\pi^2\kappa^{*2} + 64\pi^4}, -8\pi^2 - 4\kappa^{*2} + \sqrt{34\kappa^{*4} + 64\pi^2\kappa^{*2} + 64\pi^4}\right),\\
\mathcal{F}_2 &= \left(-4\pi^2 + 2\kappa^{*2}, -\pi^2 - \kappa^{*2} + \frac{15\kappa^{*4}}{8\pi^2}\right), \qquad (5.7)\\
\mathcal{F}_3 &= \left(8\pi^2 + 4\kappa^{*2} + \sqrt{34\kappa^{*4} + 64\pi^2\kappa^{*2} + 64\pi^4}, -8\pi^2 - 4\kappa^{*2} - \sqrt{34\kappa^{*4} + 64\pi^2\kappa^{*2} + 64\pi^4}\right).
\end{aligned}$$

The fixed points $\mathcal{F}_1$ and $\mathcal{F}_2$ collide at $\kappa_{\text{crit}} \approx 3.70$, analogously to the single-channel model where $\kappa_{\text{crit}} \approx 3.28$. However, instead of annihilating each other in a saddle-node bifurcation, $\mathcal{F}_1$ and $\mathcal{F}_2$ persist for all values of κ^* and instead exchange IR stability in a transcritical bifurcation. This is solely due to the presence of the non-diagonal terms $\kappa^{*2}\lambda_\pm$, which results in a positive-definite discriminant in (5.6) except at κ_{crit}, as opposed to an indefinite discriminant for the analogous cubic equation with e^*.

At fixed point $\mathcal{C}$ with $\kappa^* \approx 3.82$, $\mathcal{F}_2$ becomes fully attractive (see Table 5.1), though the proximity of κ^* to the bifurcation at κ_{crit} results in $\mathcal{F}_1$ and $\mathcal{F}_2$ being hardly distinguishable in the phase diagram of Figure 5.2. The separatrix connecting $\mathcal{F}_1$ and $\mathcal{F}_3$ remains intact, separating the chirally broken phase Ib and the chirally symmetric phase II, while $\mathcal{F}_4$ at infinity no longer connects to $\mathcal{F}_2$. The existence of such an IR attractor thus allows the Pauli-induced fixed point $\mathcal{C}$ to avoid dynamical mass generation by initializing the RG flow in phase II of Figure 5.2, without adding any further physical parameters to the three already associated to the universality class.

Moreover, a possible UV completion in the NJL sector is provided by the trajectory from $\mathcal{F}_1$. This comes at the expense of introducing a relevant NJL coupling, which should reflect fermion-fermion scattering amplitudes in the IR. As outlined in Chapter 6, non-trivial fixed points of purely fermionic NJL models in $d = 4$ often represent artefacts of the point-like limit. With a relatively small positive critical exponent indicating weak quantum corrections, $\mathcal{F}_1$ would hold some promise of surviving a resolution of momentum dependence, but the fixed point structure is already drastically altered by the inclusion of $\eta_\psi^* = -1$, as we shortly discuss in Section 5.2.2.

Table 5.1: NJL fixed points for $N_f = 1$ flavor at $\mathcal{C}$ in leading order approximation $\eta_\psi = 0$.

	$(\lambda_+^*, \lambda_-^*)$	Critical Exponents	Eigendirections
$\mathcal{F}_1$	$\begin{pmatrix}-13.3\\13.3\end{pmatrix}$	$(0.153, -3.82)$	$\begin{pmatrix}0.707\\0.707\end{pmatrix} \begin{pmatrix}0.645\\-0.764\end{pmatrix}$
$\mathcal{F}_2$	$\begin{pmatrix}-10.3\\16.0\end{pmatrix}$	$(-0.149, -3.88)$	$\begin{pmatrix}0.679\\0.734\end{pmatrix} \begin{pmatrix}0.685\\-0.729\end{pmatrix}$
$\mathcal{F}_3$	$\begin{pmatrix}288\\-288\end{pmatrix}$	$(3.82, -15.1)$	$\begin{pmatrix}0.406\\-0.914\end{pmatrix} \begin{pmatrix}0.707\\0.707\end{pmatrix}$

Multiple Fermion Flavors at $\mathcal{C}$

As for $N_f > 1$, the picture is similar, in spite of the fully IR repulsive fixed point $\mathcal{F}_4$ coming from infinity (see Table 5.2 and Figure 5.3 for the case $N_f = 2$). Once again, $\mathcal{F}_1$ and $\mathcal{F}_2$ collide and exchange stability at a critical value of the Pauli coupling κ_{crit} which increases gradually with the number N_f of fermion flavors. Extending to non-integer values of N_f by analytic continuation, we define a critical flavor number $N_{f,\,\text{crit}} \approx 5.25$ where the Pauli coupling $\kappa^* = \kappa_{\text{crit}} = 3.82$ at fixed point $\mathcal{C}$ is barely sufficient to induce the bifurcation between fixed points $\mathcal{F}_1$ and $\mathcal{F}_2$.

At even larger N_f, $\mathcal{F}_1$ is the IR attractive fixed point, though $\mathcal{F}_2$ (with one relevant direction) remains in close proximity. The phase diagram is then qualitatively akin to Figure 3.7. As such, there appears to be a one-dimensional set of asymptotically safe trajectories emanating from the purely repulsive $\mathcal{F}_4$, in addition to the two trajectories from $\mathcal{F}_2$ and $\mathcal{F}_3$. However, with critical exponents as large as $\theta_{\max} \approx 6$, the large deviations from canonical scaling at these prospective UV fixed points suggest they may not remain after partial bosonization. As N_f increases, $\mathcal{F}_3$ and $\mathcal{F}_4$ also approach each other but

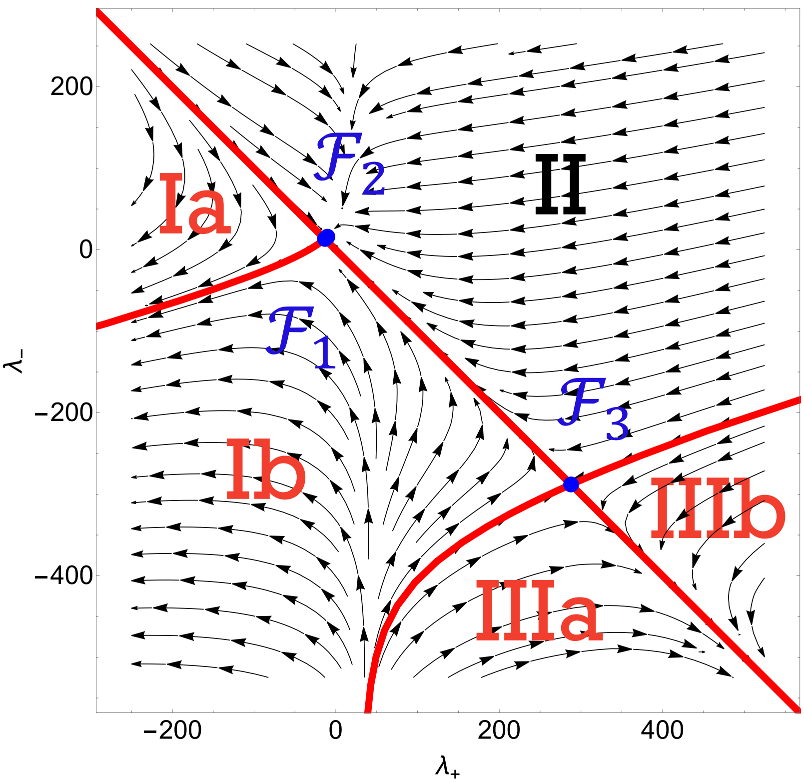

Figure 5.2: NJL phase diagram for $N_f = 1$ in the vicinity of fixed point $\mathcal{C}$ with Pauli coupling $\kappa^* = 3.82$. At leading order, the fermionic anomalous dimension $\eta_\psi = 0$ has been neglected. UV values of $\lambda_\pm^{\rm UV}$ within region II (labelled in black) are attracted towards the IR-attractive fixed point $\mathcal{F}_2$ (blue dot), avoiding dynamical generation of Planck scale fermion masses.

undergo no collision at finite N_f.

Table 5.2: NJL fixed points for $N_f = 2$ flavor at $\mathcal{C}$ in leading order approximation $\eta_\psi = 0$.

	$(\lambda_+^*, \lambda_-^*)$	Critical Exponents	Eigendirections
$\mathcal{F}_1$	$\begin{pmatrix}-12.3\\12.3\end{pmatrix}$	$(0.102, -4.41)$	$\begin{pmatrix}0.707\\0.707\end{pmatrix}\begin{pmatrix}0.657\\-0.754\end{pmatrix}$
$\mathcal{F}_2$	$\begin{pmatrix}-10.9\\13.5\end{pmatrix}$	$(-0.101, -4.44)$	$\begin{pmatrix}0.696\\0.718\end{pmatrix}\begin{pmatrix}0.672\\-0.741\end{pmatrix}$
$\mathcal{F}_3$	$\begin{pmatrix}104\\-104\end{pmatrix}$	$(4.41, -5.78)$	$\begin{pmatrix}0.508\\-0.861\end{pmatrix}\begin{pmatrix}0.707\\0.707\end{pmatrix}$
$\mathcal{F}_4$	$\begin{pmatrix}29.3\\-187\end{pmatrix}$	$(10.0, 2.75)$	$\begin{pmatrix}0.995\\-0.102\end{pmatrix}\begin{pmatrix}4.88\times10^{-4}\\1.00\end{pmatrix}$

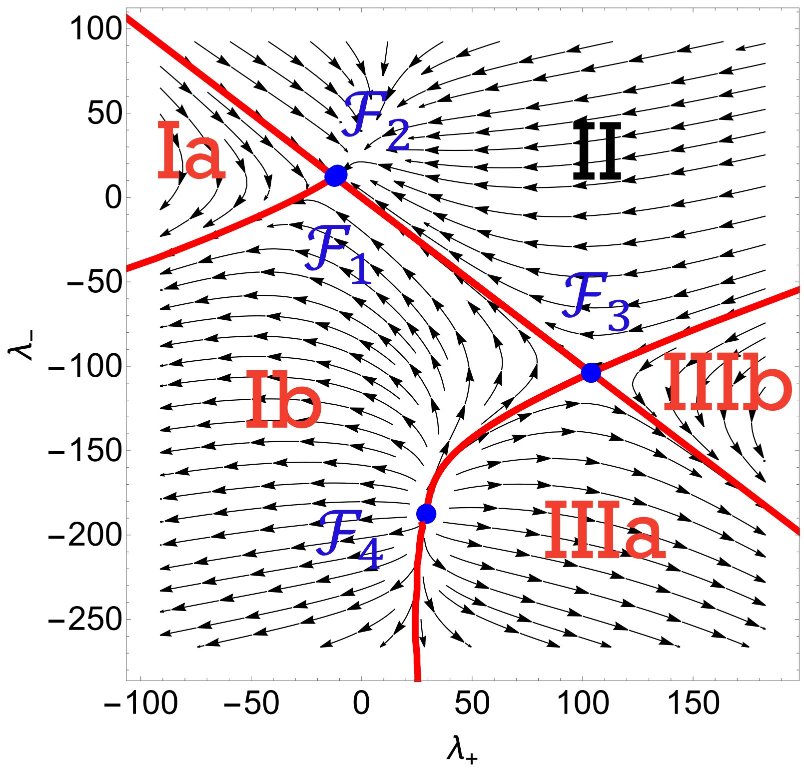

Figure 5.3: NJL phase diagram for $N_f = 2$ in the vicinity of fixed point $\mathcal{C}$ with Pauli coupling $\kappa^* = 3.82$. At leading order, $\eta_\psi = 0$ has been neglected. UV values of $\lambda_\pm^{\mathrm{UV}}$ within region II (labelled in black) are attracted towards the IR-attractive fixed point $\mathcal{F}_2$ (blue dot), avoiding dynamical generation of Planck scale fermion masses.

Fixed Point $\mathcal{B}$

Turning to the fixed point $\mathcal{B}$, the situation is qualitatively identical to $\mathcal{C}$. The NJL fixed points $\mathcal{F}_1$ and $\mathcal{F}_2$ collide and exchange stability. As with the single-channel model in Section 5.1, the non-zero mass m^* results in a higher critical value of κ_{crit}, which nonetheless remains smaller than κ^*. For large $N_f \approx 18$ (before $\mathcal{B}$ bifurcates away at larger N_f), fixed points $\mathcal{F}_3$ and $\mathcal{F}_4$ approach each other, though the large anomalous dimensions involved ($\eta_\psi^* = -2.65, \eta_A^* = 3.24$) necessitate their inclusion.

5.2.2 Non-Vanishing Anomalous Dimension

Single Fermion Flavor at $\mathcal{C}$

We now turn to the next-to-leading-order contribution from the anomalous dimension $\eta_\psi^* = -1$ at fixed point $\mathcal{C}$. It is evident that with both the linear scaling term $\sim \lambda_-$ and the self-correction term $\sim \lambda_-^2$ vanishing for $N_f = 1$, the remaining term of the beta function 5.5 in the absence of a Pauli term can only accommodate the Gaussian fixed point. The question is then whether a finite Pauli coupling could reintroduce fixed points in the NJL theory subspace.

For finite κ^*, the beta functions 5.4 and 5.5 give rise to two non-trivial fixed points, bifurcating from the Gaussian fixed point at $\kappa^* = 0$:

$$\mathcal{F}_1 = \left(-1.75\kappa^{*2}, 1.75\kappa^{*2}\right), \quad \mathcal{F}_3 = \left(8.89\kappa^{*2}, -8.89\kappa^{*2}\right), \tag{5.8}$$

both of which have one relevant direction. For $\kappa^* = 3.82$ in the vicinity of $\mathcal{C}$, the fixed points and their critical exponents are listed in Table 5.3.

Table 5.3: NJL fixed points for $N_f = 1$ flavor at $\mathcal{C}$ with anomalous dimension $\eta_\psi^* = -1$.

	$(\lambda_+^*, \lambda_-^*)$	Critical Exponents	Eigendirections
$\mathcal{F}_1$	$\begin{pmatrix}-25.5\\25.5\end{pmatrix}$	$(3.14, -2.36)$	$\begin{pmatrix}0.707\\0.707\end{pmatrix}\begin{pmatrix}-0.601\\0.799\end{pmatrix}$
$\mathcal{F}_3$	$\begin{pmatrix}130\\-130\end{pmatrix}$	$(2.36, -6.30)$	$\begin{pmatrix}0.351\\-0.937\end{pmatrix}\begin{pmatrix}-0.707\\-0.707\end{pmatrix}$

Thus, to avoid divergences in the NJL couplings $\lambda_\pm$, we would have to tune the UV values $\lambda_\pm^{\mathrm{UV}}$ to lie on certain separatrices in Figure 5.4, necessitating an additional physical parameter in the asymptotic safety scenario at $\mathcal{C}$. The trajectory directed from $\mathcal{F}_3$ to $\mathcal{F}_1$ also admits a UV completion in the NJL sector, though again the significant deviations from canonical scaling indicate substantial quantum corrections and casts doubt on whether $\mathcal{F}_3$ persists if we resolve the momentum dependence of the NJL couplings $\lambda_\pm(p_1, p_2, p_3)$.

Multiple Fermion Flavors at $\mathcal{C}$

For $N_f > 1$, the non-vanishing leading term $\sim \lambda_-^2$ maintains a similar phase diagram regardless of our treatment of the subleading linear term $\sim \lambda_-$ containing the anomalous

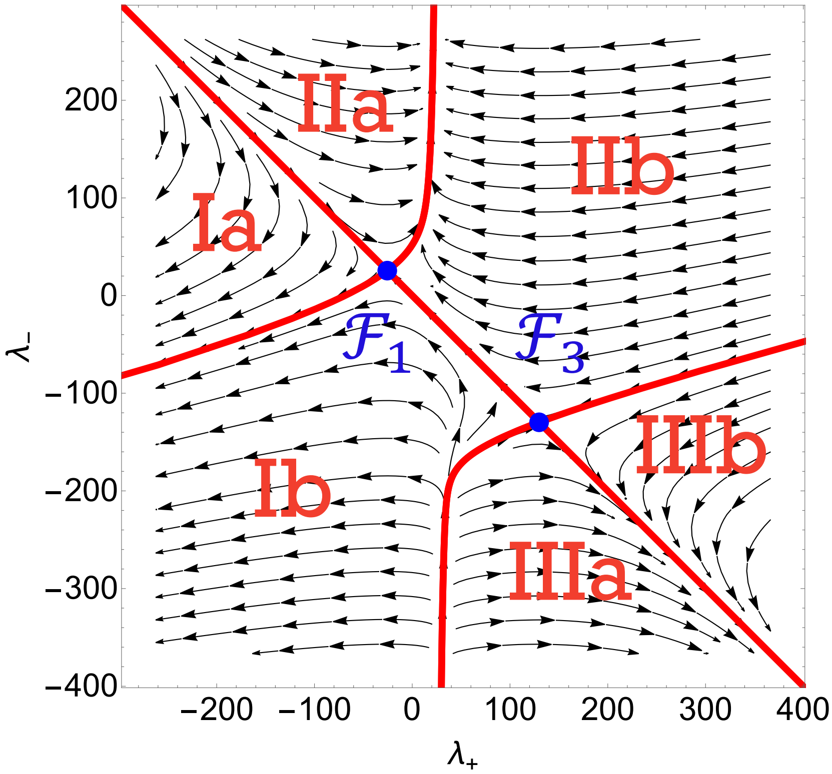

Figure 5.4: NJL phase diagram for $N_f = 1$ in the vicinity of fixed point $\mathcal{C}$ with Pauli coupling $\kappa^* = 3.82$ and fermionic anomalous dimension $\eta_\psi^* = -1$. Dynamical generation of Planck scale fermion masses can only be avoided by tuning the UV values of $\lambda_\pm^{\mathrm{UV}}$ to lie along the appropriate separatrices.

dimension η_ψ^*. In particular, there exist four fixed points whose NJL couplings $\lambda_\pm$ are proportional to κ^{*2}. For $N_f = 2$, these take the values

$$\begin{aligned} \mathcal{F}_1 &= \left(-1.38\kappa^{*2}, 1.38\kappa^{*2}\right), \quad & \mathcal{F}_2 &= \left(0.56\kappa^{*2}, 4.35\kappa^{*2}\right) \\ \mathcal{F}_3 &= \left(3.76\kappa^{*2}, -3.76\kappa^{*2}\right), \quad & \mathcal{F}_4 &= \left(2.35\kappa^{*2}, -4.61\kappa^{*2}\right), \end{aligned} \tag{5.9}$$

with $\mathcal{F}_2$ and $\mathcal{F}_4$ located at infinity for $N_f = 1$. For $N_f = 2$, the fixed points and their critical exponents are given in Table 5.4. As illustrated in Figure 5.5, $\mathcal{F}_2$ attracts the flow throughout phase II, thus maintaining light fermion masses in the IR for the asymptotic safety scenario $\mathcal{C}$. With a two-dimensional IR-critical manifold, no relevant NJL coupling is introduced as an additional physical parameter of the universality class. This persists for all N_f, with the transcritical bifurcation of $\mathcal{F}_3$ and $\mathcal{F}_4$ at $N_f \approx 4.94$, whereupon $\mathcal{F}_3$ becomes IR repulsive. As well as the possible continuum limit at $\mathcal{F}_1$, there now exists a one-dimensional set of UV-complete trajectories flowing from $\mathcal{F}_3$ to $\mathcal{F}_2$ (illustrated more clearly in Figure 5.7 for an analogous scenario at fixed point $\mathcal{B}$), though again the critical exponents are concerningly large.

Table 5.4: NJL fixed points for $N_f = 2$ flavor at $\mathcal{C}$ with $\eta_\psi^* = -1$.

	$(\lambda_+^*, \lambda_-^*)$	Critical Exponents	Eigendirections
$\mathcal{F}_1$	$\begin{pmatrix}-20.1\\20.1\end{pmatrix}$	$(2.81, -3.42)$	$\begin{pmatrix}0.707\\0.707\end{pmatrix} \begin{pmatrix}0.635\\-0.773\end{pmatrix}$
$\mathcal{F}_2$	$\begin{pmatrix}8.15\\63.5\end{pmatrix}$	$(-1.74, -6.72)$	$\begin{pmatrix}0.221\\0.975\end{pmatrix} \begin{pmatrix}0.985\\-0.173\end{pmatrix}$
$\mathcal{F}_3$	$\begin{pmatrix}54.9\\-54.9\end{pmatrix}$	$(3.42, -1.75)$	$\begin{pmatrix}0.456\\-0.890\end{pmatrix} \begin{pmatrix}0.707\\0.707\end{pmatrix}$
$\mathcal{F}_4$	$\begin{pmatrix}34.3\\-67.3\end{pmatrix}$	$(3.53, 1.53)$	$\begin{pmatrix}0.693\\-0.721\end{pmatrix} \begin{pmatrix}0.320\\0.947\end{pmatrix}$

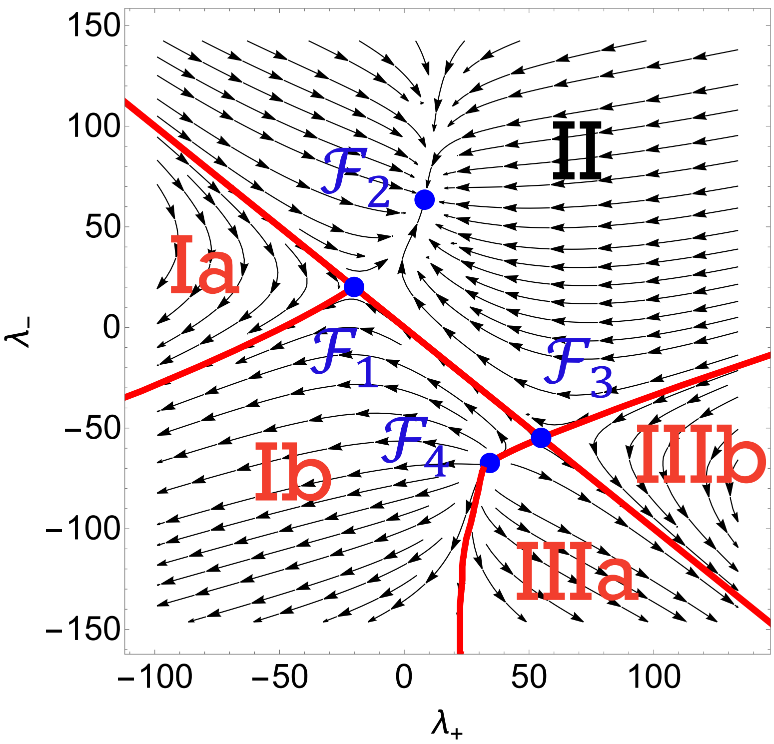

Figure 5.5: NJL phase diagram for $N_f = 2$ in the vicinity of fixed point $\mathcal{C}$ with Pauli coupling $\kappa^* = 3.82$ and fermionic anomalous dimension $\eta_\psi^* = -1$. UV values of $\lambda_\pm^{\text{UV}}$ within region II (labelled in black) are attracted towards the IR-attractive fixed point $\mathcal{F}_2$ (blue dot), avoiding dynamical generation of Planck scale fermion masses.

Fixed Point $\mathcal{B}$

At fixed point $\mathcal{B}$, the large (negative) critical exponent η_ψ^* of the fermion tends to reflect fixed points across the origin and reverse the directions of the RG flow. As a generalization of our discussion of the single-channel approximation in Section 5.1, the Gaussian fixed point $\mathcal{F}_1$ in the absence of a Pauli term is now purely IR repulsive; relevant directions in Figure 3.6 become irrelevant and vice versa. Thus, for $N_f = 1$ there is no purely IR-attractive fixed point. With the large value of η_ψ^* increasing the sizes of the threshold functions, $\mathcal{F}_1$ and $\mathcal{F}_2$ collide and exchange stability at a critical value of only $\kappa_{\text{crit}} \approx 2.76$.

At $N_f > 1$, an additional IR-attractive fixed point $\mathcal{F}_4$ comes from infinity (see Figure 5.6 for the case of $N_f = 2$). This gives rise to a similar phase diagram as for $\mathcal{C}$ in Figure 5.5, though the roles of the various fixed points are interchanged due to the large anomalous dimension $\eta_\psi^* < -1$. For $N_f = 2$, the only asymptotically safe trajectory emanates from $\mathcal{F}_3$ with maximum critical exponent $\theta_{\max} \approx 5$.

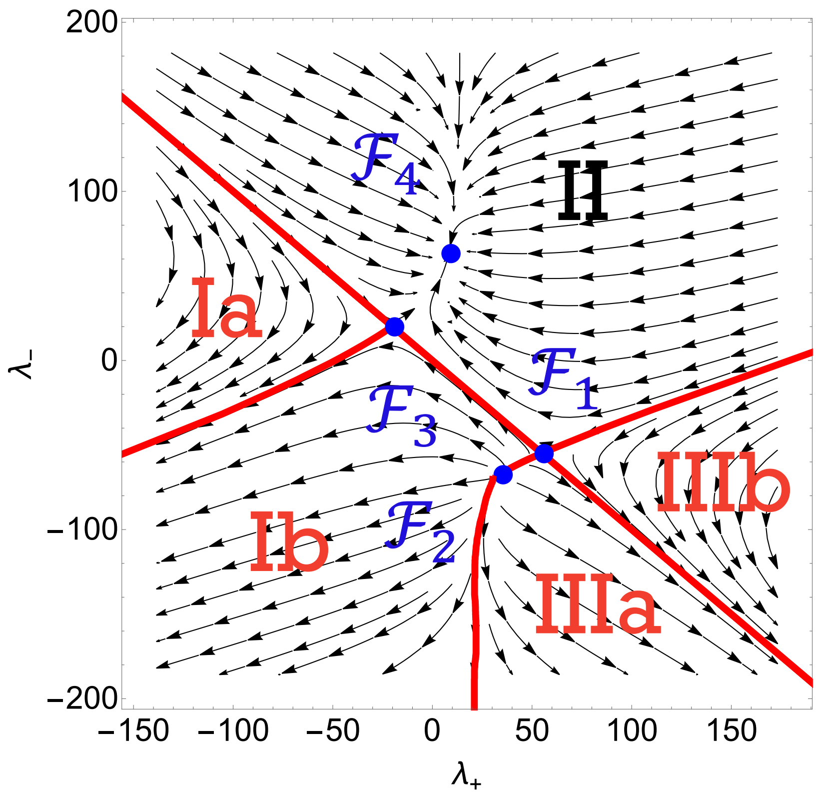

Figure 5.6: Phase diagram for $N_f = 2$ in the vicinity of fixed point $\mathcal{B}$ with Pauli coupling $\kappa^* = 5.19$, (dimensionless) mass $m^* = 0.282$, fermionic and photonic anomalous dimensions $\eta_\psi^* = -1.55, \eta_A^* = 0.904$.

For $N_f \gtrsim 3$, the fixed-point value of the Pauli coupling $\kappa^* < \kappa_{\text{crit}}$ does not exceed the critical value κ_{crit} required for the collision of $\mathcal{F}_1$ and $\mathcal{F}_2$. The significance is that $\mathcal{F}_1$ still behaves as an IR-repulsive fixed point, connected to the attractor $\mathcal{F}_4$. In contrast to the

$N_f = 2$ case, there now exists a one-dimensional set of UV-complete trajectories flowing between the two fixed points, shown in Figure 5.7 for $N_f = 4$. Asymptotic safety at $\mathcal{F}_1$ ($\theta_{\max} \approx 9$) would introduce both NJL couplings as physical parameters in addition to the two associated with $\mathcal{B}$.

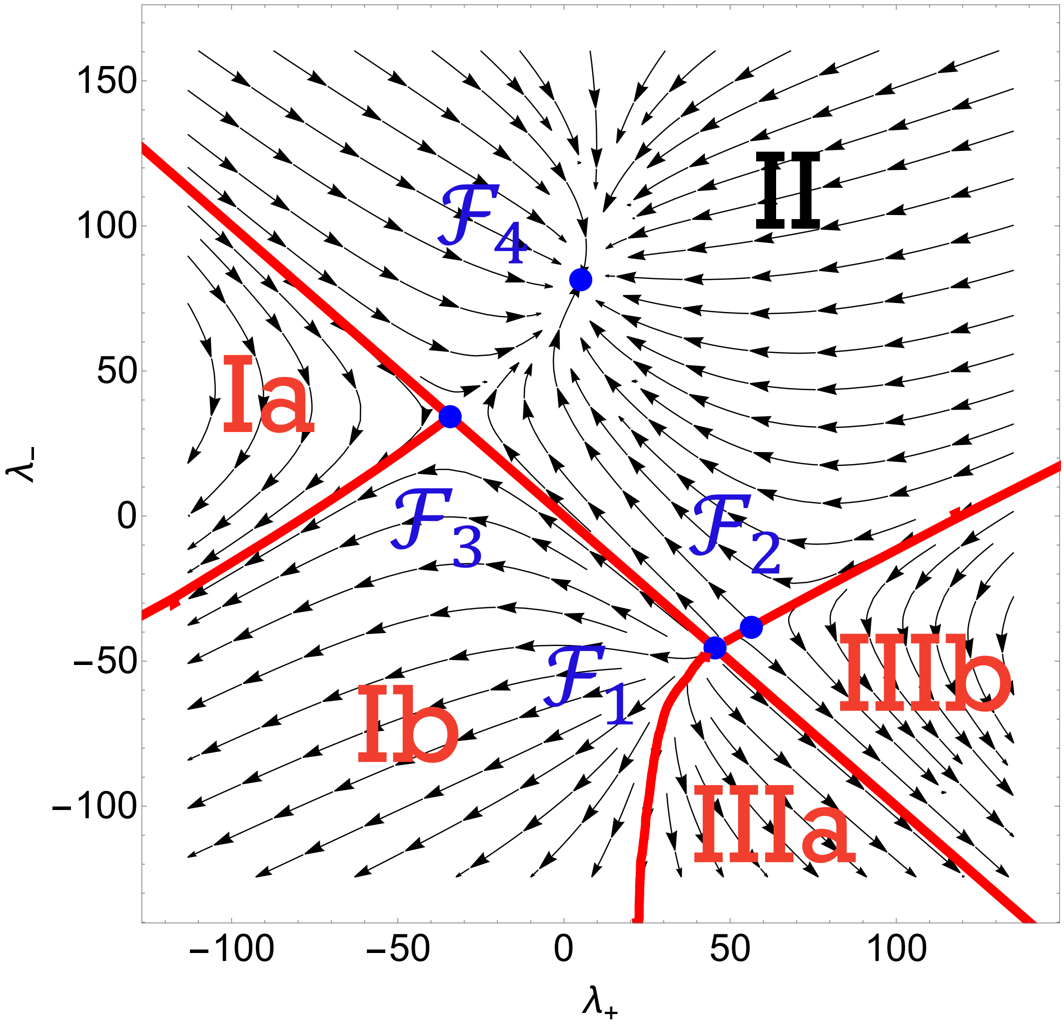

Figure 5.7: Phase diagram for $N_f = 4$ in the vicinity of fixed point $\mathcal{B}$ with Pauli coupling $\kappa^* = 5.35$, (dimensionless) mass $m^* = 0.229$, fermionic and photonic anomalous dimensions $\eta_\psi^* = -1.78, \eta_A^* = 1.41$.

Chapter 6

Conclusion

In summary, the existence of fixed points in the dimension-6 NJL sector may at first glance seem precarious, given the condition from (3.9) that at the level of truncation (3.2), a purely Pauli-induced asymptotic safety scenario $\mathcal{C}$ requires perturbatively marginal NJL couplings $\lambda_{\pm}$. Any fixed point may be maximally susceptible to the finite Pauli coupling κ^* in the first place. Nonetheless, by considering a two-channel NJL model which would be Fierz-complete under an $SU(N_f)_L \otimes SU(N_f)_R$ symmetry broken by the Pauli term, we take into account diagrams for the exchange of a single Pauli-coupled photon, thus resumming the full set of ladder diagrams in the RG flow. The mutual feedback between the RG flows of $\lambda_{\pm}$ significantly affects the phase structure in the NJL sector; instead of a fixed point annihilation at the critical value of the gauge coupling e_{crit}, we merely observe an exchange of stability in the highly non-perturbative regime beyond κ_{crit}.

For more than one flavor, there persists a fully irrelevant fixed point $\mathcal{F}_2$ which attracts the RG flow throughout a light fermion phase II, keeping the NJL couplings finite. This avoids the generation of mass at a large UV scale which would contradict observations of the Standard Model, without adding physical parameters to the three of universality class $\mathcal{C}$. For $N_f = 1$, fixed point $\mathcal{C}$ remains a viable UV completion in the gauge/Pauli sector, but at the expense of introducing a relevant four-fermion coupling which must be tuned to reproduce scattering amplitudes in the IR.

We should note that our characterization of the NJL phase diagram is based entirely on the optimized regulators of Appendix 6, which enable analytic computations. Nonetheless, their non-analytic structures (based on the Heaviside step function and derivatives thereof) may introduce artefacts to the RG flow at higher orders in the derivative expansion. In the present approximation, this is not an issue and other common regulators are expected to result in the same conclusion. Using a family of regulators with control parameters, an application of the principle of minimum sensitivity would additionally allow for an estimate of convergence in physical predictions such as the universal critical exponents [33].

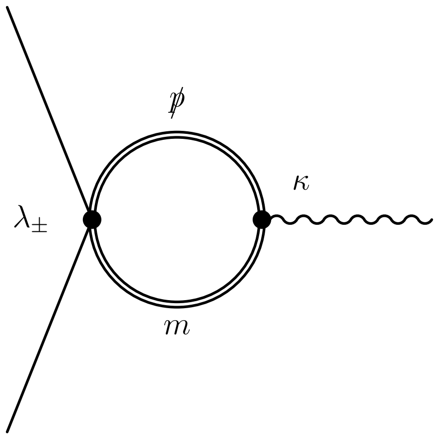

Figure 6.1: Diagram representing feedback from NJL sector to the flow of the gauge coupling e. Since the Pauli vertex is proportional to momentum, the only non-vanishing contribution must pick up mass m dependence from one leg of the fermionic loop.

Another natural line of inquiry would be to take into account the running gauge/Pauli couplings beyond the immediate vicinity of fixed points $\mathcal{B}$ and $\mathcal{C}$. The flow in the Pauli sector is anticipated to receive contributions from the diagram of Figure 6.1. The analogous diagram with the gauge coupling e vanishes at the fixed point due to modified Ward-Takahashi identities [78], but similar arguments are not expected to apply to the gauge-invariant Pauli term $\bar{\psi}\sigma_{\mu\nu}F^{\mu\nu}\psi$. Due to the momentum dependence of the Pauli vertex, diagram 6.1 survives the momentum trace only by picking up mass m dependence from one leg of the fermionic loop. With the Dirac trace of an odd product of gamma matrices vanishing, the only remaining term would be of the form

$$\lambda_\pm \kappa m \, p^\mu A^\nu \left(\bar{\psi}\gamma^\rho \not{p}\, \sigma_{\mu\nu}\gamma_\rho \psi\right) . \tag{6.1}$$

Even without performing the full computation, it is clear that the odd product of gamma matrices in this fermion bilinear can only be projected onto a contribution to the gauge coupling. Thus, the sufficient condition (3.9) for the existence of fixed point $\mathcal{C}$ at vanishing mass and gauge coupling $e^* = m^* = 0$ when $\eta_\psi^* = -1$ remains unchanged, though the critical exponents may change. One can then construct the modified flow trajectories, in an attempt to reproduce phenomenological values of QED.

Moreover, as detailed in Chapter 4, the explicit breaking of chiral symmetry by the Pauli term generates the Gross-Neveu channel outside the NJL subspace. The relevance of this scalar channel remains to be investigated, as well its feedback on the NJL subspace and the potential generation of a tensor channel. Particularly in the neighbourhood of fixed point $\mathcal{B}$, the finite mass m^* provides an additional source of explicit χSB, resulting in many additional terms in the beta functions (4.40) and (4.41). To systematically complete the truncation (4.1) to dimension-6, we can include higher derivative terms such as $\bar{\psi}\not{D}\not{D}\psi$

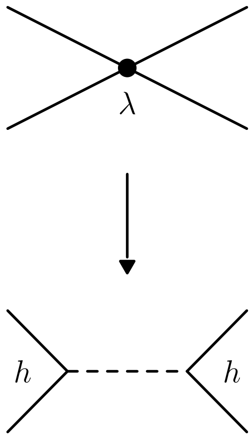

Figure 6.2: Bosonization resolves a four-fermion vertex to be mediated by a Yukawa-coupled boson corresponding to a condensate. The four-fermion coupling λ is then mapped to the ratio of the Yukawa coupling h and the exchanged boson mass.

and $F_{\mu\nu}\Box F^{\mu\nu}$.

It may be of interest to extend asymptotic safety to the NJL sector. As observed in Chapter 5, especially after accounting for the fermionic anomalous dimension $\eta_\psi^* = -1$, the significant deviations from canonical scaling at prospective UV fixed points imply that the non-Gaussian fixed points may be artefacts of the point-like limit in our purely fermionic model, as would be the case in $d = 4$ without the Pauli coupling . As alluded to in Chapter 3, the momentum dependence of four-fermion couplings can be conveniently described by partial bosonization [70]. Introducing composite bosonic fields for the condensates, the four-fermion interaction is then mediated by Yukawa-coupled bosons (Figure 6.2), with four-fermion couplings mapped to ratios of Yukawa-type coupling and boson mass. While they can be rather delicate due to the marginality of the Yukawa coupling in $d = 4$, we can search for genuine UV completions in the bosonized model.

Finally, thermal fluctuations at temperature T can be described by compactifying Euclidean time to a strip of width $\beta = 1/T$. While finite-temperature effects do not affect the UV physics at $T/k \ll 1$ and therefore the asymptotic safety scenarios $\mathcal{B}$ and $\mathcal{C}$, the fermions acquire a Matsubara mass $\sim T$ in order to satisfy anti-periodic boundary conditions, which contributes to the freeze-out from the RG flow in the IR.

Appendix A

Euclidean Dirac Algebra

Here we provide a chiral representation of the Euclidean Dirac algebra in $d = 4$:

$$\gamma^{1,2,3} = \begin{pmatrix} 0 & i\sigma^{1,2,3} \\ -i\sigma^{1,2,3} & 0 \end{pmatrix} \qquad \gamma^4 = \begin{pmatrix} 0 & \mathbb{I}_2 \\ \mathbb{I}_2 & 0 \end{pmatrix}. \tag{2}$$

We can abbreviate this as

$$\gamma^\mu = \begin{pmatrix} 0 & i\sigma^\mu \\ i\bar{\sigma}^\mu & 0 \end{pmatrix}, \tag{3}$$

where σ^i are the Pauli matrices for $i = 1, 2, 3$, $\bar{\sigma}^i = -\sigma^i$ and $\sigma^4 = \bar{\sigma}^4 = -i\mathbb{I}_2$.

$$\gamma^5 := \gamma^1\gamma^2\gamma^3\gamma^4 = \begin{pmatrix} -\mathbb{I}_2 & 0 \\ 0 & \mathbb{I}_2 \end{pmatrix} \tag{4}$$

In this chiral representation, we can express the spinors as

$$\psi := \begin{pmatrix} \psi_L \\ \psi_R \end{pmatrix}, \qquad \bar{\psi} := \psi^\dagger\gamma^4 = \begin{pmatrix} \psi_R^\dagger & \psi_L^\dagger \end{pmatrix}, \tag{5}$$

with each chirality $\psi_{L/R}$ furnishing an irreducible representation of the $SO(4)$ symmetry group of Euclidean spacetime.

Appendix B

Threshold Functions and Regulators

In general spacetime dimension d, the threshold functions used in the flow equations (4.40) and (4.41) are defined by

$$
\begin{aligned}
& l_d^{([n],X_{[x_d]}^{[x_p]},Y_{[y_d]}^{[y_p]},\ldots)}(\omega_X,\omega_Y,\ldots;\eta_X,\eta_Y,\ldots) \\
&= \frac{(-1)^{1+x_p x_d+y_p y_d+\ldots}}{2}\int dx\, x^{n+d/2-1}\tilde{\partial}_t \left[\left(\frac{\partial}{\partial x}\right)^{x_d} G_X(\omega_X)\right]^{x_p}\left[\left(\frac{\partial}{\partial x}\right)^{y_d} G_Y(\omega_Y)\right]^{y_p} \ldots, \quad (6)
\end{aligned}
$$

for particles of type X, Y etc [3]. The brackets [...] contain optional indices which would otherwise take the default values of $n = 0$, $x_d = 0$, $y_d = 0, \ldots$, $x_p = 1$, $y_p = 1, \ldots$ and the minus sign ensures that all threshold functions are positive for finite dimensionless mass parameters $\omega_{X,Y,\ldots}$ and anomalous dimensions $\eta_{X,Y,\ldots}$. $x = p^2/k^2$ denotes the momentum squared normalized to the cutoff at k^2. $G_X(\omega_X)$ is the dimensionless regularized propagator for particle X

$$
G_B(\omega_B) = \frac{1}{x_B+\omega_B}, \qquad G_F(\omega_F) = \frac{1}{x_F+\omega_F}, \qquad G_{\tilde{F}}(\omega_{\tilde{F}}) = \frac{1+r_F}{x_F+\omega_{\tilde{F}}}, \qquad (7)
$$

where

$$
x_B = x(1+r_B(x)), \qquad x_F = x(1+r_F(x))^2 \qquad (8)
$$

are the regularized momenta and r_B and r_F are the bosonic and fermionic regulator shape functions. For analytic computations, we choose to use the optimized linear regulators [70]

$$
r_B(x) = \left(\frac{1}{x}-1\right)\theta(1-x), \qquad r_F(x) = \left(\frac{1}{\sqrt{x}}-1\right)\theta(1-x), \qquad (9)
$$

where θ denotes the Heaviside step function. For massless photons with $\omega_B = 0$ and potentially massive fermions with $\omega_F = m^2$ in $d = 4$,

$$l_4^{(\mathrm{F}^2)}(m^2) = \frac{5 - \eta_\psi}{10\,(m^2+1)^2}, \tag{10}$$

$$l_4^{(\mathrm{B,F})}(0, m^2) = \frac{-5\,(m^2+1)\,\eta_A - 6\eta_\psi + 30m^2 + 60}{60\,(m^2+1)^2}, \tag{11}$$

$$l_4^{(1,\mathrm{B,F})}(0, m^2) = -\frac{7\,(m^2+1)\,\eta_A + 8\eta_\psi - 56\,(m^2+2)}{168\,(m^2+1)^2}, \tag{12}$$

$$l_4^{(\mathrm{B}^2,\mathrm{F})}(0, m^2) = -\frac{5\,(m^2+1)\,\eta_A + 3\eta_\psi - 15\,(2m^2+3)}{30\,(m^2+1)^2}, \tag{13}$$

$$l_4^{(1,\mathrm{B}^2,\mathrm{F})}(0, m^2) = -\frac{7\,(m^2+1)\,\eta_A + 4\eta_\psi - 28\,(2m^2+3)}{84\,(m^2+1)^2}, \tag{14}$$

$$l_4^{(2,\mathrm{B}^2,\mathrm{F})}(0, m^2) = -\frac{9\,(m^2+1)\,\eta_A + 5\eta_\psi - 45\,(2m^2+3)}{180\,(m^2+1)^2}. \tag{15}$$

For the Pauli-induced fixed point $\mathcal{C}$ in Table 3.1, depending on whether we take into account the anomalous dimension η_ψ^*, the threshold functions simplify to

$$l_4^{(\mathrm{F}^2)}(m^2) = \frac{1}{10}\,(5 - \eta_\psi)\,, \tag{16}$$

$$l_4^{(\mathrm{B,F})}(0, m^2) = \frac{1}{10}\,(10 - \eta_\psi)\,, \tag{17}$$

$$l_4^{(1,\mathrm{B,F})}(0, m^2) = \frac{1}{168}\,(112 - 8\eta_\psi)\,, \tag{18}$$

$$l_4^{(\mathrm{B}^2,\mathrm{F})}(0, m^2) = \frac{1}{30}\,(45 - 3\eta_\psi)\,, \tag{19}$$

$$l_4^{(1,\mathrm{B}^2,\mathrm{F})}(0, m^2) = \frac{1}{84}\,(84 - 4\eta_\psi)\,, \tag{20}$$

$$l_4^{(2,\mathrm{B}^2,\mathrm{F})}(0, m^2) = \frac{1}{180}\,(135 - 5\eta_\psi)\,. \tag{21}$$

Appendix C

Flow Equations for QED with Pauli Term

As obtained from the Wetterich equation for the truncation (3.2), the beta functions for the renormalized dimensionless couplings in (3.3) are given in general spacetime dimension d by [3]:

$$\begin{aligned}\partial_t e = e\left(\frac{d}{2}-2+\eta_\psi+\frac{\eta_A}{2}\right) &- 4v_d\frac{(d-4)(d-1)}{d}e^3\, l_d^{(1,\mathrm{B},\tilde{\mathrm{F}}^2)}(0,m^2)\\ &- 16v_d\frac{(d-2)(d-1)}{d}e\kappa^2\, l_d^{(2,\mathrm{B},\tilde{\mathrm{F}}^2)}(0,m^2) - 32v_d\frac{d-1}{d}e^2\kappa m\, l_d^{(1,\mathrm{B},\mathrm{F},\tilde{\mathrm{F}})}(0,m^2,m^2)\\ &- 4v_d\frac{(d-2)(d-1)}{d}e^3m^2\, l_d^{(\mathrm{B},\mathrm{F}^2)}(0,m^2) - 16v_d\frac{(d-4)(d-1)}{d}e\kappa^2m^2\, l_d^{(2,\mathrm{B},\mathrm{F}^2)}(0,m^2),\end{aligned} \tag{22}$$

$$\begin{aligned}\partial_t\kappa = \kappa\left(\frac{d}{2}-1+\eta_\psi+\frac{\eta_A}{2}\right) &+ 16v_d\frac{(d-4)(d-1)}{d}\kappa^3\, l_d^{(2,\mathrm{B},\tilde{\mathrm{F}}^2)}(0,m^2)\\ &- 4v_d\left(3\frac{(d-6)(d-2)}{d}+1\right)e^2\kappa\, l_d^{(1,\mathrm{B},\tilde{\mathrm{F}}^2)}(0,m^2)\\ &+ 4v_d\, e^3m\Big[\frac{d-3}{d}\Big[l_d^{(1,\mathrm{B},\mathrm{F},\tilde{\mathrm{F}}_1)}(0,m^2,m^2) - l_d^{(1,\mathrm{B},\mathrm{F}_1,\tilde{\mathrm{F}})}(0,m^2,m^2)\Big]\\ &- \frac{(d-4)(d-1)}{2d}\, l_d^{(\mathrm{B},\mathrm{F},\tilde{\mathrm{F}})}(0,m^2,m^2)\Big] + 16v_d\, e\kappa^2m\Big[\frac{5(d-4)(d-3)}{2d}\, l_d^{(1,\mathrm{B},\mathrm{F},\tilde{\mathrm{F}})}(0,m^2,m^2)\\ &+ \frac{d-3}{d}\Big[l_d^{(2,\mathrm{B},\mathrm{F},\tilde{\mathrm{F}}_1)}(0,m^2,m^2) - l_d^{(2,\mathrm{B},\mathrm{F}_1,\tilde{\mathrm{F}})}(0,m^2,m^2)\Big] - \frac{d+2}{d}\, l_d^{(1,\mathrm{B},\mathrm{F},\tilde{\mathrm{F}})}(0,m^2,m^2)\Big]\\ &+ 16v_d\left(1-\frac{(d-4)^2}{d}\right)\kappa^3m^2\, l_d^{(1,\mathrm{B},\mathrm{F}^2)}(0,m^2) + 4v_d\frac{(d-4)(d-1)}{d}e^2\kappa m^2\, l_d^{(\mathrm{B},\mathrm{F}^2)}(0,m^2),\end{aligned} \tag{23}$$

$$\begin{aligned}\partial_t m = &-m(1-\eta_\psi) - 16v_d\,(d-1)\,e\kappa\, l_d^{(1,\mathrm{B},\tilde{\mathrm{F}})}(0,m^2) + 16v_d\,(d-1)\kappa^2m\, l_d^{(1,\mathrm{B},\mathrm{F})}(0,m^2)\\ &- 4v_d\,(d-1)e^2m\, l_d^{(\mathrm{B},\mathrm{F})}(0,m^2),\end{aligned} \tag{24}$$

where $v_d = [2^{d+1}\pi^{d/2}\Gamma(d/2)]^{-1}$ is a phase space factor, such that $v_4 = 1/(32\pi^2)$. Similarly, the fermion and photon anomalous dimensions of (3.4) are given by the algebraic equations

$$\begin{aligned}\eta_\psi &= 4v_d\frac{(d-2)(d-1)}{d}e^2\, l_d^{(\mathrm{B},\tilde{\mathrm{F}})}(0,m^2) - 8v_d\frac{d-1}{d}e^2\, l_d^{(1,\mathrm{B},\tilde{\mathrm{F}}_1)}(0,m^2)\\ &+ 16v_d\frac{(d-4)(d-1)}{d}\kappa^2\, l_d^{(1,\mathrm{B},\tilde{\mathrm{F}})}(0,m^2) - 32v_d\frac{d-1}{d}\kappa^2\, l_d^{(2,\mathrm{B},\tilde{\mathrm{F}}_1)}(0,m^2)\\ &+ 32v_d\frac{d-1}{d}e\kappa m\, l_d^{(1,\mathrm{B},\mathrm{F}_1)}(0,m^2),\end{aligned} \tag{25}$$

$$\begin{aligned}\eta_A &= 8v_d\frac{d_\gamma N_f}{d+2}e^2\, l_d^{(2,\tilde{\mathrm{F}}_1^2)}(m^2) + 16v_d d_\gamma N_f\kappa^2 m^2\, l_d^{(\mathrm{F}^2)}(m^2) - 16v_d\frac{d-4}{d}d_\gamma N_f\kappa^2\, l_d^{(1,\tilde{\mathrm{F}}^2)}(m^2)\\ &- 64v_d\frac{d_\gamma N_f}{d}e\kappa m\, l_d^{(1,\mathrm{F}_1,\tilde{\mathrm{F}})}(m^2,m^2) + 8v_d\frac{d_\gamma N_f}{d}e^2 m^2\, l_d^{(1,\mathrm{F}_1^2)}(m^2).\end{aligned} \tag{26}$$

As is explicit from Appendix 6, the threshold functions themselves implicitly depend on the anomalous dimension as an RG improvement resumming over higher-loop diagrams.

References

[1] Rym Bouchendira et al. "State of the art in the determination of the fine structure constant: test of Quantum Electrodynamics and determination of". In: *Annalen der Physik* 525.7 (2013), pp. 484–492.

[2] D. Hanneke, S. Fogwell, and G. Gabrielse. "New Measurement of the Electron Magnetic Moment and the Fine Structure Constant". In: *Phys. Rev. Lett.* 100 (12 Mar. 2008), p. 120801. DOI: 10.1103/PhysRevLett.100.120801. URL: https://link.aps.org/doi/10.1103/PhysRevLett.100.120801.

[3] Holger Gies and Jobst Ziebell. "Asymptotically Safe QED". In: *Eur. Phys. J. C* 80 (2020), p. 607. DOI: 10.1140/epjc/s10052-020-8171-8. arXiv: 2005.07586 [hep-th].

[4] Kenneth G. Wilson. "The renormalization group: Critical phenomena and the Kondo problem". In: *Rev. Mod. Phys.* 47 (4 Oct. 1975), pp. 773–840. DOI: 10.1103/RevModPhys.47.773. URL: https://link.aps.org/doi/10.1103/RevModPhys.47.773.

[5] Leo P Kadanoff. "Notes on Migdal's recursion formulas". In: *Annals of Physics* 100.1 (1976), pp. 359–394. ISSN: 0003-4916. DOI: https://doi.org/10.1016/0003-4916(76)90066-X. URL: https://www.sciencedirect.com/science/article/pii/000349167690066X.

[6] Leo P. Kadanoff. "The application of renormalization group techniques to quarks and strings". In: *Rev. Mod. Phys.* 49 (2 Apr. 1977), pp. 267–296. DOI: 10.1103/RevModPhys.49.267. URL: https://link.aps.org/doi/10.1103/RevModPhys.49.267.

[7] P. Kopietz, L. Bartosch, and F. Schütz. *Introduction to the Functional Renormalization Group*. Introduction to the Functional Renormalization Group. Springer, 2010. ISBN: 9783642050930. URL: https://books.google.de/books?id=cGa5Q9BeMNUC.

[8] Bertrand Delamotte. "An Introduction to the Nonperturbative Renormalization Group". In: *Renormalization Group and Effective Field Theory Approaches to Many-Body Systems*. Ed. by Achim Schwenk and Janos Polonyi. Berlin, Heidelberg: Springer Berlin Heidelberg, 2012, pp. 49–132. ISBN: 978-3-642-27320-9. DOI: 10.1007/978-3-642-27320-9_2. URL: https://doi.org/10.1007/978-3-642-27320-9_2.

[9] Jens Braun, Holger Gies, and Daniel D. Scherer. "Asymptotic safety: A simple example". In: *Physical Review D* 83.8 (Apr. 2011). DOI: 10.1103/physrevd.83.085012. URL: https://doi.org/10.1103%2Fphysrevd.83.085012.

[10] Astrid Eichhorn. *Asymptotically safe gravity*. 2020. DOI: 10.48550/ARXIV.2003.00044. URL: https://arxiv.org/abs/2003.00044.

[11] Yu Nakayama. *Scale invariance vs conformal invariance*. 2013. DOI: 10.48550/ARXIV.1302.0884. URL: https://arxiv.org/abs/1302.0884.

[12] A. B. Zamolodchikov. "Irreversibility of the Flux of the Renormalization Group in a 2D Field Theory". In: *JETP Lett.* 43 (1986), pp. 730–732.

[13] Joseph Polchinski. “Scale and Conformal Invariance in Quantum Field Theory”. In: *Nucl. Phys. B* 303 (1988), pp. 226–236. DOI: 10.1016/0550-3213(88)90179-4.

[14] David Tong. *The Renormalization Group.* 2018. URL: https://www.damtp.cam.ac.uk/user/dbs26/AQFT/Wilsonchap.pdf.

[15] Gilles Tarjus et al. “Hierarchical reference theory of critical fluids in disordered porous media”. In: *Molecular Physics* 109.23-24 (Dec. 2011), pp. 2863–2887. DOI: 10.1080/00268976.2011.620024. URL: https://doi.org/10.1080%2F00268976.2011.620024.

[16] Michael E. Peskin and Daniel V. Schroeder. *An Introduction to quantum field theory.* Reading, USA: Addison-Wesley, 1995. ISBN: 978-0-201-50397-5.

[17] Elisabeth Kraus and Georg Weiglein. “The Callan-Symanzik equation of the electroweak standard model and its one-loop functions”. In: *Nuclear Physics B* 551.1-2 (June 1999), pp. 117–154. DOI: 10.1016/s0550-3213(99)00202-3. URL: https://doi.org/10.1016%2Fs0550-3213%2899%2900202-3.

[18] H. Osborn and D.E. Twigg. “Remarks on exact RG equations”. In: *Annals of Physics* 327.1 (Jan. 2012), pp. 29–73. DOI: 10.1016/j.aop.2011.10.011. URL: https://doi.org/10.1016%2Fj.aop.2011.10.011.

[19] Janos Polonyi. “Lectures on the functional renormalization group method”. In: *Open Physics* 1.1 (Jan. 2003), pp. 1–71. DOI: 10.2478/bf02475552. URL: https://doi.org/10.2478%2Fbf02475552.

[20] R. F. Streater and A. S. Wightman. *PCT, spin and statistics, and all that.* 1989. ISBN: 978-0-691-07062-9.

[21] Nikolai Nikolaevich Bogolubov, AA Logunov, and IT Todorov. “Introduction to axiomatic quantum field theory”. In: *Reading, Mass* (1975).

[22] R Alkofer. “The infrared behaviour of QCD Green’s functions Confinement, dynamical symmetry breaking, and hadrons as relativistic bound states”. In: *Physics Reports* 353.5-6 (Nov. 2001), pp. 281–465. DOI: 10.1016/s0370-1573(01)00010-2. URL: https://doi.org/10.1016%2Fs0370-1573%2801%2900010-2.

[23] Pieter Maris and Craig D. Roberts. “Dyson–Schwinger Equations: A Tool for Hadron Physics”. In: *International Journal of Modern Physics E* 12.03 (June 2003), pp. 297–365. DOI: 10.1142/s0218301303001326. URL: https://doi.org/10.1142%2Fs0218301303001326.

[24] C.D. Roberts and S.M. Schmidt. “Dyson-Schwinger equations: Density, temperature and continuum strong QCD”. In: *Progress in Particle and Nuclear Physics* 45 (Jan. 2000), S1–S103. DOI: 10.1016/s0146-6410(00)90011-5. URL: https://doi.org/10.1016%2Fs0146-6410%2800%2990011-5.

[25] Holger Gies. “Introduction to the Functional RG and Applications to Gauge Theories”. In: *Renormalization Group and Effective Field Theory Approaches to Many-Body Systems.* Springer Berlin Heidelberg, 2012, pp. 287–348. DOI: 10.1007/978-3-642-27320-9_6. URL: https://doi.org/10.1007%2F978-3-642-27320-9_6.

[26] J. P. Blaizot. “Non Perturbative Renormalization Group and Bose-Einstein Condensation”. In: *arXiv: Statistical Mechanics* (2007).

[27] D.-U. Jungnickel and C. Wetterich. “Effective action for the chiral quark-meson model”. In: *Phys. Rev. D* 53 (9 May 1996), pp. 5142–5175. DOI: 10.1103/PhysRevD.53.5142. URL: https://link.aps.org/doi/10.1103/PhysRevD.53.5142.

[28] Christof Wetterich. “Exact evolution equation for the effective potential”. In: *Physics Letters B* 301.1 (1993), pp. 90–94. ISSN: 0370-2693. DOI: https://doi.org/10.1016/0370-2693(93)90726-X. URL: https://www.sciencedirect.com/science/article/pii/037026939390726X.

[29] Daniel F. Litim and Jan M. Pawlowski. “Completeness and consistency of renormalization group flows”. In: *Phys. Rev. D* 66 (2 July 2002), p. 025030. DOI: 10.1103/PhysRevD.66.025030. URL: https://link.aps.org/doi/10.1103/PhysRevD.66.025030.

[30] Jürgen Berges, Nikolaos Tetradis, and Christof Wetterich. “Non-perturbative renormalization flow in quantum field theory and statistical physics”. In: *Physics Reports* 363.4-6 (June 2002), pp. 223–386. DOI: 10.1016/s0370-1573(01)00098-9. URL: https://doi.org/10.1016%2Fs0370-1573%2801%2900098-9.

[31] Richard D. Ball et al. “Scheme independence and the exact renormalization group”. In: *Physics Letters B* 347.1-2 (Mar. 1995), pp. 80–88. DOI: 10.1016/0370-2693(95)00025-g. URL: https://doi.org/10.1016%2F0370-2693%2895%2900025-g.

[32] Sen-Ben Liao, Janos Polonyi, and Michael Strickland. “Optimization of renormalization group flow”. In: *Nuclear Physics B* 567.3 (Feb. 2000), pp. 493–514. DOI: 10.1016/s0550-3213(99)00496-4. URL: https://doi.org/10.1016%2Fs0550-3213%2899%2900496-4.

[33] Jan M. Pawlowski. “Aspects of the functional renormalisation group”. In: *Annals of Physics* 322.12 (Dec. 2007), pp. 2831–2915. DOI: 10.1016/j.aop.2007.01.007. URL: https://doi.org/10.1016%2Fj.aop.2007.01.007.

[34] Léonie Canet et al. “Optimization of the derivative expansion in the nonperturbative renormalization group”. In: *Phys. Rev. D* 67 (6 Mar. 2003), p. 065004. DOI: 10.1103/PhysRevD.67.065004. URL: https://link.aps.org/doi/10.1103/PhysRevD.67.065004.

[35] D. Zappalà. “Improving the renormalization group approach to the quantum-mechanical double well potential”. In: *Physics Letters A* 290.1-2 (Nov. 2001), pp. 35–40. DOI: 10.1016/s0375-9601(01)00642-9. URL: https://doi.org/10.1016%2Fs0375-9601%2801%2900642-9.

[36] Daniel F. Litim. “Optimisation of the exact renormalisation group”. In: *Physics Letters B* 486.1-2 (July 2000), pp. 92–99. DOI: 10.1016/s0370-2693(00)00748-6. URL: https://doi.org/10.1016%2Fs0370-2693%2800%2900748-6.

[37] Daniel F. Litim. “Optimized renormalization group flows”. In: *Phys. Rev. D* 64 (10 Oct. 2001), p. 105007. DOI: 10.1103/PhysRevD.64.105007. URL: https://link.aps.org/doi/10.1103/PhysRevD.64.105007.

[38] J. S. Bell and R. Jackiw. “A PCAC puzzle: $\pi^0 \to \gamma\gamma$ in the σ model”. In: *Nuovo Cim. A* 60 (1969), pp. 47–61. DOI: 10.1007/BF02823296.

[39] Stephen L. Adler. “Axial-Vector Vertex in Spinor Electrodynamics”. In: *Phys. Rev.* 177 (5 Jan. 1969), pp. 2426–2438. DOI: 10.1103/PhysRev.177.2426. URL: https://link.aps.org/doi/10.1103/PhysRev.177.2426.

[40] H. Sazdjian. “Introduction to chiral symmetry in QCD”. In: *EPJ Web of Conferences* 137 (2017). Ed. by Y. Foka, N. Brambilla, and V. Kovalenko, p. 02001. DOI: 10.1051/epjconf/201713702001. URL: https://doi.org/10.1051%2Fepjconf%2F201713702001.

[41] Yoichiro Nambu. “Quasi-Particles and Gauge Invariance in the Theory of Superconductivity”. In: *Physical Review* 117.3 (Feb. 1960), pp. 648–663. DOI: 10.1103/PhysRev.117.648.

[42] Daniel Naegels. *An introduction to Goldstone boson physics and to the coset construction.* 2021. DOI: 10.48550/ARXIV.2110.14504. URL: https://arxiv.org/abs/2110.14504.

[43] S. P. Klevansky. “The Nambu—Jona-Lasinio model of quantum chromodynamics”. In: *Rev. Mod. Phys.* 64 (3 July 1992), pp. 649–708. DOI: 10.1103/RevModPhys.64.649. URL: https://link.aps.org/doi/10.1103/RevModPhys.64.649.

[44] S. Kim, John B. Kogut, and Maria-Paola Lombardo. “On the triviality of textbook quantum electrodynamics”. In: *Physics Letters B* 502.1-4 (Mar. 2001), pp. 345–349. DOI: 10.1016/s0370-2693(01)00201-5. URL: https://doi.org/10.1016%2Fs0370-2693%2801%2900201-5.

[45] S. Kim, John B. Kogut, and Maria-Paola Lombardo. “Gauged Nambu–Jona-Lasinio studies of the triviality of quantum electrodynamics”. In: *Physical Review D* 65.5 (Jan. 2002). DOI: 10.1103/physrevd.65.054015. URL: https://doi.org/10.1103%2Fphysrevd.65.054015.

[46] Holger Gies and Joerg Jaeckel. “Renormalization Flow of QED”. In: *Phys. Rev. Lett.* 93 (11 Sept. 2004), p. 110405. DOI: 10.1103/PhysRevLett.93.110405. URL: https://link.aps.org/doi/10.1103/PhysRevLett.93.110405.

[47] Aaron Held. *Effective asymptotic safety and its predictive power: Gauge-Yukawa theories.* 2020. DOI: 10.48550/ARXIV.2003.13642. URL: https://arxiv.org/abs/2003.13642.

[48] Daniel F. Litim and Francesco Sannino. “Asymptotic safety guaranteed”. In: *Journal of High Energy Physics* 2014.12 (Dec. 2014). DOI: 10.1007/jhep12(2014)178. URL: https://doi.org/10.1007%2Fjhep12%282014%29178.

[49] Giulio Maria Pelaggi et al. “Asymptotically safe standard model extensions?” In: *Phys. Rev. D* 97 (9 May 2018), p. 095013. DOI: 10.1103/PhysRevD.97.095013. URL: https://link.aps.org/doi/10.1103/PhysRevD.97.095013.

[50] R. B. Mann et al. “Asymptotically Safe Standard Model via Vectorlike Fermions”. In: *Phys. Rev. Lett.* 119 (26 Dec. 2017), p. 261802. DOI: 10.1103/PhysRevLett.119.261802. URL: https://link.aps.org/doi/10.1103/PhysRevLett.119.261802.

[51] René Sondenheimer. “Analytical relations for the bound state spectrum of gauge theories with a Brout-Englert-Higgs mechanism”. In: *Physical Review D* 101.5 (Mar. 2020). DOI: 10.1103/physrevd.101.056006. URL: https://doi.org/10.1103%2Fphysrevd.101.056006.

[52] A. Maas, R. Sondenheimer, and P. Törek. “On the observable spectrum of theories with a Brout–Englert–Higgs effect”. In: *Annals of Physics* 402 (Mar. 2019), pp. 18–44. DOI: 10.1016/j.aop.2019.01.010. URL: https://doi.org/10.1016%2Fj.aop.2019.01.010.

[53] U. Harst and M. Reuter. “QED coupled to QEG”. In: *Journal of High Energy Physics* 2011.5 (May 2011). DOI: 10.1007/jhep05(2011)119. URL: https://doi.org/10.1007%2Fjhep05%282011%29119.

[54] Nicolai Christiansen and Astrid Eichhorn. “An asymptotically safe solution to the U(1) triviality problem”. In: *Physics Letters B* 770 (July 2017), pp. 154–160. DOI: 10.1016/j.physletb.2017.04.047. URL: https://doi.org/10.1016%2Fj.physletb.2017.04.047.

[55] Astrid Eichhorn and Fleur Versteegen. “Upper bound on the Abelian gauge coupling from asymptotic safety”. In: *Journal of High Energy Physics* 2018.1 (Jan. 2018). DOI: 10.1007/jhep01(2018)030. URL: https://doi.org/10.1007%2Fjhep01%282018%29030.

[56] Astrid Eichhorn, Aaron Held, and Christof Wetterich. “Predictive power of grand unification from quantum gravity”. In: *Journal of High Energy Physics* 2020.8 (Aug. 2020). DOI: 10.1007/jhep08(2020)111. URL: https://doi.org/10.1007%2Fjhep08%282020%29111.

[57] D. Djukanovic, J. Gegelia, and Ulf-G. Meißner. “Triviality of Quantum Electrodynamics Revisited”. In: *Communications in Theoretical Physics* 69.3 (Mar. 2018), p. 263. DOI: 10.1088/0253-6102/69/3/263. URL: https://doi.org/10.1088%2F0253-6102%2F69%2F3%2F263.

[58] Tatsumi Aoyama, Toichiro Kinoshita, and Makiko Nio. “Theory of the Anomalous Magnetic Moment of the Electron”. In: *Atoms* 7.1 (2019), p. 28. DOI: 10.3390/atoms7010028.

[59] Konrad Osterwalder and Robert Schrader. “AXIOMS FOR EUCLIDEAN GREEN’S FUNCTIONS”. In: *Commun. Math. Phys.* 31 (1973), pp. 83–112. DOI: 10.1007/BF01645738.

[60] Holger Gies, Kevin Tam, and Jobst Ziebell. “Pauli-Term-Induced Fixed-Points in d-dimensional QED”. In: *In preparation* (2022).

[61] U. Ellwanger, M. Hirsch, and A. Weber. “Flow Equations for the Relevant Part of the Pure Yang-Mills Action”. In: (1995). DOI: 10.48550/ARXIV.HEP-TH/9506019. URL: https://arxiv.org/abs/hep-th/9506019.

[62] Daniel F. Litim and Jan M. Pawlowski. “Flow equations for Yang-Mills theories in general axial gauges”. In: *Physics Letters B* 435.1-2 (Sept. 1998), pp. 181–188. DOI: 10.1016/s0370-2693(98)00761-8. URL: https://doi.org/10.1016%2Fs0370-2693%2898%2900761-8.

[63] Matthias Vojta. “Quantum phase transitions”. In: *Reports on Progress in Physics* 66.12 (Nov. 2003), pp. 2069–2110. DOI: 10.1088/0034-4885/66/12/r01. URL: https://doi.org/10.1088%2F0034-4885%2F66%2F12%2Fr01.

[64] David J. Gross and André Neveu. “Dynamical symmetry breaking in asymptotically free field theories”. In: *Phys. Rev. D* 10 (10 Nov. 1974), pp. 3235–3253. DOI: 10.1103/PhysRevD.10.3235. URL: https://link.aps.org/doi/10.1103/PhysRevD.10.3235.

[65] Walter E Thirring. “A soluble relativistic field theory”. In: *Annals of Physics* 3.1 (1958), pp. 91–112. ISSN: 0003-4916. DOI: https://doi.org/10.1016/0003-4916(58)90015-0. URL: https://www.sciencedirect.com/science/article/pii/0003491658900150.

[66] K. Furuya, R.E.Gamboa Saraví, and F.A. Schaposnik. "Path-integral formulation of chiral invariant fermion models in two dimensions". In: *Nuclear Physics B* 208.1 (1982), pp. 159–181. ISSN: 0550-3213. DOI: https://doi.org/10.1016/0550-3213(82)90191-2. URL: https://www.sciencedirect.com/science/article/pii/0550321382901912.

[67] Moshe Moshe and Jean Zinn-Justin. "Quantum field theory in the large N limit: a review". In: *Physics Reports* 385.3-6 (Oct. 2003), pp. 69–228. DOI: 10.1016/s0370-1573(03)00263-1. URL: https://doi.org/10.1016%2Fs0370-1573%2803%2900263-1.

[68] Michael Thies and Konrad Urlichs. "Revised phase diagram of the Gross-Neveu model". In: *Phys. Rev. D* 67 (12 June 2003), p. 125015. DOI: 10.1103/PhysRevD.67.125015. URL: https://link.aps.org/doi/10.1103/PhysRevD.67.125015.

[69] Oliver Schnetz, Michael Thies, and Konrad Urlichs. "Phase diagram of the Gross–Neveu model: exact results and condensed matter precursors". In: *Annals of Physics* 314.2 (Dec. 2004), pp. 425–447. DOI: 10.1016/j.aop.2004.06.009. URL: https://doi.org/10.1016%2Fj.aop.2004.06.009.

[70] Jens Braun. "Fermion Interactions and Universal Behavior in Strongly Interacting Theories". In: *J. Phys. G* 39 (2012), p. 033001. DOI: 10.1088/0954-3899/39/3/033001. arXiv: 1108.4449 [hep-ph].

[71] Y. Nambu and G. Jona-Lasinio. "Dynamical Model of Elementary Particles Based on an Analogy with Superconductivity. I". In: *Phys. Rev.* 122 (1 Apr. 1961), pp. 345–358. DOI: 10.1103/PhysRev.122.345. URL: https://link.aps.org/doi/10.1103/PhysRev.122.345.

[72] Y. Nambu and G. Jona-Lasinio. "Dynamical Model of Elementary Particles Based on an Analogy with Superconductivity. II". In: *Phys. Rev.* 124 (1 Oct. 1961), pp. 246–254. DOI: 10.1103/PhysRev.124.246. URL: https://link.aps.org/doi/10.1103/PhysRev.124.246.

[73] Yoichiro Nambu. "From BCS to NJL: An old story retold". In: *AIP Conf. Proc.* 1388.1 (2011). Ed. by Atsushi Hosaka et al., pp. 86–92. DOI: 10.1063/1.3647355.

[74] Jens Braun and Holger Gies. "Scaling laws near the conformal window of many-flavor QCD". In: *JHEP* 05 (2010), p. 060. DOI: 10.1007/JHEP05(2010)060. arXiv: 0912.4168 [hep-ph].

[75] Holger Gies and Joerg Jaeckel. "Chiral phase structure of QCD with many flavors". In: *Eur. Phys. J. C* 46 (2006), pp. 433–438. DOI: 10.1140/epjc/s2006-02475-0. arXiv: hep-ph/0507171.

[76] Mario Mitter, Jan M. Pawlowski, and Nils Strodthoff. "Chiral symmetry breaking in continuum QCD". In: *Phys. Rev. D* 91 (2015), p. 054035. DOI: 10.1103/PhysRevD.91.054035. arXiv: 1411.7978 [hep-ph].

[77] José F. Nieves and Palash B. Pal. "Generalized Fierz identities". In: *American Journal of Physics* 72.8 (Aug. 2004), pp. 1100–1108. DOI: 10.1119/1.1757445. URL: https://doi.org/10.1119%2F1.1757445.

[78] Holger Gies, Joerg Jaeckel, and Christof Wetterich. "Towards a renormalizable standard model without a fundamental Higgs scalar". In: *Physical Review D* 69.10 (May 2004).

DOI: 10.1103/physrevd.69.105008. URL: https://doi.org/10.1103%2Fphysrevd.69.105008.

[79] Jens Braun, Christian S. Fischer, and Holger Gies. “Beyond Miransky scaling”. In: *Physical Review D* 84.3 (Aug. 2011). DOI: 10.1103/physrevd.84.034045. URL: https://doi.org/10.1103%2Fphysrevd.84.034045.

[80] Jens Braun. *Chiral Phase Boundary of QCD from the Functional Renormalization Group*. 2006. DOI: 10.48550/ARXIV.HEP-PH/0611145. URL: https://arxiv.org/abs/hep-ph/0611145.